

Strategies Towards Soft Functional Supramolecular Materials

Lovrak, Matija

DOI

[10.4233/uuid:a5fcd470-d9e2-4d27-87fd-ae883b68e42e](https://doi.org/10.4233/uuid:a5fcd470-d9e2-4d27-87fd-ae883b68e42e)

Publication date

2018

Document Version

Final published version

Citation (APA)

Lovrak, M. (2018). *Strategies Towards Soft Functional Supramolecular Materials*. [Dissertation (TU Delft), Delft University of Technology]. <https://doi.org/10.4233/uuid:a5fcd470-d9e2-4d27-87fd-ae883b68e42e>

Important note

To cite this publication, please use the final published version (if applicable). Please check the document version above.

Copyright

Other than for strictly personal use, it is not permitted to download, forward or distribute the text or part of it, without the consent of the author(s) and/or copyright holder(s), unless the work is under an open content license such as Creative Commons.

Takedown policy

Please contact us and provide details if you believe this document breaches copyrights. We will remove access to the work immediately and investigate your claim.

Strategies Towards Soft Functional Supramolecular Materials

Proefschrift

ter verkrijging van de graad van doctor
aan de Technische Universiteit Delft,
op gezag van de Rector Magnificus prof. dr. ir. T. H. J. J. van der Hagen;
voorzitter van het College voor Promoties,
in het openbaar te verdedigen op

vrijdag 26 januari 2018 om 12:30 uur

door
Matija LOVRAK

Master of Science in Chemistry,
University of Zagreb, Kroatië
geboren te Bjelovar, Kroatië

This dissertation has been approved by the
promotor: Prof. dr. J. H. van Esch
copromotor: Dr. R. Eelkema

Composition of the doctoral committee:

Rector Magnificus	chairman
Prof. dr. J. H. van Esch	Delft University of Technology
Dr. R. Eelkema	Delft University of Technology

Independent members:

Prof. dr. J. Boekhoven	Technische Universität München, Germany
Prof. dr. T. Hermans	Université de Strasbourg, France
Prof. dr. ir. M. T. Kreutzer	Delft University of Technology
Prof. dr. E. J. R. Sudhölter	Delft University of Technology
Prof. dr. S. J. Picken	Delft University of Technology, reserve member

Other members:

Dr. H. M. M. van Beusekom	Erasums MC
---------------------------	------------

The work described in this thesis was carried out in the Advanced Soft Matter group at Delft University of Technology. This research was funded by Marie Curie initial training network "SMARTNET" and NanoNextNL, a micro and nanotechnology consortium of the Government of the Netherlands and 130 partners.

© Matija Lovrak, 2018

ISBN: 978-94-6186-883-1

Printed by: Gildeprint - Enschede

All rights reserved. The author encourages the communication of scientific contents and explicitly allows reproduction for scientific purposes with proper citation of the source. Parts of this thesis have been published in scientific journals and copyright is subject to different terms and conditions.

Propositions

belonging to the thesis:

Strategies Towards Soft Functional Supramolecular Materials

by Matija Lovrak

1. Listing potential applications in scientific papers without the proof of concept should be avoided because it does not contribute to the scientific content and it is often done purely for the purpose of selling research.
He, X. M. *et al.* Synthetic homeostatic materials with chemo-mechano-chemical self-regulation. *Nature* **487**, 214-218 (2012).
2. Reaction-diffusion is a promising approach for development of useful soft materials and applications, but we have to learn how to use it properly because current number of application-related reports is rather limited.
Chapter 2 of this thesis
3. Economy, as we know it today, is unnatural.
John Médaille, (2011, April 11), Capitalism as an Unnatural System, retrieved from <http://distributistreview.com/capitalism-as-an-unnatural-system/>
4. Although not described in the way how we know it today, Liesegang patterns should be called Runge-Liesegang patterns to give deserved credit to their early discoverer.
Runge, F. F. Zur farben-chemie. Musterbildung für freunde des schönen und zum gebrauch für zeichner, maler, verzierer und zeugdrucker. Dargestellt durch chemische wechselwirkung. (E. S. Mittler & Sohn, 1850)
5. It seems that the developers of video games do not always play the games they develop themselves. Otherwise, they would not have put all kind of nonsense achievements inside.
6. Since human slavery is forbidden, animal slavery should also be forbidden. Therefore, zoos should not exist, as well as possessing pets in cages.
7. Solving a maze using reaction-diffusion should be used in all schools as a demonstration for children that chemistry can offer a solution to various problems.
Suzuno, K. *et al.* Maze solving using fatty acid chemistry. *Langmuir* **30**, 9251-9255 (2014)
8. Aging in chemistry should be more exploited because it can lead to novel useful discoveries, such as indicators of expired food.
Draper, E. R., McDonald, T. O. & Adams, D. J. A low molecular weight hydrogel with unusual gel aging. *Chem. Commun.* **51**, 6595-6597 (2015).
9. Experimental results are more valuable than the results from numerical simulations.
R. Zimmermann, U. Freudenberg, R. Schweiß, D. Küttner, C. Werner, Hydroxide and hydronium ion adsorption – A survey, *Current Opinion in Colloid & Interface Science* **15** (2010) 196-202
10. The tendency of multinational companies to push all sorts of own standards to the market, which leads to format wars, is counterproductive.
Memory Stick (Sony) vs SD Card (SD Card Association)
HD DVD (initiated by Toshiba and NEC) vs Blue-ray Disc (Sony)

These propositions are considered opposable and defensible and as such have been approved by the promotor prof. dr. Jan van Esch and copromotor dr. Rienk Eelkema.

Stellingen

behorend bij het proefschrift:

Strategies Towards Soft Functional Supramolecular Materials

door Matija Lovrak

1. Het opsommen van mogelijke toepassingen zonder *proof-of-concept* zou vermeden moeten worden omdat het niet bijdraagt aan de wetenschappelijke inhoud en omdat het vaak uitsluitend gedaan wordt om het onderzoek te verkopen.
He, X. M. *et al.* Synthetic homeostatic materials with chemo-mechano-chemical self-regulation. *Nature* **487**, 214-218 (2012).
2. Reactie-diffusie is een veelbelovende methode voor de ontwikkeling van nuttige zachte materialen en toepassingen, maar we moeten leren hoe het precies gebruikt kan worden omdat het aantal toepassingsgerelateerde artikelen gelimiteerd is.
Hoofdstuk 2 van dit proefschrift.
3. De economie, zoals we die tegenwoordig kennen, is onnatuurlijk.
John Médaille, (2011, April 11), Capitalism as an Unnatural System, retrieved from <http://distributistreview.com/capitalism-as-an-unnatural-system/>
4. Ook al was het niet beschreven op de manier die we tegenwoordig kennen, de Liesegang patronen zouden Runge-Liesegang patronen moeten heten om de eerdere ontdekker waardering te geven.
Runge, F. F. Zur farben-chemie. Musterbildung für freunde des schönen und zum gebrauch für zeichner, maler, verzierer und zeugdrucker. Dargestellt durch chemische wechselwirkung. (E. S. Mittler & Sohn, 1850)
5. Het lijkt erop dat de makers van computer games niet altijd zelf de games spelen die ze ontwikkelen. Anders zouden ze niet al die onzinnige prestaties toevoegen.
6. Omdat mensenslavernij verboden is, zou dierslavernij ook verboden moeten worden. Daarom zouden dierentuinen niet mogen bestaan en zouden huisdieren niet in kooien gehouden mogen worden.
7. Het oplossen van een doolhofpuzzel met reactie-diffusie zou op scholen gedemonstreerd moeten worden om te laten zien dat scheikunde een oplossing kan bieden voor verschillende problemen.
Suzuno, K. *et al.* Maze solving using fatty acid chemistry. *Langmuir* **30**, 9251-9255 (2014)
8. Chemische veroudering zou meer onderzocht moeten worden omdat het kan leiden tot nieuwe nuttige ontdekkingen, zoals indicatoren voor bedorven voedsel.
Draper, E. R., McDonald, T. O. & Adams, D. J. A low molecular weight hydrogel with unusual gel aging. *Chem. Commun.* **51**, 6595-6597 (2015).
9. Experimentele resultaten zijn waardevoller dan de resultaten van numerieke simulaties.
R. Zimmermann, U. Freudenberg, R. Schweiß, D. Küttner, C. Werner, Hydroxide and hydronium ion adsorption – A survey, *Current Opinion in Colloid & Interface Science* **15** (2010) 196-202
10. De neiging van multinationale ondernemingen om allerlei eigen standaarden op de markt te forceren, hetgeen leidt tot formaatoorlog, is contraproductief.
Memory Stick (Sony) vs SD Card (SD Card Association)
HD DVD (initiated by Toshiba and NEC) vs Blue-ray Disc (Sony)

Deze stellingen worden oponeerbaar en verdedigbaar geacht en zijn als zodanig goedgekeurd door de promotor prof. dr. Jan van Esch en copromotor dr. Rienk Eelkema.

Table of Contents

Table of Contents.....	5
Introduction.....	1
Self-assembly.....	2
Reaction-diffusion.....	4
Outline of the thesis.....	7
References.....	9
Free-standing Supramolecular Hydrogel Objects by Reaction-Diffusion.....	15
Introduction.....	16
Results.....	17
Conclusion.....	26
References.....	27
Supplementary Information.....	29
Control over the Formation of Supramolecular Patterns Using Reaction-Diffusion.....	51
Introduction.....	52
Results and discussion.....	53
Conclusion.....	62
References.....	64
Supplementary Information.....	65
Supramolecular Gluing of Polymeric Hydrogels.....	69
Introduction.....	70
Results and discussion.....	70
Conclusion.....	73
References.....	75
Supplementary Information.....	76
The Effect of Supramolecular Hydrogel on Cell Viability and Proliferation.....	81
Introduction.....	82
Results and discussion.....	82
Conclusion.....	86
References.....	88
Supplementary Information.....	89
Implantable Artificial Plaque as an Alternative to Atherosclerotic Animal Models.....	93
Introduction.....	94
Methods.....	95
Results.....	99
Discussion.....	101
Conclusions.....	105

References.....	106
Summary	109
Samenvatting.....	111
About the author.....	113
Acknowledgements	114



1

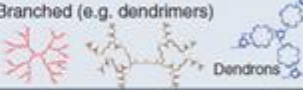
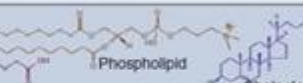
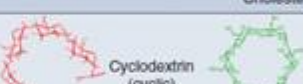
Introduction

Nature: the final frontier. For scientists, nature is an unlimited source of inspiration. For example, physicists explore nature's underlying forces and constituents all the way down to the smallest particles. Chemists aim to understand, replicate and apply the principles of nature from the level of atoms to the level of macromolecules, whereas biochemists focus on understanding the interplay of constituents that form what we call life. Out of many motifs in nature, two, which are the focus of this thesis, have attracted considerable attention of chemists. The first one is self-assembly and the second one is reaction-diffusion.

Self-assembly

Simply put, molecular self-assembly is the spontaneous organization of simple building blocks into larger constructs, usually called supramolecular structures, due to their interactions and geometry.^{1,2} Building blocks range from rather simple molecules, such as surfactants, to more complex molecules, such as DNA. A brief overview of different synthetic and biological self-assembling building blocks is given in Table 1. The interactions involved in self-assembly are noncovalent in nature, such as electrostatic interactions, hydrophobic effects, aromatic stacking, and hydrogen bonding.³ Many biological constructs are formed employing noncovalent interactions,⁵ including the light-harvesting complex, chromosomes, and cell membranes. Without noncovalent interactions, (macro)molecular building blocks would not be able to form functional constituents of living organisms and life, as we know it, probably would not exist. The occurrence of self-assembly in nature as one of the leading motifs underpins its important properties which are discussed in the rest of the paragraph. Firstly, self-assembly is a spontaneous process. Simply mixing self-assembling components suffices to form larger structures without any additional input. The reason for such simplicity is that the information necessary for molecules to assemble is encoded into the molecules themselves. This encoding is achieved by the presence of different, appropriately spatially arranged functional groups which allow interaction with other molecules through one of the aforementioned noncovalent interactions. Secondly, self-assembly is reversible. Since building blocks of supramolecular structures are usually held together by large number of interactions, their total energy of interaction is big. However, single noncovalent interactions are (much) weaker than covalent interactions (in terms of energy). The relatively small individual non-covalent interactions allow supramolecular structures to be much more dynamic at ambient temperatures compared to molecules consisting of covalently connected moieties. For example, easy exchange of one type of a building block with another, or easy repair of a damaged supramolecular structure, are some of possibilities. Thirdly, supramolecular assemblies of defined structure spanning over several orders of magnitude in size can be made by simply mixing nanometer-sized building blocks of the appropriate geometry and spatial disposition of interactions. Finally, as already mentioned, these self-assembling building blocks can be often made

Table 1. Synthetic and biological building blocks used in supramolecular self-assembly for obtaining diverse complex structures and their potential biomedical applications. Reproduced from reference.⁵

Building-Blocks		Supramolecular Assemblies	Applications	
Synthetic	Polymers	Linear (e.g. block-co-polymers)  Branched (e.g. dendrimers) 	 Micelles, Vesicles, Tubes	Nanoreactors; artificial organelles; nanocarriers drug delivery ^{21, 22}
	Surfactants	Anionic, Neutral, Cationic 	 Micelles, Vesicles	Drug and gene delivery systems; antimicrobial and antifungal activity ^{26, 27}
	Others	Porphyrin, Rotaxane, Graphene 	 Nanotubes, Toroids, Carbon nanotubes	Nanomedicine; drug delivery; hydrogels ^{8, 28, 29}
	Viruses	CPMV, λ phage, hHPBV 	 Aligned phage film, Fibrils, Particles	Biomaterials; cell culture substrates ³⁰⁻³³
Biological	Nucleic acids	RNA, DNA 	 DNA origami	Therapeutics (vehicles for drug delivery); diagnostics (biosensing) ^{11, 34, 35}
	Lipids	Fatty acid, Phospholipid, Cholesterol 	 Lipid bilayer, Vesicles, Films	Nanoreactors; artificial organelles; controlled drug delivery ^{19, 36-37}
	Saccharides	Amylose (helical), Cyclodextrin (cyclic) 	 Double helix, Nanotube, Spherical micelle	Drug delivery; biosensors ^{38,39}
	Peptides	VSYK, EACO 	 Random coil, β-sheet, α-helix, Helix protein	Hydrogel biomaterials; drug delivery; tissue engineering; 3D cell culture ⁴⁰⁻⁴⁸

employing well-understood chemical reactions, but yield supramolecular structures that might be very difficult, if not impossible, to synthesize. Therefore, scientist have recognized the potential of self-assembly as a bottom-up approach for making artificial, man-made, functional materials. The very first examples of man-made self-assembly were focused on reconstructing the self-assembly of viruses from their building blocks.^{8,9} Since that time, this research area has widely expanded and examples of different self-assembled materials can be found in literature today, ranging from rather simple assemblies of nanoparticles¹¹ to DNA origami¹².

One class of self-assembled materials are hydrogels - specifically, supramolecular hydrogels. Hydrogels are a special class of materials that are made of water (usually more than 95 %) and the small amount of structured solid matter, usually in the form of entangled fibers forming a network. This fibrillar network entraps water and stops it from flowing. Even that small amount of solid matter can make hydrogels exert some properties of solids. Therefore, hydrogels can exhibit some properties of both types of materials – solids (e.g. similar mechanical behavior under stress) and liquids (e.g. easy diffusion of small molecules). Hydrogels can be divided in two categories – polymeric hydrogels and supramolecular hydrogels. Polymeric hydrogels consist of long polymers

that are covalently crosslinked or held together by noncovalent interactions. They can be made from biological components, such as agar or gelatin, or synthetic polymers, such as polyacrylamide. Contrary to their polymeric counterparts, supramolecular hydrogels are made out of small molecules called low molecular weight gelators (LMWGs).¹⁵ LMWG molecules usually self-assemble via noncovalent interactions into fibers that subsequently form a fibrous network which entraps water thus forming a self-supporting gel. So far, many LMWGs have been discovered, either by molecular iteration of already know examples, or accidentally. However, designing LMWGs is very difficult because small changes in the molecular structure can turn a gelator into a non-gelator. Although certain sets of rules can be deduced from already existing examples¹⁶, general design rules that would always yield a LMWG molecule do not exist yet. In general, hydrogels are widely useful materials, with applications in foods¹⁷, cosmetics¹⁸, tissue engineering¹⁹ and medicine²⁰ amongst others. The same areas of applications are also envisioned for supramolecular hydrogels. Supramolecular hydrogels might offer advantage in some application areas due to rather easy synthesis and simple chemical modification to yield different properties. On the other hand, mechanical properties could be the limitation of supramolecular hydrogels when compared to their polymeric counterparts. They can rarely reach mechanical strengths (expressed as elastic modulus or storage modulus) of several hundred kPa, and not even compete with the strongest polymeric hydrogels which can reach strengths of more than 1 MPa.²¹ The resistance to mechanical deformation can be especially important when hydrogels are used as injectable materials, for example for drug delivery. Therefore, the strategies to significantly improve the mechanical properties of supramolecular gels are waiting to be discovered. Because of the extensive literature on self-assembled materials the interested reader is referred to some review articles for more details.^{5,22,23}

Reaction-diffusion

One of the crucial mechanisms to sustain life is reaction-diffusion (RD). RD is essentially the combination of two processes – reaction and diffusion. In a simple configuration, reactive components are physically separated in space by a medium such as hydrogel, for example, and they are brought together by diffusion (Figure 1). In the case when chemical reaction between the components is negligible or even absent, diffusion leads to homogenization of their spatial distribution. However, when reaction is faster than diffusion, thereby preventing homogenization, spatial organization can be achieved through localized reaction of components at diffusional fronts. Building and maintaining of microtubules²⁴ or skin patterns on animals²⁵⁻²⁷ (see Figure 2a) are some examples from nature that find an origin in reaction-diffusion. Additionally, living organisms employ a huge number of reactions in their bodies (cells) to enable their everyday functioning. To exert their function, biomolecules must be delivered to the

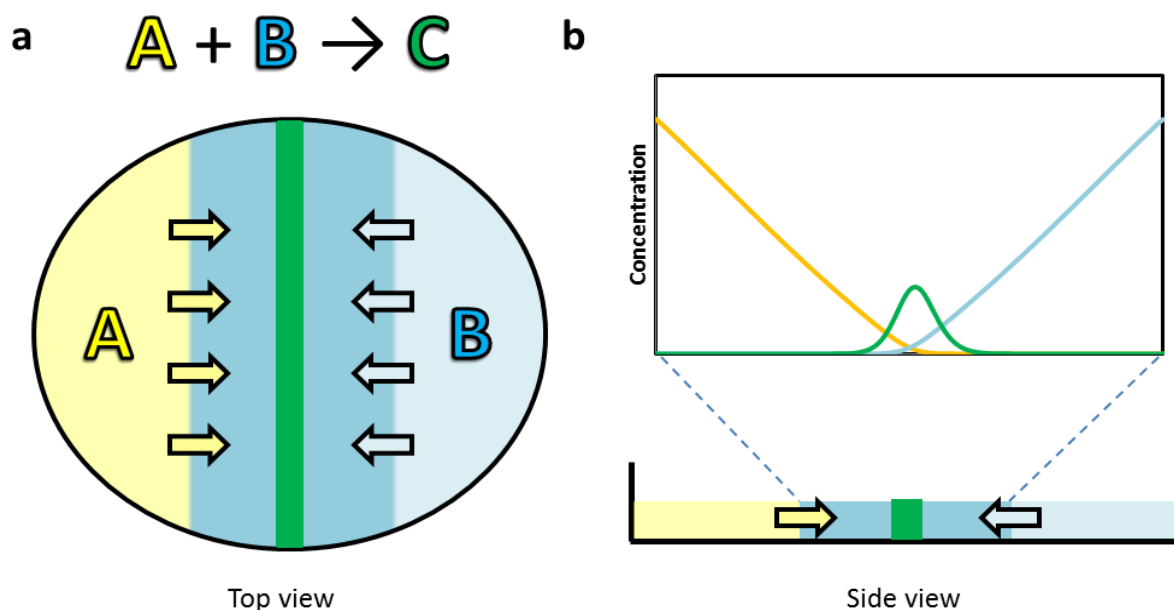


Figure 1. Scheme of a simple reaction-diffusion setup. a) A hypothetical chemical reaction between the compounds **A** and **B** leads to the formation of **C**. When **A** and **B** are separated by a medium that allows diffusion, they diffuse through it (indicated with arrows), forming the compound **C** upon collision of their diffusional fronts. In this way, **C** is formed only at locations where **A** and **B** come into contact. b) The concentration profiles of **A**, **B**, and **C** along diffusional matrix.

right spot at the right time. Since diffusion is a spontaneous process that does not cost energy, it is part of various regulatory processes in living organisms.^{28,29} However, diffusion itself is often not enough because it is slow. Therefore, diffusive transport is combined with a series of transport enzymes to increase efficiency. In this way, the series of enzymatic chemical reactions is coupled to diffusional transport between enzymes thus forming RD system. Examples include calcium waves^{30,31}, glucose-induced oscillations³², and transport of ATP to ATP-deficient sites³³⁻³⁵. RD can be also invoked to explain events including multiple cells. For example, growth of bacteria under insufficient nutrient conditions³⁶⁻³⁸ as well as some undesirable health conditions, such as ventricular tachycardia and fibrillation³⁹⁻⁴².

Despite its utmost importance in living systems, examples of RD can be also found in inanimate systems. RD based on simple, inorganic chemistries forms spatially extended structures in inanimate systems. For example, the alternate deposition of two minerals, chalcedony and quartz, causes the formation of patterns in iris agates⁴³, as shown in Figure 2d. Many other natural minerals, such as augite, garnet, plagioclase and zebra spa rock,⁴⁴⁻⁴⁹ are composed of alternating layers of different types of precipitates which gives them characteristic textures. Other examples include formation of cave stalactites⁴⁹, dendritic structures on surface of limestone⁵⁰ and formation and pigmentation of intricate seashells⁵¹.

Since its importance in nature, RD did not remain unnoticed by chemists. The first written evidence of reaction-diffusion related research dates back to 1855. That

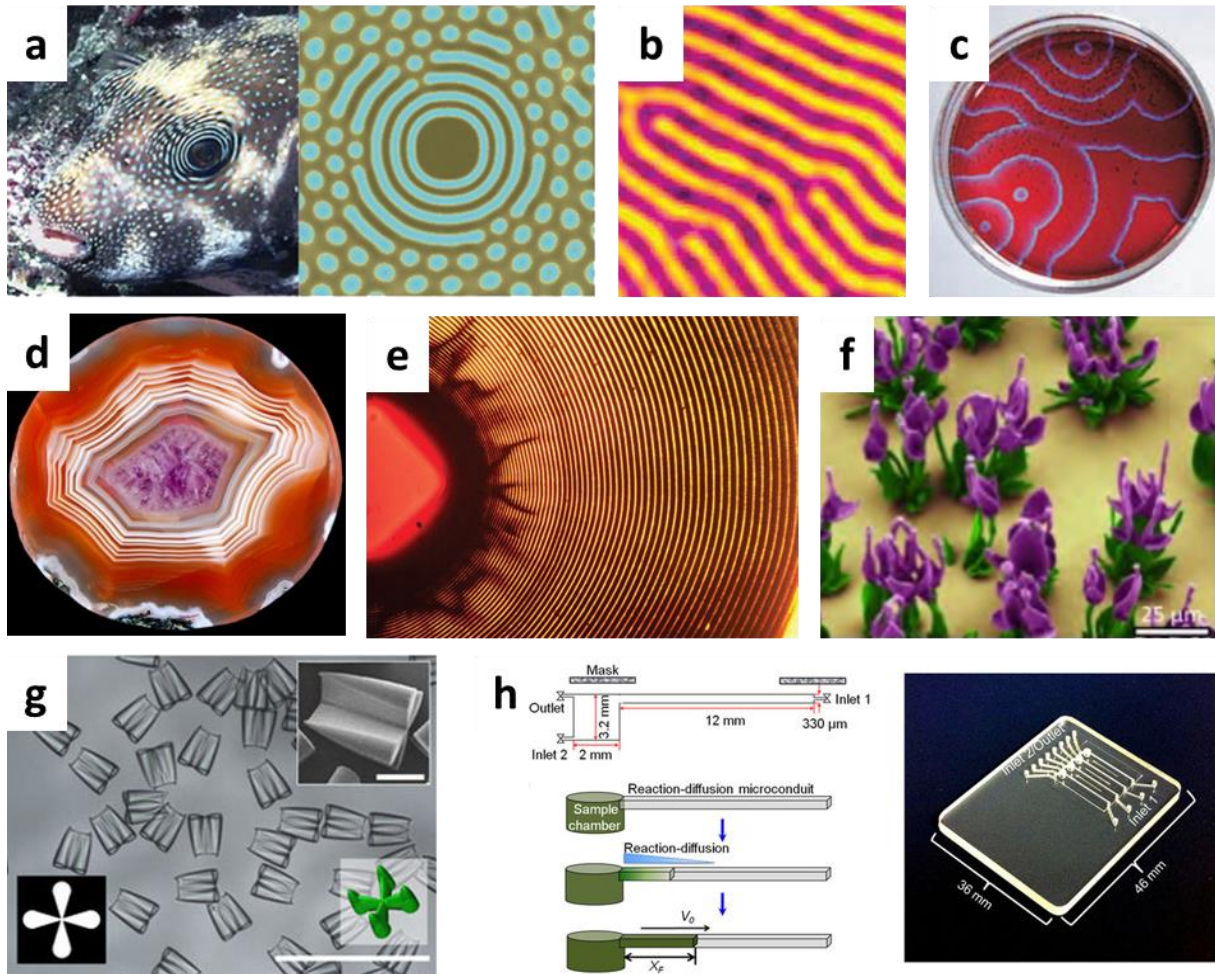


Figure 2. Biological and artificial RD systems. **a)** Pattern on a fish. Reproduced from reference.⁴ **b)** Turing pattern formed by CIMA reaction. Reproduced from reference.⁶ **c)** Traveling waves in the Belousov-Zhabotinsky chemical system. Reproduced from reference.⁶ **d)** Liesegang rings formed by precipitation of $\text{Ag}_2\text{Cr}_2\text{O}_7$. Reproduced from reference.⁶ **e)** Pattern on Lake Superior Carnelian Amethyst Agate. Reproduced from reference.⁷ **f)** Complex artificial microstructures produced using inorganic precipitation reactions. Reproduced from reference.¹⁰ **g)** Artificial microstructures made using polymerization reaction. Reproduced from reference.¹³ **h)** A functional device for quantification of nucleic acids based on RD. Reproduced from reference.¹⁴

year Friedlieb Ferdinand Runge discovered reaction-diffusion systems and published two books about them.⁵²⁻⁵⁵ Nevertheless, this first discovery was forgotten until 1896 when Raphael Liesegang⁵⁶ did similar experiments and from that year extensive research on this kind of systems has been done. Runge and Liesegang observed that some reactive pairs of inorganic salts form bands of a precipitate when they diffuse through a gel matrix (Figure 2e). These bands were named Liesegang rings/patterns⁵⁷⁻⁶⁰ after their discoverer. This discovery was the proof that reaction-diffusion systems are different from conventional reactions in bulk, because a mechanism of precipitation does not imply the formation of patterns, but only the formation of precipitate.

First evidence that RD is linked to living systems was provided by Alan Turing⁶¹ and Boris Belousov⁶² on the examples of oscillatory reactions. Turing predicted theoretically that a homogeneous mixture of activator and inhibitor can spontaneously

lead to the formation of stationary concentration variations, as shown in Figure 2b. It is important to note that such concentration variations can occur only in the case when not all species have similar diffusion coefficients. Belousov discovered a system in which diffusion and reactions are nonlinearly coupled which leads to chemical oscillations in space and/or time (Figure 2c). Since various regulatory processes in living organisms employ versatile combinations of nonlinear coupling and feedback loops, their discoveries were indeed an important link between RD and origin of life.

Until this date, it has been shown that various pairs of inorganic salts can produce various kinds of patterns using gel-on-gel printing.⁶ Nevertheless, the reaction-diffusion systems are far from only-for-demonstration experiments. They are useful for micro- and nanoscale fabrication. In that sense, RD is used for the deposition of metal foils at gel interfaces, for gold, glass, and silicon etching, and for the structuring metal films.⁶³⁻⁶⁶ They can also be applied for amplification and sensing.⁶⁷⁻⁶⁹ In the end, they are not limited only to produce 1D or 2D patterns, but can be also applied in 3D, producing very complex microstructures (Figure 2f).^{6,10} Although RD systems have been extensively investigated until this date, mainly inorganic systems have been reported. The reports of RD systems employing organic or biomolecules are scarce. Examples include determination of protein-ligand binding constants⁷⁰, DNA circuits for edge detection⁷¹, enzymatic network for threshold sensing⁷², and propagation of a synthetic replicator⁷³. Also, complex polymeric microstructures can be easily made (Figure 2g).¹³ Even a functional device for quantifying nucleic acids based on RD can be constructed, as can be seen in Figure 2h.¹⁴ These examples show that RD offers extraordinary possibilities. Nevertheless, taking into account the immense number of organic compounds and organic reactions it is clear that the full potential of RD is yet to be reached.

Outline of the thesis

The next step in technological development would be combining self-assembly and reaction-diffusion in similar ways to how nature does. In this way the advantages of both would be brought together yielding means towards the development of new materials that could not be made in other ways. For example, spatial control over self-assembly is usually achieved by templating. By combining it with a reaction-diffusion approach, self-assembling building blocks could be brought together by diffusion, and would assemble only at locations where all necessary components are present without need for any template. Alternatively, supramolecular structures exerting certain function or carrying a cargo could diffuse through a hydrogel matrix and exert function or release the cargo only at locations where chemical “instructions” for this specific action are present. These kinds of materials could be used as platforms for investigation of drug-delivery properties. In the end, possibilities are almost limitless and depend only on our imagination and our needs.

The aim of this work is to explore the strategies of using self-assembly and reaction-diffusion approaches for the production of novel soft functional materials with potential cell related and medical applications. The second chapter of this thesis describes reaction-diffusion approach for assembling a small molecular weight gelator into patterns imbedded in agar and free-standing hydrogel objects ranging in size from the micrometer to centimeter scale. Our experimental results are supported with a mathematical model of RD. Strikingly, this is the first report of this sort which shows implications of combining reaction-diffusion approach with supramolecular chemistry. The third chapter is about the details of supramolecular pattern formation. More precisely, we investigated how controllable experimental parameters define the dimensions of the pattern. We showed that the experimental results are in good agreement with the RD model, confirming that modelling of RD is crucial tool for predicting outcomes of these non-linear processes. The fourth chapter describes simple approach for gluing gels. We developed simple method based on RD and self-assembly of the small molecular weight gelator to attach two or more pieces of hydrogel together. This approach contributes to possible solutions for attaching pieces of soft matter together, which is generally a rather challenging task. In the fifth chapter we investigate the potential of the double network gel consisting of alginate and supramolecular gel to act as an extracellular matrix. First, we relate the cell survival to different components of this hybrid gel network, and then we discuss requirements and potential solutions for further improvements of this double network gel towards being fully compatible extracellular matrix. Finally, in the sixth chapter, we describe the preparation of first implantable artificial plaque for evaluation of drug-coated endovascular technologies. We developed artificial plaque based on self-assembled lipids dispersed throughout a hydrogel matrix. Our solution presents a cheaper alternative to atherosclerotic animal models.

References

- 1 Whitesides, G. M. & Grzybowski, B. Self-assembly at all scales. *Science* **295**, 2418-2421 (2002).
- 2 Grzybowski, B. A., Wilmer, C. E., Kim, J., Browne, K. P. & Bishop, K. J. M. Self-assembly: From crystals to cells. *Soft Matter* **5**, 1110-1128 (2009).
- 3 Bishop, K. J. M., Wilmer, C. E., Soh, S. & Grzybowski, B. A. Nanoscale forces and their uses in self-assembly. *Small* **5**, 1600-1630 (2009).
- 4 Kondo, S. & Miura, T. Reaction-diffusion model as a framework for understanding biological pattern formation. *Science* **329**, 1616-1620 (2010).
- 5 Mendes, A. C., Baran, E. T., Reis, R. L. & Azevedo, H. S. Self-assembly in nature: Using the principles of nature to create complex nanobiomaterials. *Wiley Interdiscip. Rev.: Nanomed. Nanobiotechnol.* **5**, 582-612 (2013).
- 6 Grzybowski, B. A. *Chemistry in motion: Reaction-diffusion systems for micro- and nanotechnology.* (Wiley, 2009).
- 7 Gitche Gume Agate and History Museum Grand Marais, M. *Agate basics*, <<http://www.agatelady.com/agate-basics.html>> (2017).
- 8 Bancroft, J. B., Hills, G. J. & Markham, R. A study of the self-assembly process in a small spherical virus formation of organized structures from protein subunits in vitro. *Virology* **31**, 354-379 (1967).
- 9 Poglazov, B. F., Mesyanzhinov, V. V. & Kosourov, G. I. A study of the self-assembly of protein of the bacteriophage t2 head. *J. Mol. Biol.* **29**, 389-394 (1967).
- 10 Noorduyn, W. L., Grinthal, A., Mahadevan, L. & Aizenberg, J. Rationally designed complex, hierarchical microarchitectures. *Science* **340**, 832-837 (2013).
- 11 Kalsin, A. M. *et al.* Electrostatic self-assembly of binary nanoparticle crystals with a diamond-like lattice. *Science* **312**, 420-424 (2006).
- 12 Rothmund, P. W. K. Folding DNA to create nanoscale shapes and patterns. *Nature* **440**, 297-302 (2006).
- 13 Shim, T. S., Yang, S. M. & Kim, S. H. Dynamic designing of microstructures by chemical gradient-mediated growth. *Nat. Commun.* **6**, 6584 (2015).
- 14 Liu, C. *et al.* Nucleometer: A reaction-diffusion based method for quantifying nucleic acids undergoing enzymatic amplification. *Sci. Rep.* **4** (2014).
- 15 Hanabusa, K. & Suzuki, M. Physical gelation by low-molecular-weight compounds and development of gelators. *Bull. Chem. Soc. Jpn.* **89**, 174-182 (2016).
- 16 van Esch, J. H. & Feringa, B. L. New functional materials based on self-assembling organogels: From serendipity towards design. *Angewandte Chemie International Edition* **39**, 2263-2266 (2000).
- 17 Shewan, H. M. & Stokes, J. R. Review of techniques to manufacture micro-hydrogel particles for the food industry and their applications. *J. Food Eng.* **119**, 781-792 (2013).
- 18 Parente, M. E., Andrade, A. O., Ares, G., Russo, F. & Jimenez-Kairuz, A. Bioadhesive hydrogels for cosmetic applications. *Int. J. Cosmet. Sci.* **37**, 511-518 (2015).
- 19 Kumar, A. & Han, S. S. Pva-based hydrogels for tissue engineering: A review. *Int. J. Polym. Mater. Polym. Biomater.* **66**, 159-182 (2017).
- 20 Pinho, E., Grootveld, M., Soares, G. & Henriques, M. Cyclodextrin-based hydrogels toward improved wound dressings. *Crit. Rev. Biotechnol.* **34**, 328-337 (2014).
- 21 Gong, J. P., Katsuyama, Y., Kurokawa, T. & Osada, Y. Double-network hydrogels with extremely high mechanical strength. *Adv. Mater.* **15**, 1155-1158 (2003).
- 22 Palivan, C. G. *et al.* Bioinspired polymer vesicles and membranes for biological and medical applications. *Chem. Soc. Rev.* **45**, 377-411 (2016).
- 23 Jang, Y. & Champion, J. A. Self-assembled materials made from functional recombinant proteins. *Acc. Chem. Res.* **49**, 2188-2198 (2016).

- 24 Tabony, J., Glade, N., Demongeot, J. & Papaseit, C. Biological self-organization by way of
microtubule reaction-diffusion processes. *Langmuir* **18**, 7196-7207 (2002).
- 25 Kondo, S. The reaction-diffusion system: A mechanism for autonomous pattern formation in the
animal skin. *Genes Cells* **7**, 535-541 (2002).
- 26 Kondo, S. & Asai, R. A reaction-diffusion wave on the skin of the marine angelfish pomacanthus.
Nature **376**, 765-768 (1995).
- 27 Jiang, T. X. *et al.* Integument pattern formation involves genetic and epigenetic controls: Feather
arrays simulated by digital hormone models. *Int. J. Dev. Biol.* **48**, 117-135 (2004).
- 28 Soh, S., Byrska, M., Kandere-Grzybowska, K. & Grzybowski, B. A. Reaction-diffusion systems in
intracellular molecular transport and control. *Angew. Chem., Int. Ed.* **49**, 4170-4198 (2010).
- 29 Soh, S., Banaszak, M., Kandere-Grzybowska, K. & Grzybowski, B. A. Why cells are microscopic: A
transport-time perspective. *J. Phys. Chem. Lett.* **4**, 861-865 (2013).
- 30 Newman, E. A. & Zahs, K. R. Calcium waves in retinal glial cells. *Science* **275**, 844-847 (1997).
- 31 Straub, S. V., Giovannucci, D. R. & Yule, D. I. Calcium wave propagation in pancreatic acinar cells -
functional interaction of inositol 1,4,5-trisphosphate receptors, ryanodine receptors, and
mitochondria. *J. Gen. Physiol.* **116**, 547-559 (2000).
- 32 Mair, T., Warnke, C., Tsuji, K. & Muller, S. C. Control of glycolytic oscillations by temperature.
Biophys. J. **88**, 639-646 (2005).
- 33 Dzeja, P. P. & Terzic, A. Phosphotransfer networks and cellular energetics. *J. Exp. Biol.* **206**, 2039-
2047 (2003).
- 34 Reich, J. G. & Sel'kov, E. E. *Energy metabolism of the cell: A theoretical treatise.* (Academic Press,
1981).
- 35 Dzeja, P. P. & Terzic, A. Phosphotransfer reactions in the regulation of atp-sensitive k⁺ channels.
FASEBJ. **12**, 523-529 (1998).
- 36 Budrene, E. O. & Berg, H. C. Complex patterns formed by motile cells of escherichia-coli. *Nature*
349, 630-633 (1991).
- 37 Budrene, E. O. & Berg, H. C. Dynamics of formation of symmetrical patterns by chemotactic
bacteria. *Nature* **376**, 49-53 (1995).
- 38 Ben-Jacob, E., Cohen, I. & Levine, H. Cooperative self-organization of microorganisms. *Adv. Phys.*
49, 395-554 (2000).
- 39 Terman, D. & Wang, D. L. Global competition and local cooperation in a network of neural
oscillators. *Physica D* **81**, 148-176 (1995).
- 40 Hess, B. Periodic patterns in biology. *Naturwissenschaften* **87**, 199-211 (2000).
- 41 Garfinkel, A. *et al.* Preventing ventricular fibrillation by flattening cardiac restitution. *Proc. Natl.*
Acad. Sci. U. S. A. **97**, 6061-6066 (2000).
- 42 Gray, C. M., Konig, P., Engel, A. K. & Singer, W. Oscillatory responses in cat visual-cortex exhibit
inter-columnar synchronization which reflects global stimulus properties. *Nature* **338**, 334-337
(1989).
- 43 Heaney, P. J. & Davis, A. M. Observation and origin of self-organized textures in agates. *Science*
269, 1562-1565 (1995).
- 44 Haase, C. S., Chadam, J., Feinn, D. & Ortoleva, P. Oscillatory zoning in plagioclase feldspar. *Science*
209, 272-274 (1980).
- 45 Allegre, C. J., Provost, A. & Jaupart, C. Oscillatory zoning - a pathological case of crystal-growth.
Nature **294**, 223-228 (1981).
- 46 Reeder, R. J., Fagioli, R. O. & Meyers, W. J. Oscillatory zoning of mn in solution-grown calcite
crystals. *Earth-Sci. Rev.* **29**, 39-46 (1990).
- 47 Yardley, B. W. D., Rochelle, C. A., Barnicoat, A. C. & Lloyd, G. E. Oscillatory zoning in metamorphic
minerals - an indicator of infiltration metasomatism. *Mineral. Mag.* **55**, 357-365 (1991).
- 48 Krug, H. J., Jacob, K. H. & Dietrich, S. The formation and fragmentation of periodic bands through
precipitation and ostwald ripening. *Fractals and Dynamic Systems in Geoscience*, 269-282 (1994).

- 49 Short, M. B. *et al.* Stalactite growth as a free-boundary problem: A geometric law and its platonic ideal. *Phys. Rev. Lett.* **94** (2005).
- 50 Bates, R. L. & Jackson, J. A. *Glossary of geology*. (American Geological Institute, 1987).
- 51 Fowler, D. R., Meinhardt, H. & Prusinkiewicz, P. *Comp. Graph.* **26** (1992).
- 52 Runge, F. F. *Zur farben-chemie. Musterbildung für freunde des schönen und zum gebrauch für zeichner, maler, verzierer und zeugdrucker. Dargestellt durch chemische wechselwirkung*. (E. S. Mittler & Sohn, 1850).
- 53 Runge, F. F. *Das od als bildungstrieb der stoffe, veranschaulicht in selbstständig gewachsenen bildern*. (Published by the author, 1866).
- 54 Bussemas, H. H., Harsch, G. & Etre, L. S. Runge, friedlieb, ferdinand (1794-1867) - self-grown pictures as precursors of paper-chromatography. *Chromatographia* **38**, 243-254 (1994).
- 55 Anft, B. Friedlieb ferinand runge: A forgotten chemist of the nineteenth century. *J. Chem. Educ.* **32**, 566 (1955).
- 56 Liesegang, R. E. Ueber einige eigenschaften von gallerten. *Naturwiss. Wochenschr.* **11**, 353 (1896).
- 57 Flicker, M. & Ross, J. Mechanism of chemical instability for periodic precipitation phenomena. *J. Chem. Phys.* **60**, 3458-3465 (1974).
- 58 Hantz, P. Regular microscopic patterns produced by simple reaction-diffusion systems. *PCCP* **4**, 1262-1267 (2002).
- 59 Muller, S. C. & Ross, J. Spatial structure formation in precipitation reactions. *J. Phys. Chem. A* **107**, 7997-8008 (2003).
- 60 Bensemann, I. T., Fialkowski, M. & Grzybowski, B. A. Wet stamping of microscale periodic precipitation patterns. *J. Phys. Chem. B* **109**, 2774-2778 (2005).
- 61 Turing, A. M. The chemical basis of morphogenesis. *Philos. Trans. R. Soc. London, Ser. B* **237**, 37-72 (1952).
- 62 Zaikin, A. N. & Zhabotinsky, A. M. Concentration wave propagation in two-dimensional liquid-phase self-oscillating system. *Nature* **225**, 535-537 (1970).
- 63 Smoukov, S. K., Bishop, K. J. M., Campbell, C. J. & Grzybowski, B. A. Freestanding three-dimensional copper foils prepared by electroless deposition on micropatterned gels. *Adv. Mater.* **17**, 751-+ (2005).
- 64 Smoukov, S. K., Bishop, K. J. M., Klajn, R., Campbell, C. J. & Grzybowski, B. A. Cutting into solids with micropatterned gels. *Adv. Mater.* **17**, 1361-1365 (2005).
- 65 Smoukov, S. K. & Grzybowski, B. A. Maskless microetching of transparent conductive oxides (ito and zno) and semiconductors (gaas) based on reaction-diffusion. *Chem. Mater.* **18**, 4722-4723 (2006).
- 66 Campbell, C. J., Smoukov, S. K., Bishop, K. J. M., Baker, E. & Grzybowski, B. A. Direct printing of 3d and curvilinear micrometer-sized architectures into solid substrates with sub-micrometer resolution. *Adv. Mater.* **18**, 2004-2008 (2006).
- 67 Bishop, K. J. M., Gray, T. P., Fialkowski, M. & Grzybowski, B. A. Microchameleons: Nonlinear chemical microsystems for amplification and sensing. *Chaos* **16** (2006).
- 68 Bishop, K. J. M., Fialkowski, M. & Grzybowski, B. A. Micropatterning chemical oscillations: Waves, autofocusing, and symmetry breaking. *J. Am. Chem. Soc.* **127**, 15943-15948 (2005).
- 69 Bishop, K. J. M. & Grzybowski, B. A. Localized chemical wave emission and mode switching in a patterned excitable medium. *Phys. Rev. Lett.* **97** (2006).
- 70 Wei, Y., Wesson, P. J., Kourkine, I. & Grzybowski, B. A. Measurement of protein-ligand binding constants from reaction-diffusion concentration profiles. *Anal. Chem.* **82**, 8780-8784 (2010).
- 71 Chirieleison, S. M., Allen, P. B., Simpson, Z. B., Ellington, A. D. & Chen, X. Pattern transformation with DNA circuits. *Nat. Chem.* **5**, 1000-1005 (2013).
- 72 Semenov, S. N., Markvoort, A. J., de Greef, T. F. & Huck, W. T. Threshold sensing through a synthetic enzymatic reaction-diffusion network. *Angew. Chem., Int. Ed.* **53**, 8066-8069 (2014).

- 73 Bottero, I., Huck, J., Kosikova, T. & Philp, D. A synthetic replicator drives a propagating reaction-diffusion front. *J. Am. Chem. Soc.* **138**, 6723-6726 (2016).

Free-standing Supramolecular Hydrogel Objects by Reaction-Diffusion

Abstract

Self-assembly provides access to a variety of molecular materials, yet spatial control over structure formation remains difficult to achieve. Here we show how reaction-diffusion (RD) can be coupled to a molecular self-assembly process to generate macroscopic free-standing objects with control over shape, size, and functionality. In RD, two or more reactants diffuse from different positions to give rise to spatially defined structures upon reaction. We demonstrate that RD can be used to locally control formation and self-assembly of hydrazone molecular gelators from their non-assembling precursors, leading to soft, free-standing hydrogel objects with sizes from several hundred micrometers up to centimeters. Different chemical functionalities and gradients can easily be integrated in the hydrogel objects by using different reactants. Our methodology, together with the vast range of organic reactions and self-assembling building blocks, provides a general approach towards the programmed fabrication of soft microscale objects with controlled functionality and shape.

Introduction

Over the past decades the self-assembly of a wide variety of building blocks has become an established technology for the bottom-up fabrication of objects and materials with structural features ranging from nano- up to micrometer length scales.^{1,2} The general approach to create objects and structures of dimensions beyond the nanoscale is to increase the size of the building blocks. However, this comes with new challenges - to fabricate these larger building blocks with sub-micron features and to manage the delicate balance of forces between building blocks, diffusion, and inertia. Reaction-diffusion (RD) plays a key role in natural structure-forming processes, including self-assembly and cell proliferation, which control the formation of a wide variety of structures, ranging from actin filaments, extracellular matrix, to organs and skin patterns.^{1,3-5} In RD, two or more reactants diffuse when locally released at different positions, giving rise to spatial concentration patterns, which may lead to local structure formation, like Liesegang rings, polymerization or self-assembly, upon reaction.^{6,7} In recent years, almost exclusively inorganic RD systems have expanded into a wide range of scientific and technological areas, such as biomineralization⁸, microfabrication⁹⁻¹³, the formation of microlenses^{7,9,14}, the formation of microparticles and microspheres^{15,16}, and dynamic materials¹⁷. The reported RD patterns and structures reach high levels of complexity and resolution¹⁸, but so far the application of RD to control structure formation of organic materials has been limited. Organic chemistry offers both an extremely wide range of chemical reactions and functional materials, as well as the possibility to precisely control chemical kinetics across multiple time scales. Only a few examples of RD using biological reactants have shown that chemical gradients can be programmed using DNA-based autocatalytic reaction networks¹⁹⁻²¹, and enzymes^{22,23}. With organic compounds, RD has been used to fabricate anisotropic structures²⁴, and, only very recently, to achieve spatial control over the formation of micro-objects by a polymerization reaction²⁵.

Here we describe the combined reaction-diffusion and self-assembly (RD-SA) of a supramolecular gelator leading to the formation of free-standing macroscopic structures with controllable shape, size, and chemical functionalization. In this system, multiple components diffuse towards each other, to react at the crossing of the diffusional fronts and form hydrogelator molecules, eventually leading to a supramolecular structure through self-assembly. We show that the patterned structures can be chemically functionalized and functionalization can be used to form permanent chemical gradients inside the final structures. The methodology developed here provides a general approach towards the programmed fabrication of soft microscale objects with controlled functionality and shape, and we anticipate that it may be applied for the creation of new functional soft biomaterials with a wealth of shapes, sizes, and chemical functionality.

Results

Fabrication of 1D reaction-diffusion pattern. We use RD-SA to control the spatial distribution of supramolecular materials (Figure 1). RD-SA requires a multicomponent reaction inducing a self-assembly process, to allow independent diffusion of reactants and self-assembly of products at the crossing of the diffusional fronts. We have recently reported a supramolecular hydrogelator that is formed in the gelation medium by a multicomponent chemical reaction.²⁶ In this work, the acid-catalyzed reaction of hydrazide **H** and aldehyde **A** leads to the formation of the trishydrazone gelator **HA₃** (Figure 1a).²⁷ When **HA₃** reaches concentrations above its critical aggregation concentration (CAC), it self-assembles into fibers and *in-situ* forms a non-transparent supramolecular network. The rate of formation of the supramolecular network is controlled through the hydrazine-forming reaction, which depends on the concentration of reactants and the presence of an acid catalyst.^{27,28} In our RD-SA approach, reactants **H** and **A** diffuse over a distance and react upon crossing of the moving fronts, forming **HA₃**, which subsequently self-assembles into a supramolecular material. In a typical RD-SA experiment, **H** and **A** are placed at the opposite sides of an agar gel matrix (acting as a diffusion medium), and left to diffuse and react over time (Figure 1b). We observed that the formed **HA₃** forms a non-transparent supramolecular structure within the agar matrix, manifesting as the appearance of a turbid line structure at the intercept of the two diffusion fronts. Structure formation started after ~7 hours, and the formed line typically achieved a width of 2.5 mm within 24 hours (Figure 2a and Supplementary Movie 1) when using 2 cm wide agar gels at general experimental conditions. The supramolecular structure forming the line (referred to as a 1D pattern) extends vertically from the bottom to the top of the 3.5 mm thick agar matrix, and is stable for months.

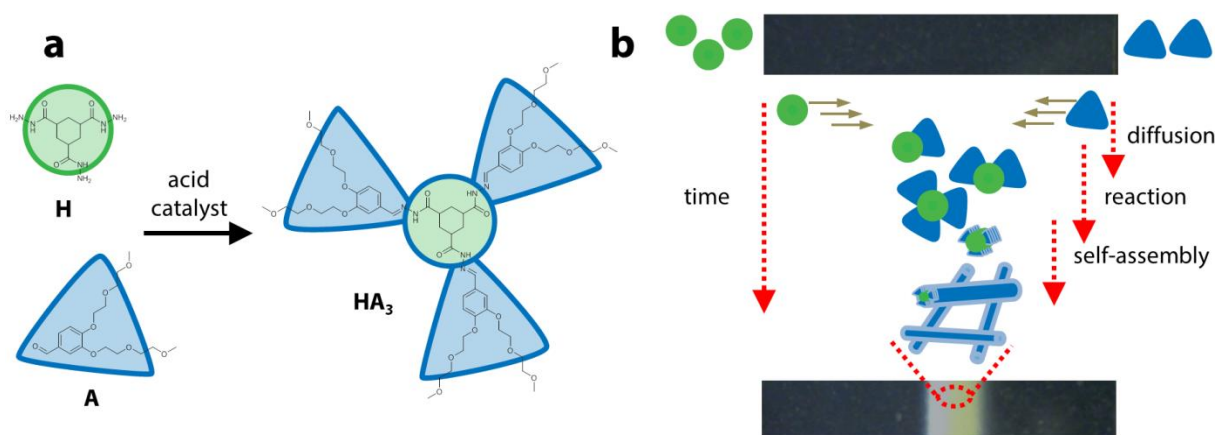


Figure 1. Reaction-diffusion of a two component self-assembling gelator. (a) Hydrazide **H** and aldehyde **A** react to form gelator **HA₃** under ambient conditions in water, with acid acting as a catalyst. (b) The space-time plot illustrates the RD-SA process. Reactants **H** (green circle, left) and **A** (blue triangle, right) are placed on the opposite sides of the agar gel matrix. Over time **H** and **A** diffuse through the matrix, and react upon crossing to form gelator **HA₃**, which self-assembles into a fibrous gel network. This process results in the formation of a turbid white line consisting of gel fibers, within the diffusion matrix.

Fabrication of more complex RD patterns. With this result in hand, we set out to explore the potential of RD-SA to control shape and dimensions of the formed structures. We started by investigating the influence of initial localization of reactants, diffusion distance, and type of reactant on the resulting shapes. By positioning the reactants in pre-designed locations, we anticipated obtaining a variety of two-dimensional (2D) shapes. We observed the local formation of the supramolecular structure at the crossing of diffusional fronts of **H** and **A** (Figure 2a). More complex shapes and patterns such as waves, grids, circles and triangles were easily made using

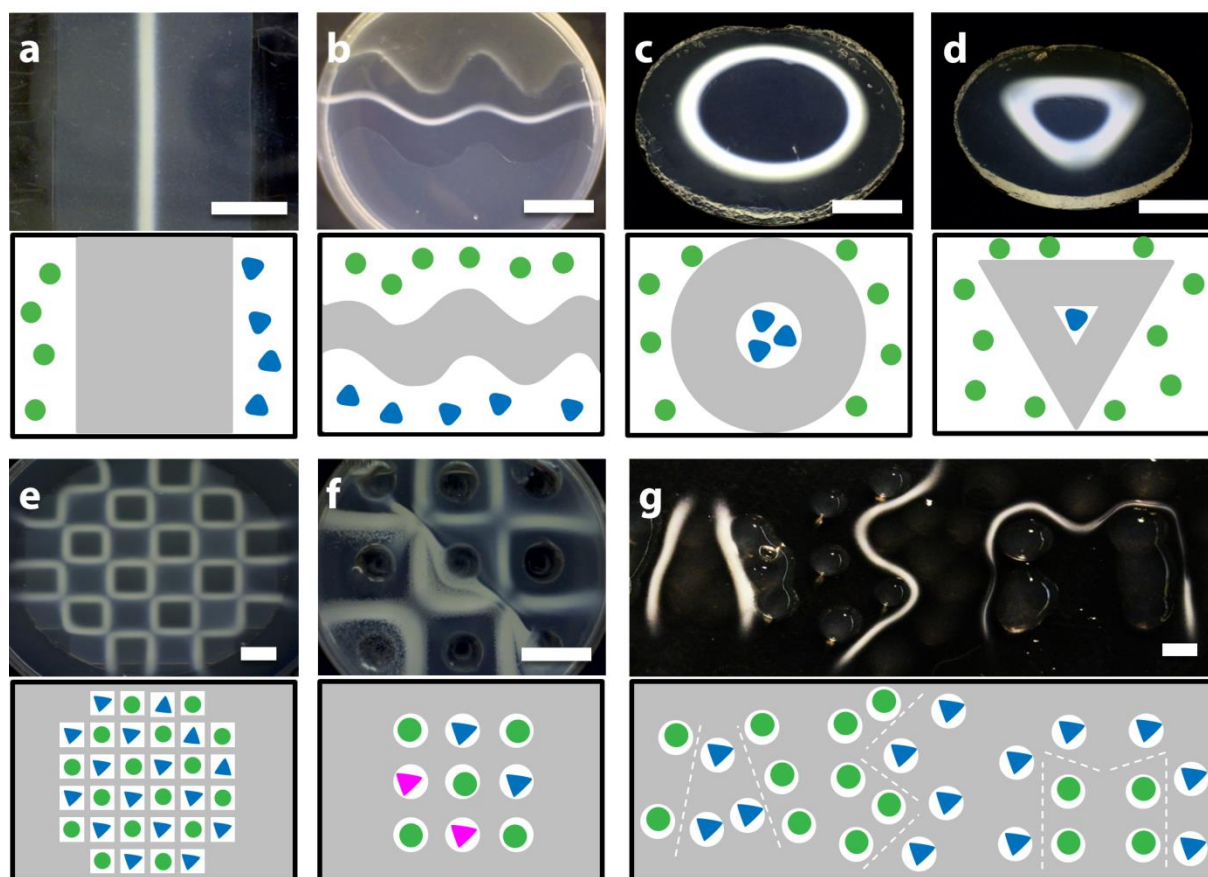


Figure 2. The initial location of reactants control structure formation in RD-SA. In a-g, the gel structure formed through RD-SA (photograph, top) resulted from a starting point configuration as shown in the cartoon below. In the cartoons, the grey areas denote the agar matrix, white areas are the reservoirs, which are filled with hydrazide **H** (green circles) and aldehyde **A** (blue triangles). (a) A 1D pattern formed by RD of **H**, from the left, and **A**, from the right, in an agar diffusion matrix. Method: reservoirs in the agar matrix. (b) By shaping the agar matrix, the RD-SA formed patterns were obtained in different shapes, such as waves. Method: reservoirs in the agar matrix. (c,d) To show the versatility of the RD-formed gel structures, different designs were used to obtain a circle and a triangle. Method: a PDMS mold below the agar matrix. (e) A grid formed by RD-SA. Method: a PDMS mold below the agar matrix. (f) An RD-SA grid made from aldehydes **A** and **A*** to compare the difference in self-assembly behavior, (magenta: **A***, blue: **A**). Method: reservoirs in the agar matrix. (g) Using the RD-SA approach to ‘write’ our research group name (ASM). Method: droplets of reactants in agar solutions were placed on top of an agar matrix, to diffuse and form supramolecular structures at the intersection of the diffusion gradients (Supplementary Methods). Scale bars: 1 cm.

three types of approaches for reactant injection: by cutting reservoirs for the reactants into the agar matrix (Figure 2a, b and f and Supplementary Movie 2), by placing reservoirs into a polydimethylsiloxane (PDMS) mold placed under the agar matrix (Figure 2c-e), or by printing droplets with reactants as point sources on a flat agar matrix (Figure 2g). When the PDMS mold consists of a grid of reservoirs, the formed structures consist of several connected segments generated in the regions where the reactants, after diffusing from their reservoir, meet and react (Figure 2e). A close look at a segment reveals that the center is more opaque than the edges as a consequence of the neighboring reservoirs being physically further apart diagonally than side-by-side. This separation, in turn, causes the diffusional fronts of **H** and **A** to overlap with time delay at the edges. To demonstrate that the choice of reactants is important for the final appearance of produced patterns, we prepared a pattern using structurally similar 3,4-dihydroxybenzaldehyde (**A***) simultaneously with **A** (Figure 2f). It can be seen that the **HA₃*** pattern is thicker and looks precipitate-like compared to the **HA₃** pattern. By precise positioning of reactant reservoirs with the aforementioned methods, we were able to generate a range of shapes, including squares, circles, grids, triangles, and even letters (Figure 2g).

Mechanical properties and morphology of hybrid gel network. We then aimed at making free-standing objects using RD-SA. Making free-standing objects requires removal of the diffusional matrix after completion of the RD-SA process. Also, the objects have to be sufficiently mechanically strong to carry their own weight. To facilitate straightforward removal of the matrix, we used calcium alginate instead of agar as a diffusional matrix. Alginate gels can be dissolved and subsequently removed by the addition of ethylenediaminetetraacetic acid (EDTA) solution, removing the crosslinking divalent ions between the alginate chains. We confirmed that changing the matrix from agar to alginate does not significantly influence the resulting RD-SA pattern (Supplementary Fig. 11).

We investigated the mechanical properties of the RD-SA structures in alginate gels. Alginate/**HA₃** hybrid gels with varying compositions were subjected to compression tests (see Supplementary Fig. 3 and Supplementary Methods for details of preparation). We find that the formation of a supramolecular network inside an alginate gel leads to a hybrid material displaying a hugely increased yield stress when compared to pure gels formed from either alginate or **HA₃** (Figure 3a-b). For instance, a material consisting of 1.5% alginate gel and a hydrazone network made from 40 mM **H** (denoting the initial concentration of **H** in alginate, with **A** in excess) has a yield stress of 62 kPa, compared to only 7 kPa for the pure 1.5 % alginate gel, and 0.7 kPa for a pure 30 mM **HA₃** gel (see Supplementary Methods for detailed explanation).

To explain why the mechanical properties of alginate/**HA₃** improved compared to the separate gel networks, we investigated the microstructure of the formed gel patterns with confocal fluorescence microscopy. To distinguish between the self-assembled hydrazone structure and the alginate matrix, we labeled **HA₃** with a pyrene

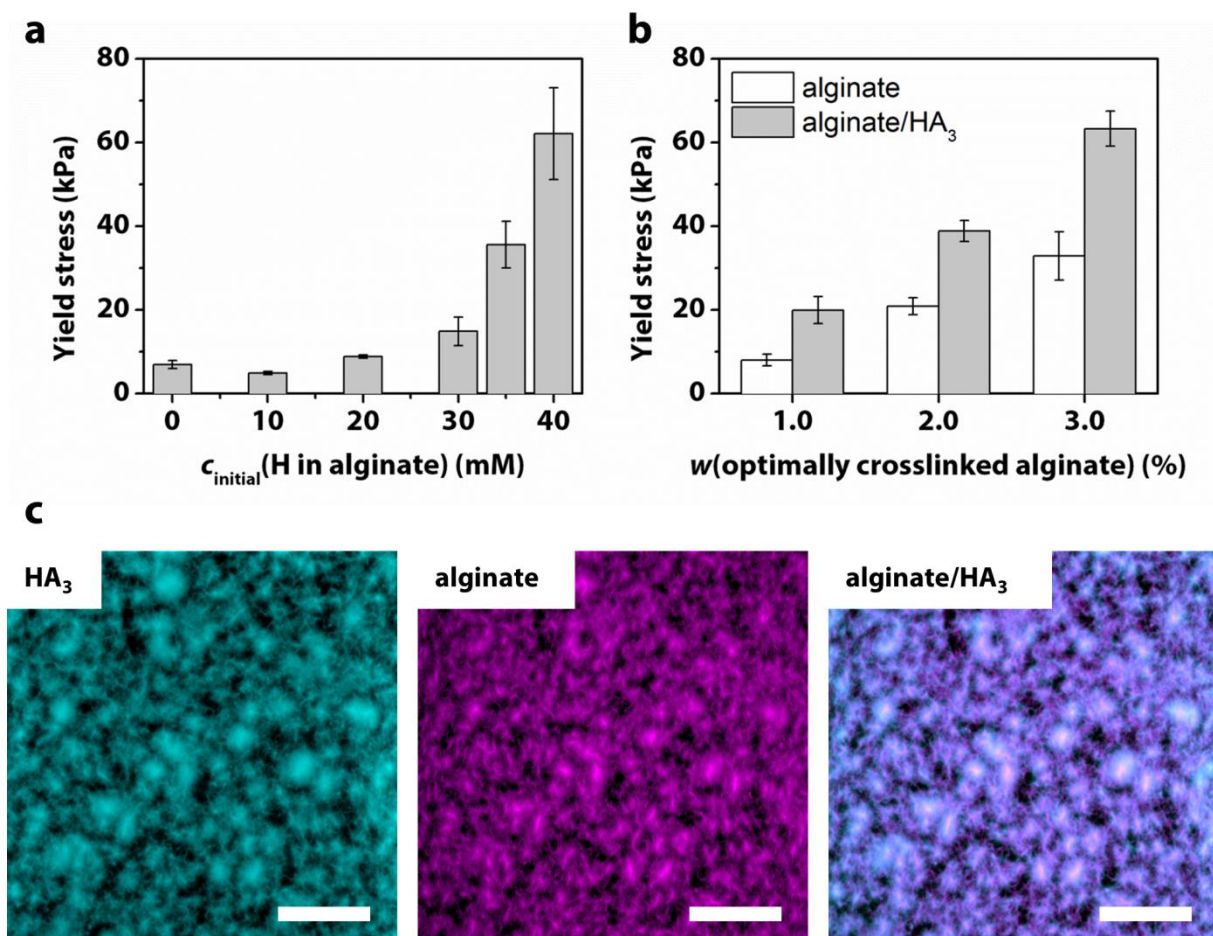


Figure 3. Mechanical properties and structure of the formed hybrid network gels. (a) The effect of the initial concentration of hydrazide **H** in alginate on the compressive strength of the alginate/HA₃ hybrid network material. Compression rate was 50 mN min⁻¹. (b) The effect of the concentration of the optimally cross-linked alginate on the compressive strength of alginate and alginate/HA₃ hybrid network material. Compression rate was 250 mN min⁻¹. (c) Confocal fluorescence micrographs of HA₃, alginate, and overlay images of alginate/HA₃. HA₃ is labeled with a pyrene-functionalized benzaldehyde (**AP**, $\lambda_{\text{ex}} = 405$ nm) and alginate is labeled with BODIPY TR ($\lambda_{\text{ex}} = 543$ nm). The error bars in **a** and **b** were calculated as a standard deviation of at least three measurements. Scale bars: 50 μm .

fluorophore **AP** (see Supplementary Fig. 1 and Supplementary Methods), and alginate with a BODIPY TR fluorophore (Supplementary Methods). As can be seen in Figure 3c, the fibers of HA₃ are co-localized with the alginate chains, which suggests that HA₃ and alginate form a hybrid network material. It is known that networks consisting of two different gels often exhibit vastly improved mechanical properties.²⁹ We did not investigate how the interactions or synergy between HA₃ and alginate lead to improved mechanical properties, but we hypothesize that HA₃ fibers wrap around the alginate chains and create cross-links between the alginate chains in addition to already existing calcium cross-links, most likely in a similar fashion as recently has been reported by Kiriya *et al.*³⁰ This additional crosslinking, in turn, would improve the mechanical properties of alginate/HA₃ hybrid network material.

Fabrication of free-standing objects. The excellent mechanical strength of the alginate/HA₃ hybrid network material encouraged us to further investigate the possibilities of making free-standing objects. We used a similar approach as in the experiments with agar, now including an additional step for removing the alginate matrix (Figure 4a). Following the proposed scheme, we successfully made free-standing objects with distinct shapes (Figure 4b), where the width of the lines constructing the object is in the millimeter range and the size of the full object is in the centimeter range. We subsequently looked at downscaling the RD-SA process to extend RD-SA to applications at sub-millimeter length scales. Creating diffusion patterns through the manual cutting approach did not allow us to achieve the required resolution. Therefore, we turned to wet stamping (WETS) as an alternative approach.^{7,31}

In the wet stamping approach, a substrate and a stamp were both made from alginate or agar gel. The substrate contained **A** and the stamp contained **H**. Upon bringing the stamp and the substrate into contact, **H** from the stamp diffuses into the substrate and **A** from the substrate diffuses into the stamp. After 60 minutes of stamp-substrate contact, the stamp was removed and the substrate was left standing overnight to allow RD-SA to take place. We observed formation of HA₃ patterns in the substrate. The patterns were examined using a confocal microscope before and after dissolution of the alginate substrate (Figure 4d). Objects as small as 300 μm (measured as the width of a single line) were successfully prepared (Figure 4c). When we tried to use the stamp with a 200 μm feature size with 200 μm spacing, objects could not be successfully separated from each other upon dissolution of the alginate substrate.

Functionalization of patterns and free-standing objects. With all the tools established, we set out to explore the potential of RD-SA to control chemical differentiation and functionalization of the formed structures. Exploratory experiments were performed in agar diffusion matrices. We showed previously that the hydrazide-aldehyde reactive gelator system is very tolerant towards the use of different aldehydes.³² Combined with RD-SA, this feature can be exploited to create patterned supramolecular gels with spatially differentiated zones of chemical functionalities, by placing different aldehydes at different locations before diffusion. Indeed, by using different fluorescent aldehydes at different diffusion locations with this approach, we were able to fabricate 2D gel patterns with stable spatially-varying differences in fluorescence and color that were visible by confocal fluorescence microscopy and even by eye (Figure 5a,b).

Next, we investigated the possible formation of permanent chemical gradients within the formed supramolecular patterns. Such chemical gradients can, for instance, be useful to control cell differentiation in space.³³ We mixed **H** in agar. **A** was mixed with an aldehyde-functionalized fluorescent probe in buffer and allowed to diffuse in from one side of the agar matrix. After two weeks we analyzed the material within the agar

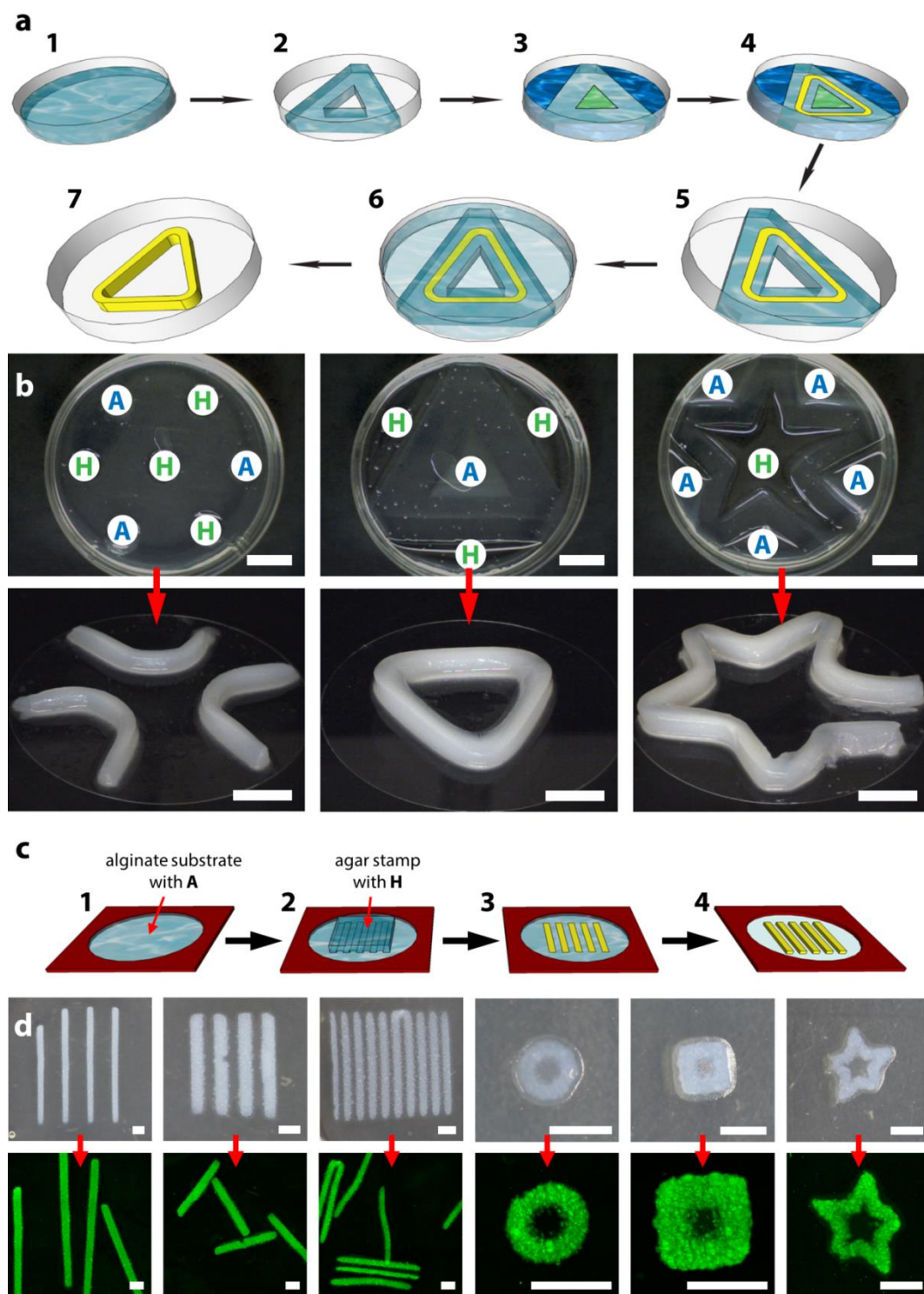


Figure 4. Free-standing hydrogel objects. (a) General method of preparing free-standing objects using the cutting approach. 1) An alginate hydrogel is prepared in a Petri dish. 2) An arbitrary shape is cut out of the alginate. 3) Solutions of hydrazide **H** (green) and aldehyde **A** (blue) are placed into the reservoirs. 4) **H** and **A** diffuse through the alginate matrix and react at the diffusion fronts to form HA_3 , which then self-assembles into a gel structure (yellow). 5) The remaining solutions are removed. 6) A solution of EDTA is poured into the Petri dish until it completely covers the alginate containing the formed pattern. 7) After all alginate is dissolved (as observed by visual inspection), the remaining solution is removed and the free-standing hydrogel object is obtained. (b) Free-standing hydrogel objects prepared using the cutting

approach. (c) A wet stamping approach for the preparation of micro-sized free-standing objects: 1) A 1 mm thick layer of alginate is prepared on a glass slide and loaded with **A**. 2) A stamp containing **H** and rhodamine B-benzaldehyde (**AR**) is placed on the substrate for 60 minutes and is then removed. 3) After standing overnight, the pattern of **HA**₃ appears. 4) Dissolving the remaining substrate produces the free-standing objects. (d) Photographs and confocal images of the patterns of **HA**₃ and free-standing objects. The dimensions of the stamps for lines (from left to right): 500 μm feature/1500 μm spacing, 500 μm feature/500 μm spacing, and 300 μm feature/300 μm spacing. Scale bars: 1 cm in **b**; 1 mm in **d**.

matrix using confocal microscopy, showing an 8 mm wide permanent fluorescence gradient within the formed fiber network (Figure 5c-d). The experimental time was significantly longer than in the formation of 1D patterns, because here the diffusion of **A** was hindered by immediate formation of **HA**₃ at the gel/solution interface (see Supplementary Fig. 3 for the experimental details). This gradient in fiber network density was quantified by measuring the fluorescence intensity over the full distance. Surprisingly, the gradient was not completely gradual, but showed the formation of a band as the normalized fluorescence had a local minimum at ~ 1 mm distance from the source of **A**, after which it gradually decreases towards the end. This phenomenon was observed in repeated experiments and shows up in both local fiber density as well as in the summed fluorescence intensity, and may have an origin similar to the Liesegang patterns observed in precipitation systems.^{7,34} Although in principle this phenomenon could have occurred in all of our other experiments, we observed it only in the experiments when pH was around 7.0 (Supplementary Fig. 12).

To further capitalize on the potential of chemical differentiation of organic materials made by RD-SA, we attempted to functionalize these structures with molecular recognition sites for proteins. Here, the modular nature of the self-assembling system employed in this work plays a pivotal role.³² We used the extensively described non-covalent binding of the lectin Concanavalin A (**ConA**) to mannose as a protein-ligand interaction³⁵. Using the mannose-functionalized benzaldehyde **AM**, we loaded the reservoirs of a Plexiglass holder with **A** and **A+AM**, and allowed diffusion and reaction with **H** using the RD-SA approach shown in Supplementary Fig. 2. This resulted in the formation of millimeter-scale supramolecular shapes within the agar matrix. To test **ConA** binding, we loaded the holder such that one of the two formed shapes was labelled with mannose. Next, fluorescein-labelled **ConA** was allowed to diffuse into the matrix, to bind to the mannose groups on the fibers. The entire matrix was subsequently soaked in buffer solution for several days to remove unbound or nonspecifically bound protein. Fluorescence microscopy shows that, after soaking, the amount of **ConA** decreases more on the fiber structures without mannose functional groups, when compared to those that do contain mannose (Figure 5e-f). The relative stability of **ConA** on the mannose-functionalized supramolecular structures shows the potential of RD-SA to chemically differentiate supramolecular structures with biological functionalities in space.

Finally, we combined several demonstrated principles to make a free-standing object with a permanent chemical gradient. To achieve that, we positioned solutions of **H**, **A** and **A+AR** (rhodamine B-functionalized benzaldehyde) into reservoirs in an

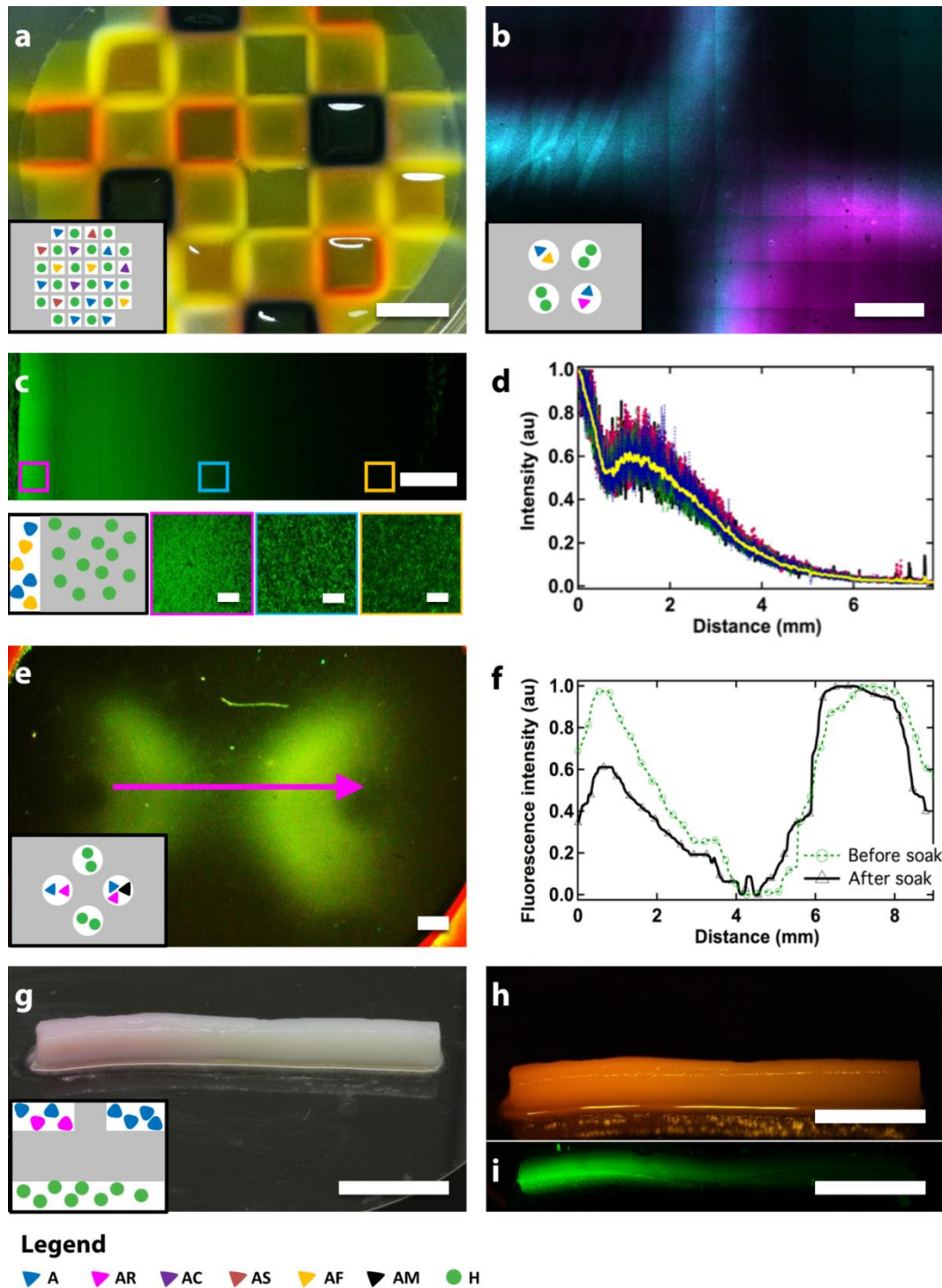


Figure 5. Functional and gradient patterns and objects obtained by RD-SA. (a) A large grid made with several benzaldehyde-functionalized dyes, (yellow, orange, and purple), added for chemical differentiation within a single structure (Supplementary Methods). (b) Chemically differentiated gel objects, with two aldehyde-functionalized dyes (**AF** with $\lambda_{\text{ex}} = 488$ nm and **AR** with $\lambda_{\text{ex}} = 543$ nm) incorporated into the gel fibers, as imaged by confocal fluorescence microscopy. The image is composed of 10×8 individual micrographs, leading to visible edges (Supplementary Methods). (c) A permanent chemical gradient formed by letting **A** diffuse from the left into an agar gel containing **H**, imaged by fluorescence imaging (Supplementary Methods). The confocal micrographs below show magnifications of the gradient, highlighting the change in fiber density. (d) Fluorescence intensity measured from left to right in c. The

yellow line is the average of multiple lines in the same image. (e) Fluorescence image of **ConA** bound to a gel pattern made by RD-SA, in which mannose groups are incorporated in the structure on the right. The image was recorded after partially removing unbound **ConA** by soaking the structure in buffer (Supplementary Methods). (f) Fluorescence intensity measured in e, along the magenta arrow. The green dashed data is before soaking in buffer, black is after soaking in buffer. (g) Photograph of a free-standing bar of alginate/**HA**₃ with incorporated gradient of fluorescence (**AR** was used as a fluorophore). (h) Photograph of the object in g illuminated with a LED (540 nm). The photo was taken through a filter (cutoff wavelength was 580 nm). (i) A confocal micrograph of the object in g. Scale bars: 1 cm in a, g, h and i; 1 mm in b, c (top), and e; 50 μm in c (bottom). Schematic insets in a, b, c, e and g show the scheme of the formation of corresponding patterns. The grey areas denote the gel matrix and the white areas denote the reservoirs. **H** is hydrazide; **A** is aldehyde; **AC** is benzaldehyde labeled with cyanine; **AF** is benzaldehyde labeled with fluorescein; **AP** is benzaldehyde labeled with sulfonated pyrene; **AR** is benzaldehyde labeled with rhodamine B; **AS** is benzaldehyde labeled with styryl; **AM** is benzaldehyde labeled with mannose.

alginate matrix. After 24 hours, we dissolved the alginate and the formed object was left standing in a large amount of water overnight to remove unreacted compounds, after which it was imaged. As can be seen in Figure 5g, the red color intensity gradually decreases along the object from left to right, showing a gradient of functionalization along the object. The same gradient was also visualized using fluorescence (Figure 5h-i).

Quantitative analysis of 1D pattern formation. To better understand pattern formation through RD-SA, we developed a simple reaction-diffusion model describing the formation of the line structure in the basic experiment shown in Figure 2a. The required reaction rate constants were determined using a kinetic model in which we considered the **HA**₃ formation reaction as a 3-step forward reaction (Supplementary Fig. 7, Supplementary Fig. 8, Supplementary Table 2 and Supplementary Methods), followed by a gelation step. Diffusion of species was described using Fick's first law, where we set the diffusion coefficient of **HA**₃ close to zero to incorporate the gelation step. We solved the reaction-diffusion model (Supplementary Methods) for a range of diffusion coefficients for the other species and obtained their value (see Supplementary Table 3) by finding the best fit between simulated and experimentally observed temporal development of the width of the 1D pattern at pH = 4.0 (see Supplementary Fig. 6 for details about the determination of width). We note that it is important to hereby take into account that the diffusion depends on the local formation of **HA**₃ gel, which was done by considering diffusion coefficients that depend on the local concentration of **HA**₃ (Supplementary Fig. 9 and Supplementary Methods). Figure 6a shows the resulting spatial and temporal variation of the concentrations of **H** (green), **A** (blue), and **HA**₃ (yellow) along the gel. It can be seen that the temporal concentration profile of **HA**₃ from the model resembles the measured temporal intensity profile of line formation as shown in Figure 6b. Since change in intensity is related to the formation of **HA**₃, this result is in good qualitative agreement with the experimental data. Next, we used the model to predict the response of the system to RD parameters that can be easily controlled in an experiment – namely, the diffusion distance, the initial reactant concentrations, and pH (controlling the reaction rates). The model predicts, after reaching a steady value after about 50 hours, a weak dependence of the width of the 1D pattern on the diffusion

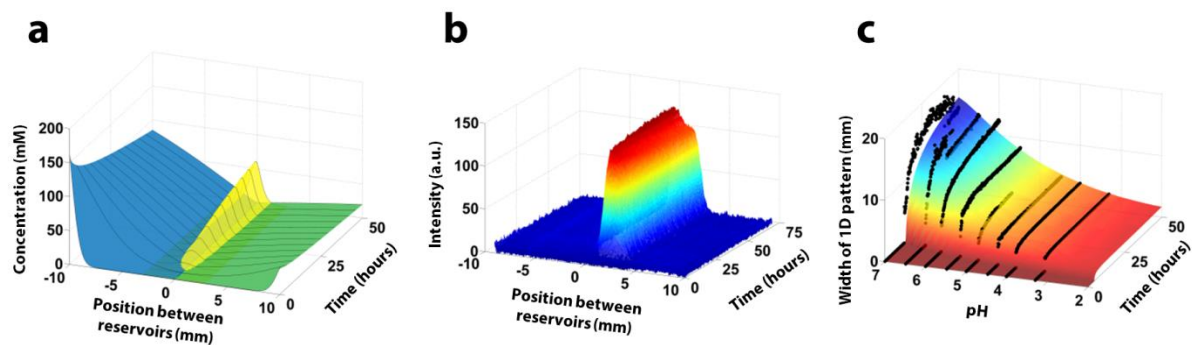


Figure 6. Predicting control over 1D pattern dimensions using reaction-diffusion modelling. (a) The temporal concentration profiles of hydrazide **H** (green), aldehyde **A** (blue), and gelator **HA₃** (yellow) obtained from the model (pH = 4.0). (b) The temporal intensity profile along the distance between the reservoirs of **H** and **A**, as obtained from experiment (pH = 4.0). The increase in intensity signifies the formation of **HA₃**. (c) Comparison between the RD model (colored surface) and experiment (black dots). The reaction rate in the experiments was controlled by varying the pH between 3.3 (fast reaction) and 7.0 (slow reaction).

distance (Supplementary Fig. 10), while a much stronger dependence was predicted for the pH. According to the model, reducing the pH from 7 to 3.3 causes a five-fold decrease of the line width, which is in excellent quantitative agreement with the experimentally observed line widths within this pH range (Figure 6c). Because the pH mainly influences the reaction rates (see Supplementary Fig. 4, Supplementary Fig. 5, Supplementary Table 1 and Supplementary Methods for details), these results clearly indicate that within the current experimental setup the reaction rates for hydrazone formation limit the minimum attainable width to around 2 mm (see Supplementary Discussion for extended explanation). The fabrication of objects with smaller structural features would require either substantially higher reaction rates and hence different chemistry, and/or a different experimental setup. Here, the WETS approach, although with its own limitations, has been shown to be an excellent tool for further downscaling of the pattern dimensions.

Conclusion

In conclusion, we have demonstrated that self-assembly of a supramolecular gelator can be coupled to reaction-diffusion to fabricate free-standing objects of variable size, shape, and chemical functionality. The objects can vary in size from several hundred micrometers to centimeters, and chemical functionalities such as fluorophores or molecular recognition sites can be easily incorporated in this modular system. Through reaction-diffusion, there is control over the location and density profile of chemical functionality in these gel objects. Taking into account the versatility of self-assembling systems, and the vast number of organic reactions, this approach could be easily extended to any organic system for production of functional materials with defined shapes, sizes, and functionalities.

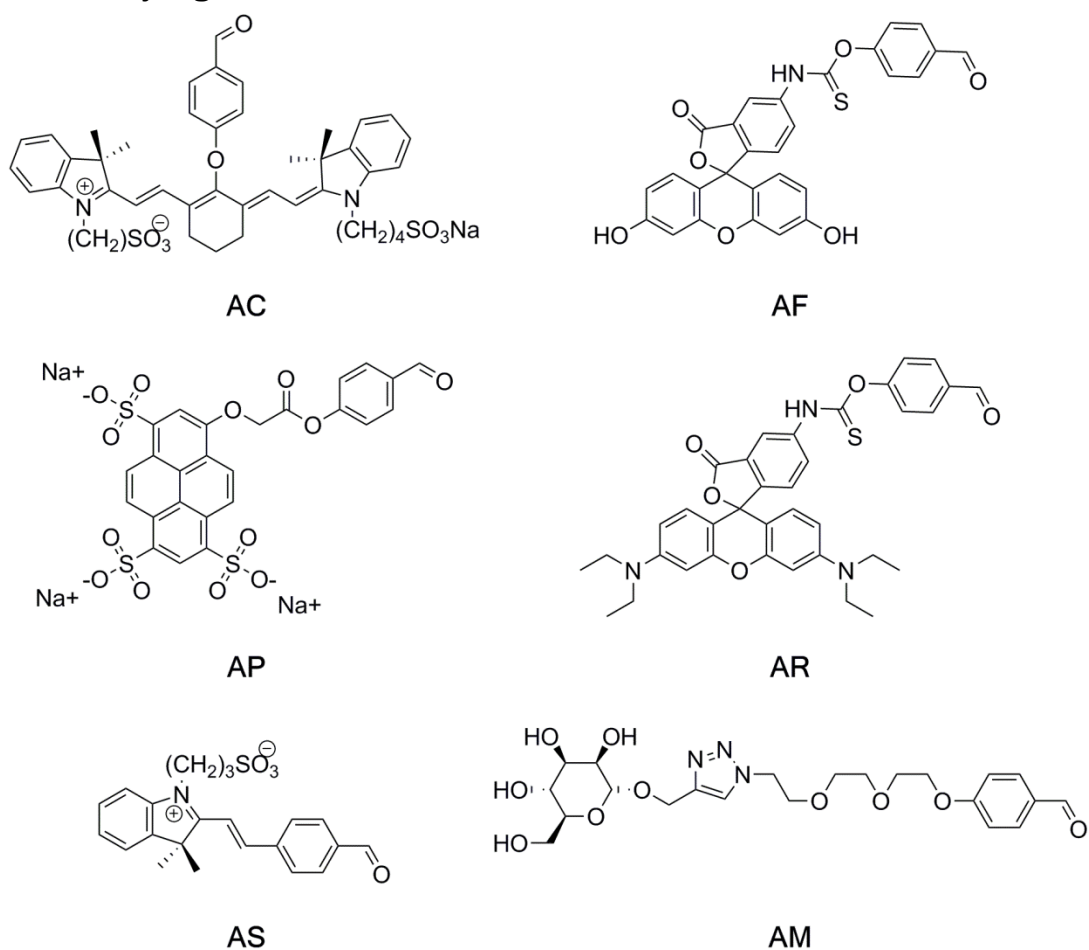
References

- 1 Whitesides, G. M. & Grzybowski, B. Self-assembly at all scales. *Science* **295**, 2418-2421 (2002).
- 2 Bishop, K. J. M., Wilmer, C. E., Soh, S. & Grzybowski, B. A. Nanoscale forces and their uses in self-assembly. *Small* **5**, 1600-1630 (2009).
- 3 Kondo, S. & Miura, T. Reaction-diffusion model as a framework for understanding biological pattern formation. *Science* **329**, 1616-1620 (2010).
- 4 Soh, S., Byrska, M., Kandere-Grzybowska, K. & Grzybowski, B. A. Reaction-diffusion systems in intracellular molecular transport and control. *Angew. Chem. Int. Ed.* **49**, 4170-4198 (2010).
- 5 Mikhailov, A. S. & Hess, B. Self-organization in living cells: networks of protein machines and nonequilibrium soft matter. *J. Biol. Phys.* **28**, 655-672 (2002).
- 6 Epstein, I. R. & Xu, B. Reaction-diffusion processes at the nano- and microscales. *Nat. Nanotech.* **11**, 312-319 (2016).
- 7 Grzybowski, B. A. *Chemistry in Motion: Reaction-Diffusion Systems for Micro- and Nanotechnology*. (Wiley, 2009).
- 8 Ramadan, Y. *et al.* Obtaining new composite biomaterials by means of mineralization of methacrylate hydrogels using the reaction-diffusion method. *Mater. Sci. Eng. C-Mater. Biol. Appl.* **42**, 696-704 (2014).
- 9 Campbell, C. J., Klajn, R., Fialkowski, M. & Grzybowski, B. A. One-step multilevel microfabrication by reaction-diffusion. *Langmuir* **21**, 418-423 (2005).
- 10 Smoukov, S. K., Bishop, K. J. M., Klajn, R., Campbell, C. J. & Grzybowski, B. A. Cutting into solids with micropatterned gels. *Adv. Mater.* **17**, 1361-1365 (2005).
- 11 Smoukov, S. K. & Grzybowski, B. A. Maskless microetching of transparent conductive oxides (ITO and ZnO) and semiconductors (GaAs) based on reaction-diffusion. *Chem. Mater.* **18**, 4722-4723 (2006).
- 12 Grzybowski, B. A. & Campbell, C. J. Fabrication using 'programmed' reactions. *Mater. Today* **10**, 38-46 (2007).
- 13 Grzybowski, B. A. & Bishop, K. J. Micro- and nanoprinting into solids using reaction-diffusion etching and hydrogel stamps. *Small* **5**, 22-27 (2009).
- 14 Campbell, C. J., Smoukov, S. K., Bishop, K. J. M., Baker, E. & Grzybowski, B. A. Direct printing of 3D and curvilinear micrometer-sized architectures into solid substrates with sub-micrometer resolution. *Adv. Mater.* **18**, 2004-2008 (2006).
- 15 Walliser, R. M. *et al.* Growth of nanoparticles and microparticles by controlled reaction-diffusion processes. *Langmuir* **31**, 1828-1834 (2015).
- 16 Al Akhrass, G. A., Ammar, M., El-Rassy, H. & Al-Ghoul, M. Self-assembled lanthanum hydroxide microspheres within a reaction-diffusion framework: synthesis, characterization, control and application. *RSC Adv.* **6**, 3433-3439 (2016).
- 17 Kleiman, M., Brubaker, K. S., Nguyen, D. T. & Esser-Kahn, A. P. Bio-inspired morphogenesis using microvascular networks and reaction-diffusion. *Chem. Mater.* **27**, 4871-4876 (2015).
- 18 Noorduyn, W. L., Grinthal, A., Mahadevan, L. & Aizenberg, J. Rationally designed complex, hierarchical microarchitectures. *Science* **340**, 832-837 (2013).
- 19 Chirieleison, S. M., Allen, P. B., Simpson, Z. B., Ellington, A. D. & Chen, X. Pattern transformation with DNA circuits. *Nat. Chem.* **5**, 1000-1005 (2013).
- 20 Zadorin, A. S., Rondelez, Y., Galas, J. C. & Estevez-Torres, A. Synthesis of programmable reaction-diffusion fronts using DNA catalyzers. *Phys. Rev. Lett.* **114**, 068301 (2015).
- 21 Allen, P. B., Chen, X. & Ellington, A. D. Spatial control of DNA reaction networks by DNA sequence. *Molecules* **17**, 13390-13402 (2012).
- 22 Semenov, S. N. *et al.* Ultrasensitivity by molecular titration in spatially propagating enzymatic reactions. *Biophys. J.* **105**, 1057-1066 (2013).

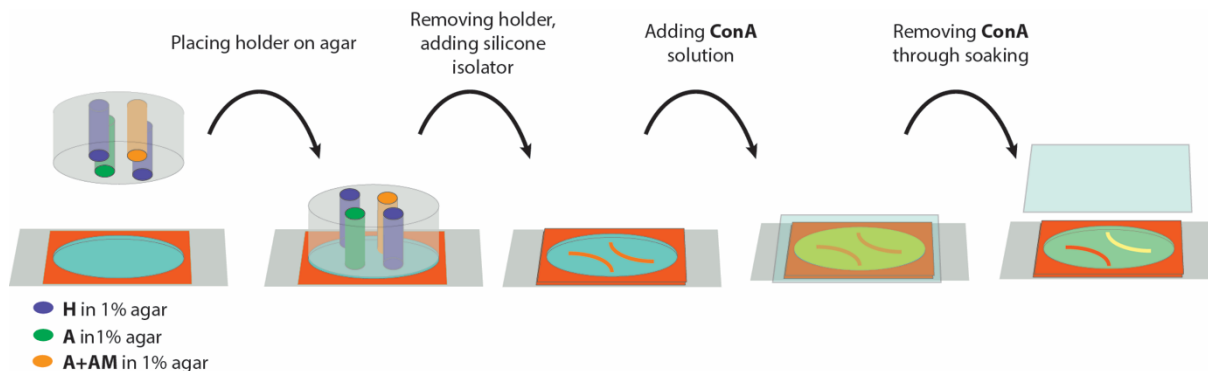
- 23 Semenov, S. N., Markvoort, A. J., de Greef, T. F. & Huck, W. T. Threshold sensing through a synthetic enzymatic reaction-diffusion network. *Angew. Chem. Int. Ed.* **53**, 8066-8069 (2014).
- 24 Ziemecka, I., Koper, G. J. M., Olive, A. G. L. & van Esch, J. H. Chemical-gradient directed self-assembly of hydrogel fibers. *Soft Matter* **9**, 1556-1561 (2013).
- 25 Shim, T. S., Yang, S. M. & Kim, S. H. Dynamic designing of microstructures by chemical gradient-mediated growth. *Nat. Commun.* **6**, 6584 (2015).
- 26 Trausel, F. *et al.* Catalysis of supramolecular hydrogelation. *Acc. Chem. Res.* **49**, 1440-1447 (2016).
- 27 Boekhoven, J. *et al.* Catalytic control over supramolecular gel formation. *Nat. Chem.* **5**, 433-437 (2013).
- 28 Poolman, J. M. *et al.* Variable gelation time and stiffness of low-molecular-weight hydrogels through catalytic control over self-assembly. *Nat. Protoc.* **9**, 977-988 (2014).
- 29 Gong, J. P., Katsuyama, Y., Kurokawa, T. & Osada, Y. Double-network hydrogels with extremely high mechanical strength. *Adv. Mater.* **15**, 1155-1158 (2003).
- 30 Kiriya, D. *et al.* Meter-long and robust supramolecular strands encapsulated in hydrogel jackets. *Angew. Chem. Int. Ed.* **51**, 1553-1557 (2012).
- 31 Klajn, R. *et al.* Multicolour micropatterning of thin films of dry gels. *Nat. Mater.* **3**, 729-735 (2004).
- 32 Poolman, J. M. *et al.* A toolbox for controlling the properties and functionalisation of hydrazone-based supramolecular hydrogels. *J. Mat. Chem. B* **4**, 852-858 (2016).
- 33 Ashe, H. L. & Briscoe, J. The interpretation of morphogen gradients. *Development* **133**, 385-394 (2006).
- 34 Liesegang, R. E. Ueber einige Eigenschaften von Gallerten. *Naturwiss. Wochenschr.* **11**, 353 (1896).
- 35 Tagawa, K. *et al.* Recognition of novel amphiphiles with many pendent mannose residues by Con A. *Bioconjugate Chem.* **10**, 354-360 (1999).
- 36 Draget, K. I., Ostgaard, K. & Smidsrod, O. Alginate-based solid media for plant-tissue culture. *Appl. Microbiol. Biotechnol.* **31**, 79-83 (1989).

Supplementary Information

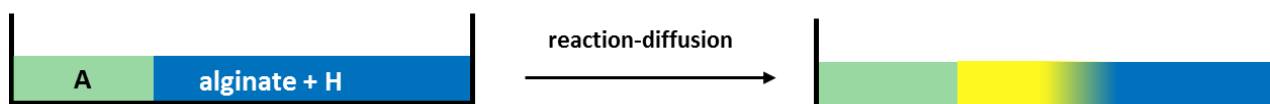
Supplementary Figures



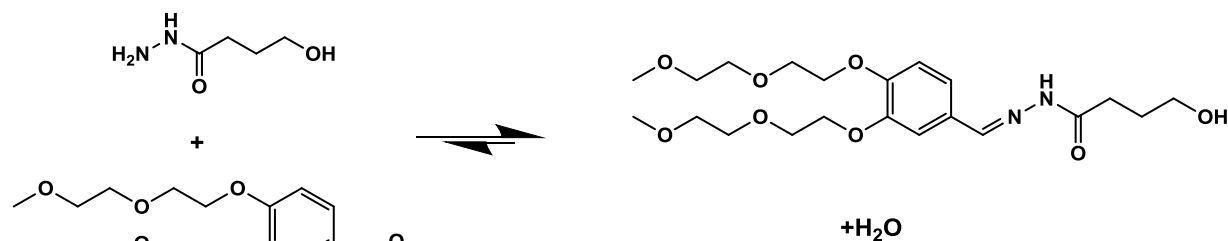
Supplementary Figure 1. Chemical structures of functionalized benzaldehydes. AC is benzaldehyde labeled with cyanine; AF is benzaldehyde labeled with fluorescein; AP is benzaldehyde labeled with sulfonated pyrene; AR is benzaldehyde labeled with rhodamine B; AS is benzaldehyde labeled with styryl; AM is benzaldehyde labeled with mannose.



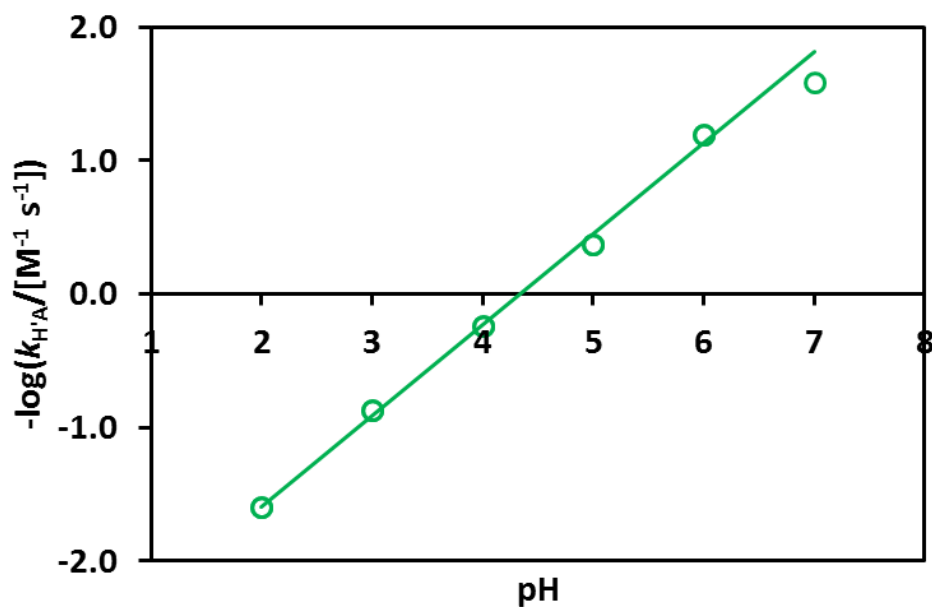
Supplementary Figure 2. Scheme of the process used for the ConA binding setup. A Plexiglass holder was loaded with solutions of hydrazide **H**, aldehyde **A**, and **A + AM** in agar. The holder was placed on top of an agar matrix prepared in a well created by putting a Press-to-Seal™ silicone isolator on top of a glass slide and the holder was left standing for 8 hours. Next, the holder was removed, one Press-to-Seal™ silicone isolator was added on top of the previous one and the resulting well was filled with the solution of **ConA** (2 mM, pH = 7). This well was closed with a glass slide and left standing for 12 hours. Afterwards, the solution of **ConA** was removed and replaced with fresh buffer solution to remove non-bound **ConA**. The solution was exchanged every 24 hours for 72 hours in total.



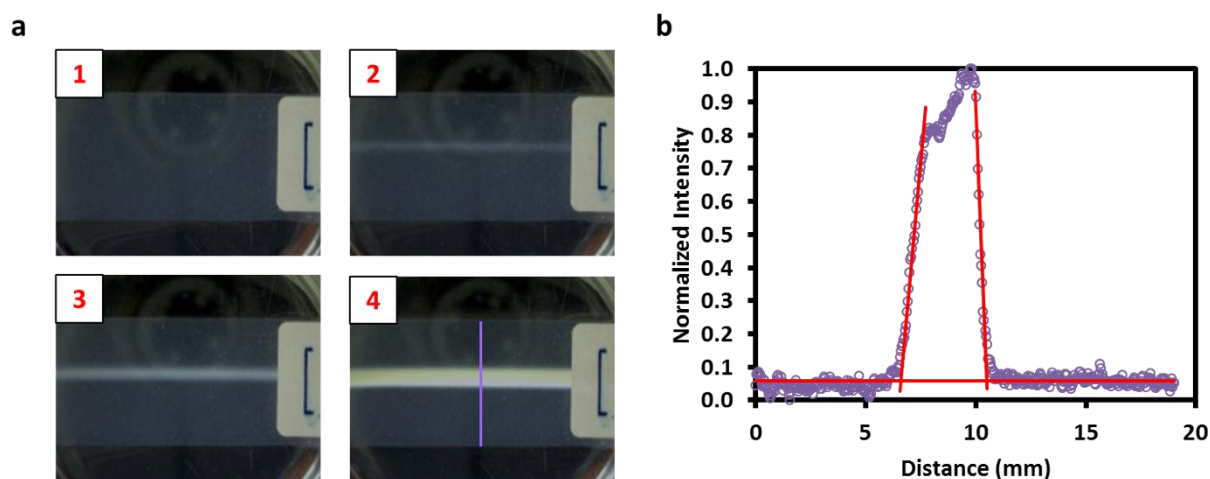
Supplementary Figure 3. The scheme of the formation of hybrid network gels for compression tests. The yellow region represents the alginate/ HA_3 hybrid network.



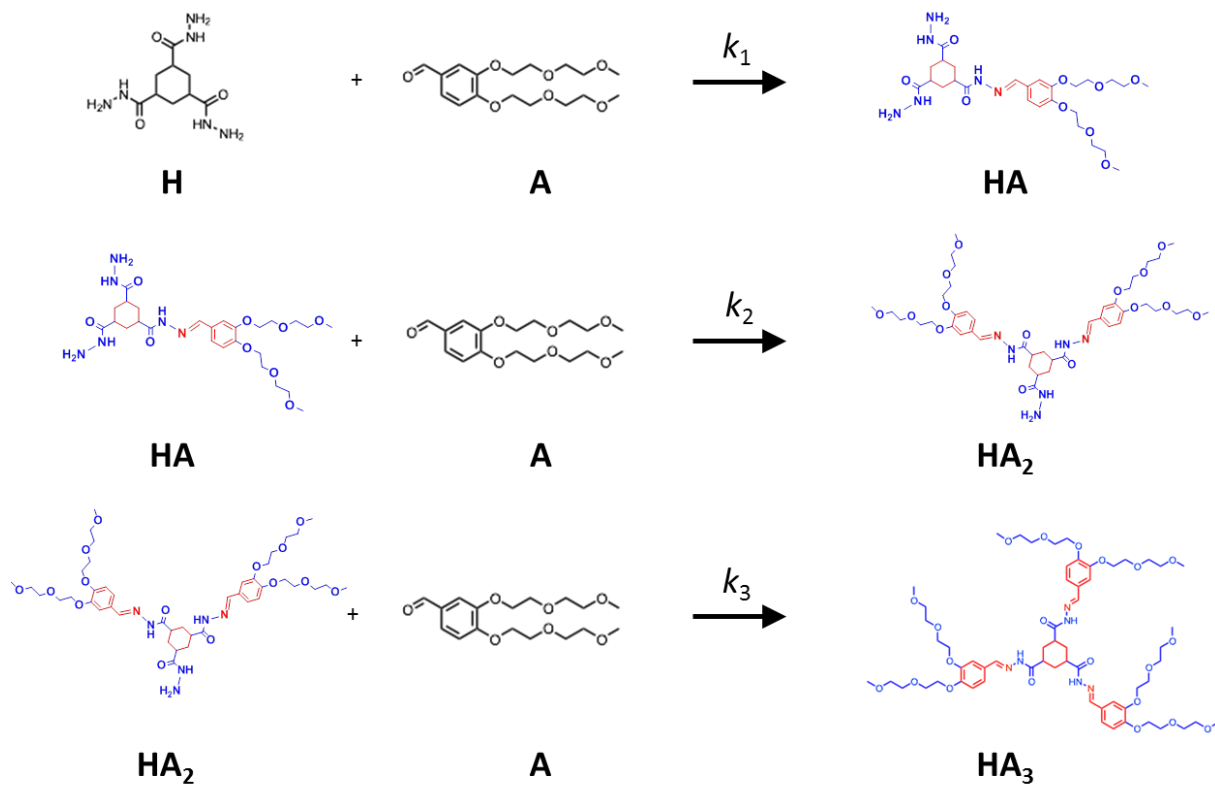
Supplementary Figure 4. One-step reaction for kinetic analysis. A simplified reaction used to determine the pH dependence of reaction rate constant.



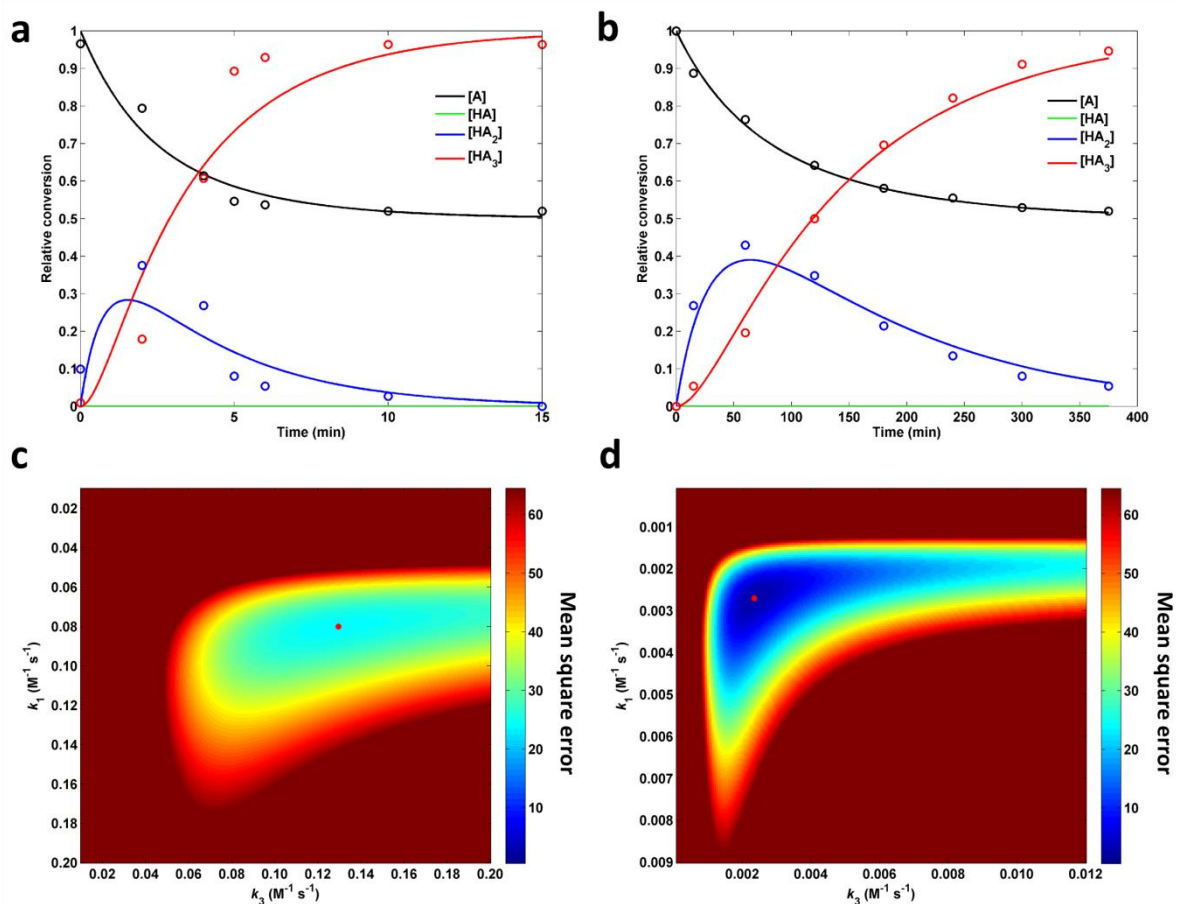
Supplementary Figure 5. Dependence of the rate constant on pH for the one-step reaction.



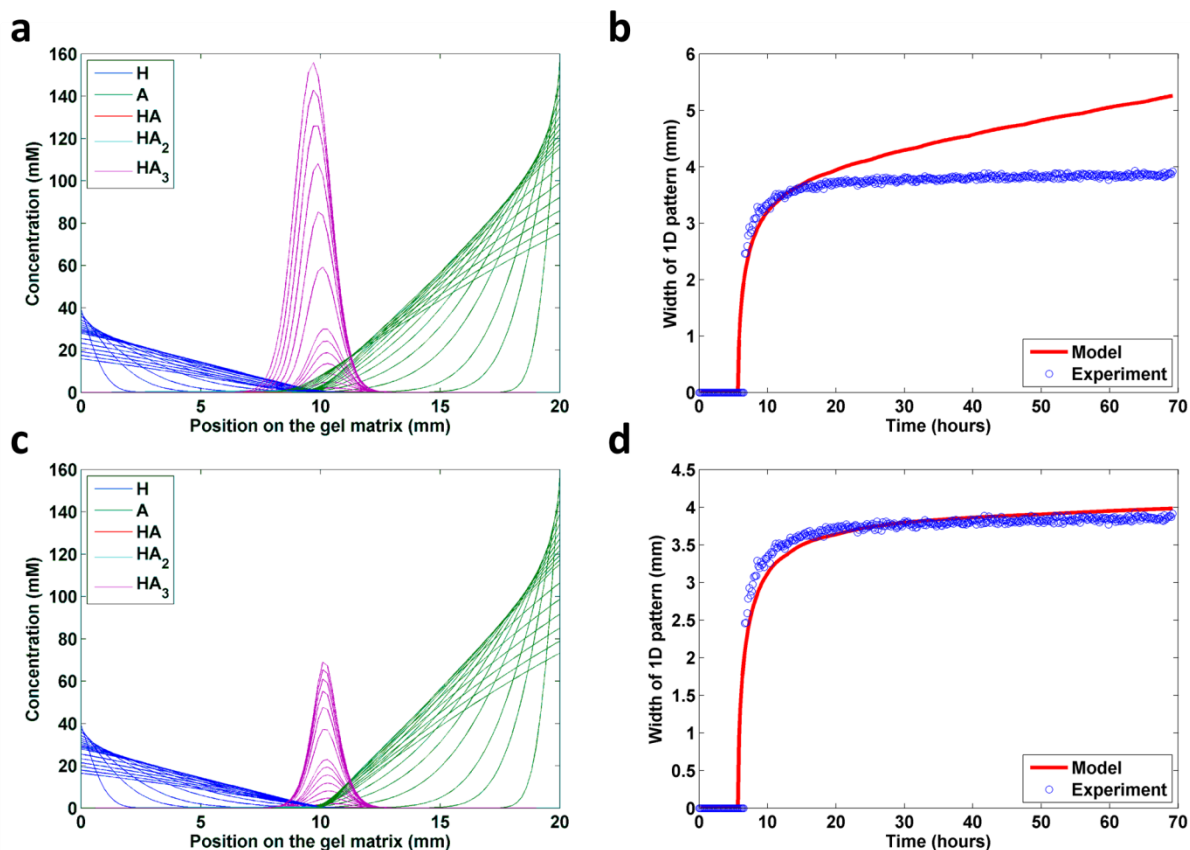
Supplementary Figure 6. Formation of supramolecular hydrogel lines over time at pH = 4.0. a) Photo 1, $t = 0$ min; photo 2, $t = 400$ min; photo 3, $t = 470$ min; photo 4, $t = 2000$ min b) The normalized intensity profile was obtained from the intensity measured along the purple line, shown in photo 4, to determine the temporal development of the width of the 1D pattern as the distance between points where two slopes intersect a base line.



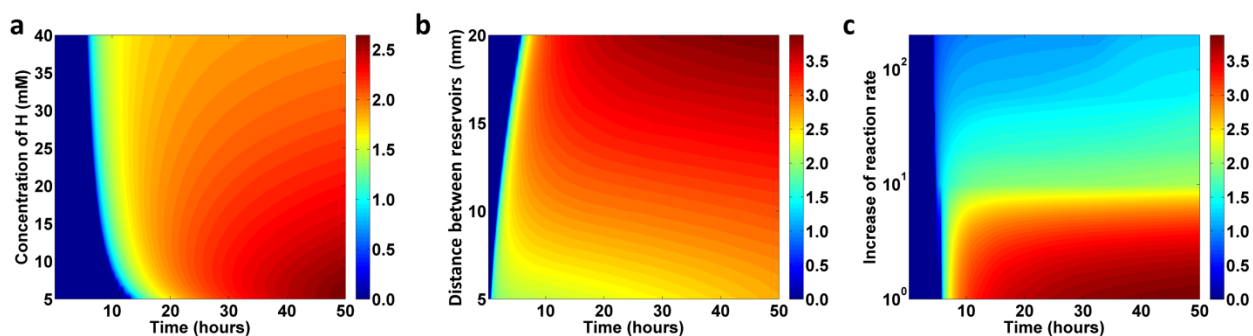
Supplementary Figure 7. Formation of gelator HA₃.



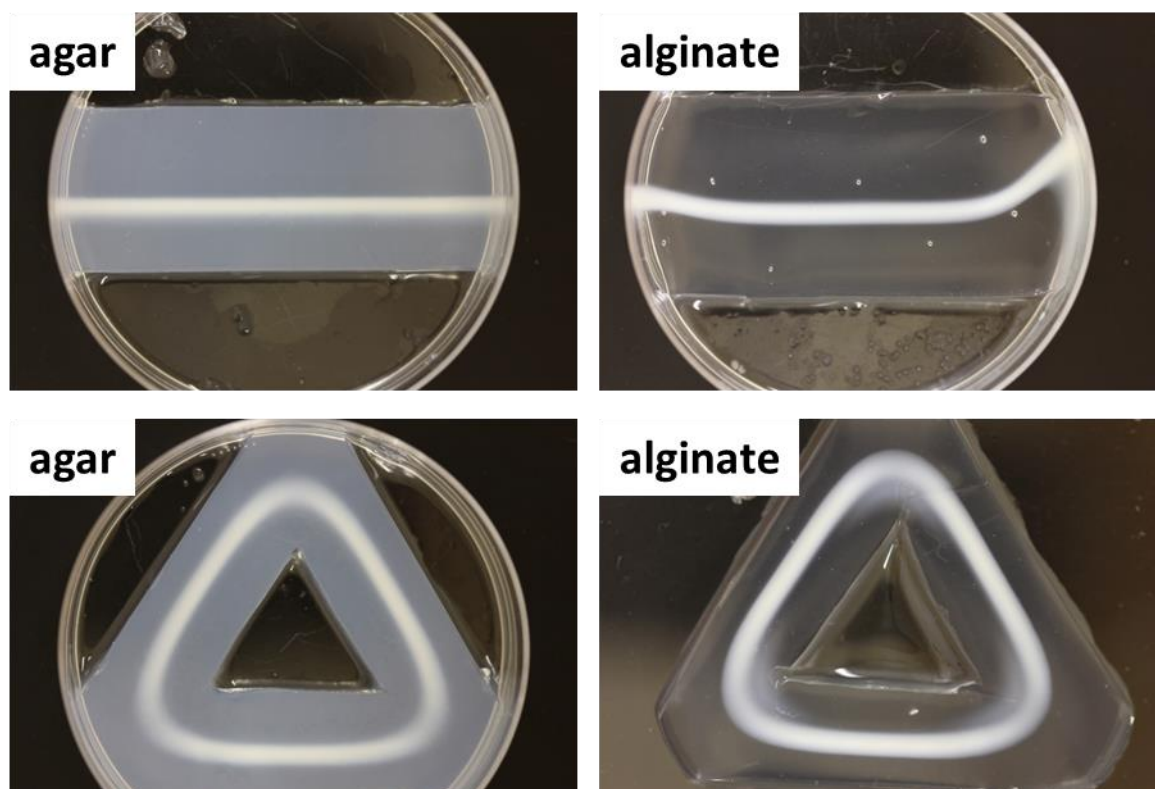
Supplementary Figure 8. The kinetics of gelator formation at pH = 5 (a) and pH = 7 (b). a, b) The experimental data is shown as circles and the lines show the best fit obtained from numerical simulations. The relative conversion for each component was calculated as its concentration normalized by the initial concentration of **H**, except for **A**, which was normalized by its own initial concentration. c, d) Plots show mean square error for different combinations of constants k_1 and k_3 at pH = 5 (c) and pH = 7 (d). The red dot indicates the combination that gave the best fit.



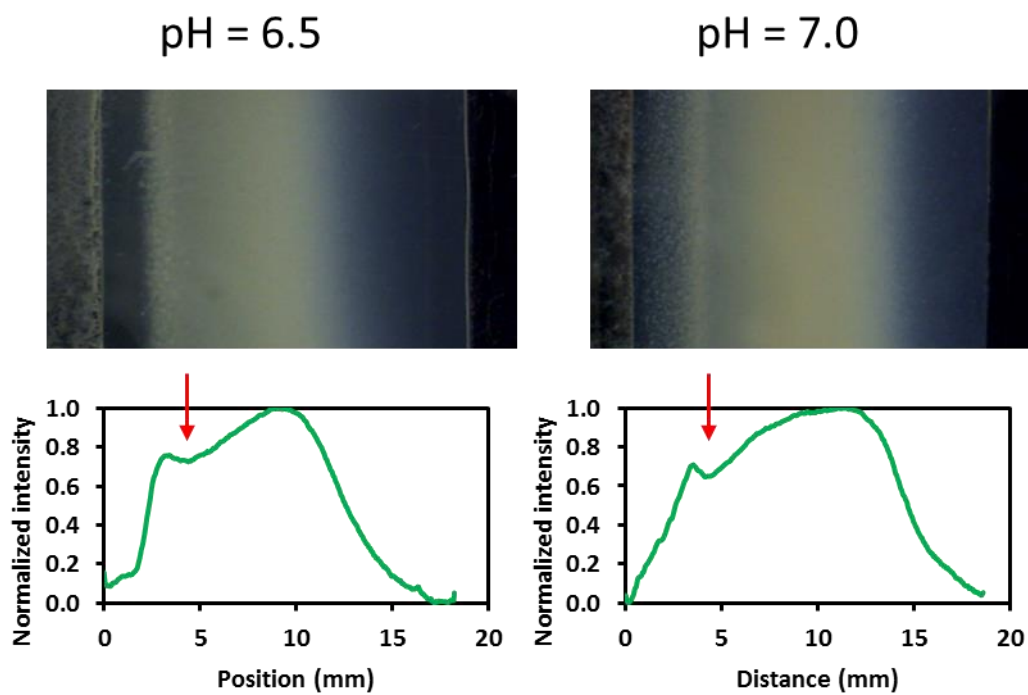
Supplementary Figure 9. Time-dependent structure formation in the RD model at pH = 4.0. **a)** The concentration profiles of all species in space and time for the model without the decrease of diffusion coefficient of all species depending on the concentration of HA_3 . **b)** The width of 1D pattern for the model without the decrease of diffusion coefficient of all species depending on the concentration of HA_3 . **c)** The concentration profiles of all species in space and time for the model with the decrease of diffusion coefficient of all species depending on the concentration of HA_3 . **d)** The width of 1D pattern for the model with the decrease of diffusion coefficient of all species depending on the concentration of HA_3 . Different lines in **a** and **c** represent different time points with the first 10 lines being separated by 1.7 hours and the following lines being separated by 8.3 hours. The width of the 1D pattern from the model was extracted from the concentration profile of HA_3 (as a horizontal distance between two points of the profile at 1 mM).



Supplementary Figure 10. Predictions from the model. a) Effect of initial concentrations of **H** on the width of the 1D pattern. **b)** Effect of distance between reservoirs with **H** and **A** on the width of 1D pattern. **c)** Effect of rate constant on the width of 1D pattern. The increase in reaction rate designates how many times the reaction rate constants k_1 , k_2 , and k_3 are bigger than their values at pH = 4.0. The color bars represent the width of 1D pattern in mm. It should be noted that dark blue areas represent the time points when pattern has not started forming yet, i.e. the HA_3 concentration is below 1 mM.



Supplementary Figure 11. Comparison between agar and alginate. All experiments were conducted using the same basic conditions: 40 mM **H** and 160 mM **A** at pH = 4.5 in a 5 cm Petri dish. The only difference was either the use of agar (1 %, left) or calcium alginate (1 %, right).



Supplementary Figure 12. Band formation at high pHs. All experiments were conducted using the same basic conditions: 40 mM **H** and 160 mM **A** at $d = 2$ cm. Red arrow indicates the band with less **HA**₃.

Supplementary Tables

Supplementary Table 1. Dependence of rate constant on pH for the one-step reaction as determined from UV-VIS measurements.

pH	$k_{H'A}$ [$M^{-1} s^{-1}$]
2.0	40
3.0	7.4
4.0	1.7
5.0	4.3×10^{-1}
6.0	6.4×10^{-2}
7.0	2.6×10^{-2}

Supplementary Table 2. Rate constants of HA₃ formation. The rate constants were obtained from the kinetic model by determining the smallest error between the experimental data and the data from the model. The rate constants of the one-step reaction are given for comparison.

pH	$k_{H'A}$ [$M^{-1} s^{-1}$]	k_1 [$M^{-1} s^{-1}$]	k_3 [$M^{-1} s^{-1}$]
5.0	4.3×10^{-1}	0.8×10^{-1}	1.3×10^{-1}
7.0	2.6×10^{-2}	2.7×10^{-3}	2.4×10^{-3}

Supplementary Table 3. Parameters used in the RD model. The column “Default value” indicates values that were used throughout the model. The column “If changed” indicates other values that were used in certain instances. Only one parameter was changed at a time while keeping other parameters at their default values. Column “Shown” indicates which figures show the result of changing parameters.

Parameter	Default value	If changed	Shown
D_H	$5.40 \times 10^{-6} \text{ cm}^2 \text{ s}^{-1}$		
D_A	$4.50 \times 10^{-6} \text{ cm}^2 \text{ s}^{-1}$		
D_{HA}	$2.76 \times 10^{-6} \text{ cm}^2 \text{ s}^{-1}$		
D_{HA2}	$1.95 \times 10^{-6} \text{ cm}^2 \text{ s}^{-1}$		
D_{HA3}	$10^{-11} \text{ cm}^2 \text{ s}^{-1}$		
pH (determines rate constants)	4	2 – 7	Supplementary Figure 12c
Distance between reservoirs, L	20 mm	5 – 20 mm	Supplementary Figure 12b
c_H	40 mM	5 – 40 mM	Supplementary Figure 12a
c_A	160 mM	$4 \times c_H$	Supplementary Figure 12a

Supplementary Methods

Materials. All reagents were purchased from commercial sources and used as provided, unless stated otherwise. Hydrazide **H**, aldehyde **A**, aldehydes labelled with cyanine (**AC**), fluorescein (**AF**), rhodamine (**AR**), styryl (**AS**), and mannose (**AM**) were synthesized according to reported methods.^{27,32} All experiments were performed using MilliQ water as a solvent, unless mentioned otherwise. All stock solutions of **A**, **H** or labelled aldehydes were prepared in 100 mM phosphate buffer (pH = 4.0). The stability of the pH was checked by measuring the pH before and after the experiment and no significant differences were detected.

Press-to-Seal™ silicone isolators with adhesive, one well, were bought from Life Technologies. They were 20 mm in diameter and 0.5 mm deep.

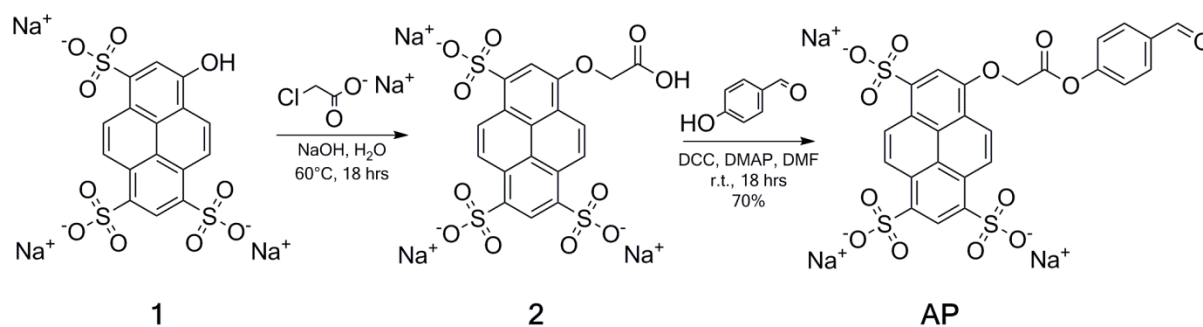
Equipment. UV-VIS spectroscopic measurements were performed on an Analytik Jena Specord 250 spectrophotometer. Confocal Laser Scanning Microscopy (CLSM) micrographs were obtained using a Zeiss LSM 710 confocal laser scanning microscope, equipped with 2.5× and 10× air objectives and a 40× oil immersion objective. The sensitivity of detectors and filters was adjusted in order to obtain maximum signal to noise ratio. Time-lapse movies were recorded with a MicroCapture USB camera connected to a standard desktop computer, with suitable software. Data analysis was performed using MATLAB® 2012b and ImageJ (<http://imagej.nih.gov>). The compression test were performed using a dynamic mechanical analyzer DMA 7e (Perkin Elmer Instruments).

Preparation of agar gels. Phosphate buffer was prepared at the desired pH by dissolving the appropriate amounts of acid-base pair of phosphate salts at a total concentration of 100 mM in water. If necessary, the pH was adjusted with NaOH or H₃PO₄ solutions. A diffusion matrix was made of 1% agar (mass fraction, *w*) by dissolving agar in the appropriate amount of phosphate buffer. The experiments were conducted using this composition of diffusion matrix, unless stated differently. To completely dissolve the agar, the mixture was heated and stirred at ~100 °C until the solution turned transparent. The solution was subsequently allowed to cool down and left to solidify.

Preparation of alginate gels. Alginate gels were prepared according to the procedure proposed by Draget *et al.*³⁶ Briefly, a powder of CaCO₃ was dispersed in water. Then, dry sodium alginate was added and this dispersion was heated at 100 °C in a closed vial until all alginate and CaCO₃ was dissolved. The solution was subsequently allowed to cool to room temperature. Finally, an aqueous solution of glucono- δ -lactone (**GDL**) was added, and the resulting solution was stirred briefly and transferred to a Petri dish. 10 mL of solution per Petri dish was used. The alginate gel was formed by leaving the solution standing overnight. Unless otherwise stated, final concentrations of CaCO₃, alginate, and

GDL were 12.5 mM, 1.5 % (mass fraction, w), and 40 mM, respectively, giving alginate gels with pH = 4.5. To prepare alginate gels labelled with BODIPY TR, 3 % (mass fraction, w) of alginate-BODIPY TR was added with respect to the total mass of alginate.

Synthesis of AP



AP was prepared from **1** by carboxymethylation followed by esterification with 4-hydroxybenzaldehyde. Both steps were adapted from reported methods.^{1,2}

8-Hydroxypyrenetrisulfonate trisodium salt **1** (1 g), sodium hydroxide (92 mg, 1.2 eq.), and sodium chloroacetate (335 mg, 1.2 eq.) were dissolved in demineralized water (25 ml). The resulting mixture was subsequently heated to 60 °C, magnetically stirred for 18 hours, cooled down to room temperature, acidified with hydrochloric acid to pH = 3.0, and dried in vacuum. Dry residue was repeatedly washed with boiling ethanol and dried overnight at 60°C in vacuum to afford 685 mg of **2**. ¹H NMR (400 MHz, D₂O) δ, ppm: 9.13 (s, 1H), 9.07 (d, 1H), 8.93 (q, 2H), 8.68 (d, 1H), 8.26 (s, 1H)

Next, DMAP (120 mg, 1 eq.) and 4-hydroxybenzaldehyde (412 mg, 3 eq.) were added to the solution of **2** (680 mg) in anhydrous DMF (20 ml). DCC (255 mg, 1.1 eq.) was then added and the mixture was stirred overnight at 25°C. DMF was removed in vacuum. Solid residue was repeatedly washed with boiling ethanol to remove impurities, and dried overnight at 60°C in vacuum to afford 600 mg of **AP**. ¹H NMR (400 MHz, D₂O) δ, ppm: 9.31 (s, 1H), 9.10 (s, 1H), 9.02 (d, 1H), 8.83 (q, 2H), 8.63 (d, 1H), 8.16 (s, 1H), 7.34 (d, 2H), 6.53 (d, 2H); ¹³C NMR (100 MHz, D₂O) δ, ppm: 197.12, 196.79, 166.72, 158.81, 142.09, 136.31, 136.19, 135.36, 133.57, 132.61, 129.99, 129.04, 128.95, 127.72, 127.29, 127.06, 125.96, 124.12, 123.68, 121.19, 118.76, 118.65, 53.33; ESI-MS (neg. mode): 257 (hydrolyzed AP+2H⁺); 558 (hydrolyzed AP+2Na⁺). We could not observe the molecular ion either by ESI or MALDI-ToF MS.

Labeling of alginate with BODIPY® TR Cadaverine (5-(((4-(4,4-Difluoro-5-(2-Thienyl)-4-Bora-3a,4a-Diaza-s-Indacene-3-yl)phenoxy)acetyl)amino)pentylamine, Hydrochloride).

Alginate-BODIPY TR conjugate was prepared using the following procedure. 1-Ethyl-3-(3-dimethylaminopropyl)carbodiimide hydrochloride (EDC, 3.67 mg) and *N*-hydroxysuccinimide (NHS, 2.57 mg) were added to a solution of sodium alginate (104.1 mg) in water (10 mL), followed by the addition of a solution of BODIPY® TR Cadaverine

(1.16 mg) in DMSO (100 μ L). The resulting mixture was stirred overnight at 25°C, transferred to a dialysis tube (Spectra/Por®, MWCO = 6500 Da), dialyzed against 5 \times 1 L of demineralized water over 3 days, and freeze-dried. The resulting powder was stored at -20 °C.

RD-SA experiments by cutting reservoirs in agar gels. To prepare the agar gel matrix for reaction-diffusion self-assembly (RD-SA) experiments, 10 mL of agar solution was heated until dissolved. When still warm, this solution was poured in a plastic Petri dish (diameter *ca.* 50 mm, height *ca.* 15 mm) and left to gelate upon cooling. The same type of Petri dishes were used in other experiments, unless stated otherwise. A slab of the agar matrix with desired dimensions was made by manually cutting two parallel lines at equal distance from the center of the Petri dish for the experiment in Figure 2a. The two outer segments of agar were removed, forming two reservoirs for the solutions of **H** and **A**. These reservoirs were completely separated from each other, as the agar gel extends fully to the sides of the Petri dish, ensuring that no mixing of solutions can occur other than by diffusion through the gel matrix. Solutions of **H** (40 mM) and **A** (160 mM) were prepared in the same buffer as used for the agar gel preparation. The two solutions were then pipetted in the two reservoirs and left to diffuse in a closed humidified environment, which prevented evaporation of liquids. The experiment in Figure 2b was performed using a similar approach, except for making reservoirs in the agar with non-straight edges, and for filling the reservoirs with solutions of **A** and **H** in agar instead of in buffer. For the experiment with the two-dimensional grid of reservoirs in Figure 2f, reservoirs with a diameter of 5 mm were cut in the gelled agar and filled with buffer solutions of **A** and **H** in an alternating pattern.

RD-SA by using a PDMS mold. To form RD-SA patterns in a flat agar matrix without reservoirs at the sides, we used a two layer approach. The first layer is a PDMS mold with reservoirs for H and A, and the second layer is a flat agar matrix in which the RD-SA patterns form. The PDMS mold was either made by manually cutting a layer of PDMS cured in a Petri dish in the form of the circular and triangular mold shown in gray in Figure 2c-d, or by curing liquid PDMS in a Petri dish against a Teflon mold containing an array of squares (8 \times 8 \times 3 mm, 2 mm separation between them; Figure 2e). The reservoirs were completely filled with agar solutions containing H (40 mM) and A (160 mM). The PDMS mold with the agar was left to cool down to room temperature, to allow the agar to gelate. Then, a new agar layer was poured on top of the PDMS mold, which serves as the diffusion and reaction layer in which the RD-SA patterns form. After gelation of this layer, the Petri dish was placed in a closed humidified environment. After 24 – 78 hours it was taken out and the PDMS mold was gently removed from the agar layer by pushing a glass slide between the PDMS mold and the agar layer, which contained the formed RD-SA patterns.

RD-SA by drop deposition (Figure 2g). To form letters by RD-SA, we used the following procedure. A plastic Petri dish (8.5 cm in diameter) was filled with an agar solution and left to gelate. This layer acts as the diffusion and reaction medium. After cooling, solutions containing **H** (40 mM) and **A** (160 mM) in agar were deposited as droplets on top of the agar layer. The droplets (50 μ L) were pipetted at opposite sides of the outline of the letters, along their contour (see the cartoon in Figure 5g), forming the “ASM” abbreviation. Careful deposition prevented direct contact between droplets, which gelate in less than a minute. The sample was left standing for ~5 hours in a closed humidified environment to allow the diffusion of **H** and **A**.

Chemically differentiated grid (Figure 5a). To make the chemically differentiated grid, we followed the procedure described in section 3.2, except for filling some of the reservoirs with solutions of **A** containing different benzaldehyde-functionalized dyes (**AC**, **AF** or **AS**), according to the configuration shown in Supplementary Figure 3a. The concentration of **A** was 160 mM if only **A** was used and 144 mM if mixed with the dye. The concentration of dye was 10 mM.

Chemical differentiation by fluorescent labeling of RD-SA patterns (Figure 5b). In this experiment, we used a cylindrical Plexiglass holder to deliver compounds into the gel matrix. The holder was 2.5 cm in diameter and 2 cm in height with four through holes symmetrically staggered around the center. The holes were 2 mm in diameter and their centers 5 mm apart. To chemically label the formed RD-SA patterns, we prepared solutions of **A** (160 mM) + **AF** (40 μ M) and **A** (160 mM) + **AR** (40 μ M) in agar. These two solutions were injected in two holes, while the other holes were filled with a solution containing **H** (40 mM), see Supplementary Figure 4 and Figure 3b. The solutions were left to gelate for 20 minutes after which the holder was placed on a flat agar matrix and left standing for 8 hours in a closed humidified environment. The resulting patterns were analyzed by confocal microscopy, using the following settings: **AF** (λ_{ex} = 488 nm, λ_{em} = 500-550 nm), **AR** (λ_{ex} = 548 nm, λ_{em} = 580-700 nm).

Chemical gradient (Figure 5c). An agar matrix loaded with **H** (40 mM) was prepared in a Petri dish. A reservoir for the solution of **A** was made by manually cutting out a circular segment of agar (the central angle defining the circular segment was 110°), see Supplementary Figure 3c. The solution of **A** (200 mM) + **AF** (8 mM) was placed in the reservoir and the setup was left standing for 2 weeks. The solutions and agar matrix were prepared using phosphate buffer of pH = 6.5.

Chemical labeling for enzyme binding to RD-SA patterns (Figure 5e). To make RD-SA patterns capable of binding ConcanavalinA (**ConA**), solutions of **A** (160 mM) + **AR** (40 μ M) and **A** (160 mM) + **AM** (1.6 mM) + **AR** (40 μ M) in agar were prepared. These solutions were pipetted in two separate holes in a Plexiglass holder. The other two holes were filled with a solution containing **H** (40 mM) according to the configuration shown

in Supplementary Figure 4 and Supplementary Figure 3d, and the solutions were left to gelate. The experiment was then performed according to the procedure in Supplementary Figure 4. In short: the holder was placed on top of the agar gel prepared in the well formed by putting a Press-to-Seal™ silicone isolator on a glass slide and left to diffuse in a closed humidified environment for 8 hours. The time was kept intentionally short to prevent the formation of a dense supramolecular network, which would not allow the **ConA** to penetrate. Subsequently, the holder was removed and another Press-to-Seal™ silicone isolator was placed on top and the resulting well was filled with a buffered solution of **ConA** (2 mM, pH = 7). This well was closed with a glass slide to prevent evaporation and left to stand in a closed humidified environment for 12 hours. After this period, the sample was analyzed using fluorescence microscopy. To remove the non-bound **ConA**, the top glass slide was removed, the **ConA** solution was removed, and the sample was immersed into buffer (at least several mL) and left to stand for 72 hours, while buffer being refreshed every 24 hours. The final sample was again imaged by fluorescence microscopy. Images were analyzed with ImageJ to extract the fluorescence intensity profiles.

The formation of free-standing macroscopic hydrogel objects. The experiments were conducted in Petri dishes. Alginate gels were prepared according to the described procedure. Reservoirs were manually cut into the gel in various configurations shown in Figure 4b. The solutions of **H** (40 mM) and **A** (160 mM), both prepared in phosphate buffer of pH = 4.5, were placed in the reservoirs. Depending on the configuration, the reservoirs can hold up to 2.5 mL of solution. After the sample was left overnight, the remains of the solutions of **H** and **A** were removed. Free-standing patterns were obtained by adding a solution of EDTA (0.5 M) into the Petri dish and waiting until the alginate was dissolved (confirmed by visual inspection). Then, the resulting solution was removed with a pipette and the remaining hydrogel pattern was washed several times with water.

The free-standing gradient object shown in Figure 5g-i was made following a similar procedure with the arrangement shown in Supplementary Figure 2e.

RD by wet stamping. 3 % (mass fraction, *w*) agar stamps were used in all wet stamping (WETS) experiments. Stamps were prepared by dissolving agar in an appropriate amount of water (heated to 100 °C) and casting the hot solution on PDMS molds in a Petri dish. After cooling, gel stamps were cut out and soaked in a solution of **H** (40 mM) + **AR** (30 μM) for at least 12 hours. Gels used as substrates were 2% (weight/volume) alginate. The substrates were prepared by dissolving alginate in an appropriate amount of water (heated to 100 °C) and casting the cold solution into the well made by sticking two Press-to-Seal™ silicone isolators on top of each other on a glass slide (giving a height of 1 mm). A dialysis membrane was placed on top and gently pressed. The membrane was used to allow diffusion of calcium into the liquid alginate and to prevent alginate from leaving the well. The whole setup was then immersed into a 100 mM

solution of CaCl_2 for at least 12 hours. Subsequently, the membrane was gently removed and the substrate was soaked in a solution of **A** (300 mM) for at least 12 hours. The surfaces of the substrate and the stamp were air-dried before stamping. The stamp was gently put on the substrate and left for 60 minutes, after which the stamp was removed. The substrate was left standing overnight in a humid atmosphere to prevent drying. Alginate substrates were dissolved with a 0.5 M solution of EDTA by pipetting several drops of the solution onto the substrate. When all alginate was dissolved (confirmed by visual inspection), the solution was removed by careful pipetting and the remaining objects were carefully washed with water. Imaging of substrates and free-standing objects was done with a MicroCapture USB microscope camera and a confocal fluorescence laser scanning microscope. The solutions of **H** (40 mM) + **AR** (30 μM) and **A** (300 mM) were prepared in phosphate buffer of $\text{pH} = 4.5$.

Formation of hybrid network materials for compression tests (Figure 3a/b).

Alginate gels containing **H** were prepared similarly to pure alginate gels, but now dispersing CaCO_3 powder in an aqueous solution of **H** instead of in water. 10 mL of this solution was added to a Petri dish and left to gelate. Then, we manually cut out a circular segment of agar (the central angle defining the circular segment was 110°) to make a reservoir (Supplementary Figure 5). The solution of **A** was placed in the reservoir and the reaction was left running for at least three weeks (until the patterned region was more than 1 cm wide). Cylinders of 8 mm in diameter were punched out from the alginate/ HA_3 hybrid network region using a circular puncher and subjected to compression tests.

To prepare gels with varying initial concentration of **H** in alginate (10, 20, 30, 35 and 40 mM **H**), the following conditions were kept constant: $w(\text{alginate}) = 1.5\%$, $c(\text{CaCO}_3) = 12.5\text{ mM}$, $c(\text{GDL}) = 40\text{ mM}$, $c(\text{A}) = 400\text{ mM}$. The final pH of the gel depends on the ratio of concentrations of CaCO_3 and **GDL**. The current conditions gave a pH of 4.5. It should be noted that when the initial concentration of **H** in alginate was 30 mM, the final concentration of HA_3 in hybrid network gel was around 70 mM. Since the solubility of **H** in water is 40 mM we could not measure the yield stress of pure 70 mM HA_3 . Nevertheless, we do not expect that it would be significantly higher than the yield stress of 30 mM HA_3 , especially taking into account that the pure 30 mM HA_3 was physically so weak (as confirmed by the yield stress of only 0.7 kPa) that it was challenging to transfer it from a Petri dish to the instrument for measurement. Therefore, we have not attempted to measure pure 10 mM and 20 mM HA_3 to get a trend of increase of mechanical properties versus the concentration of HA_3 . Because of noted and confirmed low mechanical performance of 30 mM HA_3 we assumed that the increase of mechanical properties of HA_3 versus the concentration of HA_3 cannot be significant compared to the effect of the formation of hybrid network.

To prepare optimally crosslinked gels with varying mass fraction of alginate (1, 2 and 3 %), the following conditions were kept constant: $c_{\text{initial}}(\text{H in alginate}) = 30\text{ mM}$, $c(\text{A}) =$

400 mM, pH = 4.5. The optimal crosslinking was controlled by adjusting the amount of CaCO₃, and the final pH (4.5) was controlled by adjusting the amount of **GDL**.

The kinetics of hydrazone formation, measured using one-step reaction. We explored how the reaction constant of hydrazone formation varies with pH. Since the formation of **HA₃** is a three-step reaction, it would be complicated to investigate its dependence on pH. Therefore, we used a one-step reaction of monohydrazide **H'** with aldehyde **A** giving monohydrazone **H'A** (Supplementary Figure 6). This reaction can be easily followed using UV-VIS spectroscopy. Briefly, the absorbance of a well-mixed reaction mixture containing **H'** (60 μM) and **A** (60 μM) was measured at 308 nm until no significant change in absorbance was observed. The evolution of the concentration of **H'A** was obtained from the absorbance curve using a separately constructed calibration curve. The initial rate of **H'A** formation was determined from the linear least-square fit of the initial increase of **H'A** concentration, and used in combination with the initial concentrations of **H'** and **A** to calculate the rate constant under the assumption that the kinetics of the reaction is first order in both reactants, i.e. $dC_{H'A}/dt = k_{H'A}C_{H'}C_A$. The resulting rate constants for different pHs are summarized in Supplementary Table 1 and Supplementary Figure 7, and agree well with reported values for a similar hydrazone formation reactions.³

Dynamics of 1D pattern formation. To study the dynamics of 1D pattern formation, we performed a set of experiments using the basic configuration shown in Figure 2a in which the width of the 1D pattern increases over time. A plastic Petri dish was filled with agar at the desired pH and left to gelate. A 2 cm wide agar strip was made with two parallel cuts, at equal distance from the center. The outer agar segments were removed, creating two reservoirs. Before injecting buffer solutions of **H** and **A** in these reservoirs, the Petri dish was placed on a flat Plexiglass plate above a digital microscope camera. The recording started at the moment that the two solutions were injected. Images were taken every 10 minutes, over the course of 20 to 120 hours depending on experimental conditions. They were analyzed using ImageJ, extracting the intensity profile along a line between the two reservoirs (Supplementary Figure 8a, purple line in photo 4). This was done for multiple lines in the same image and the resulting profiles were averaged to reduce noise. The resulting intensity profile was then normalized by subtracting the minimum intensity value from the raw intensity profile and subsequently dividing the resulting intensities with respect to the peak intensity. The width of the 1D pattern was determined as the distance between points where two slopes intersect a base line (Supplementary Figure 8b). This baseline was determined as the average value of the first ten points of the intensity profile. This was done for all images in a time lapse, yielding the evolution of the width of the formed 1D pattern.

Kinetic model for HA₃ formation. The formation of gelator **HA₃** proceeds in three consecutive steps as shown in Supplementary Figure 9. Assuming that the rate constants

of the three steps k_1 , k_2 , and k_3 are independent and that they are first order in reactant concentration, the concentration of species in a well-mixed system without diffusion limitations changes in time according to:

$$\frac{d[\mathbf{H}]}{dt} = -k_1[\mathbf{H}][\mathbf{A}] \quad (1.1)$$

$$\frac{d[\mathbf{A}]}{dt} = -k_1[\mathbf{H}][\mathbf{A}] - k_2[\mathbf{HA}][\mathbf{A}] - k_3[\mathbf{HA}_2][\mathbf{A}] \quad (1.2)$$

$$\frac{d[\mathbf{HA}]}{dt} = k_1[\mathbf{H}][\mathbf{A}] - k_2[\mathbf{HA}][\mathbf{A}] \quad (1.3)$$

$$\frac{d[\mathbf{HA}_2]}{dt} = k_2[\mathbf{HA}][\mathbf{A}] - k_3[\mathbf{HA}_2][\mathbf{A}] \quad (1.4)$$

$$\frac{d[\mathbf{HA}_3]}{dt} = k_3[\mathbf{HA}_2][\mathbf{A}]. \quad (1.5)$$

To validate this model and find the values of the rate constants, we performed a set of experiments in a system where diffusion plays no role. Briefly, we mixed solutions of **H** (20 mM) and **A** (120 mM) and measured the concentrations using HPLC to find the temporal concentration changes of **A**, **HA**, **HA₂** and **HA₃** (see reference 2 for complete experimental procedure details). We compared the experimental data with the concentration data obtained by solving the model equations using a MATLAB code using the same initial concentrations for **A** and **H** as in the experiment. We solved the set of equations for a wide range of reaction constants k_1 and k_3 , while k_2 was set to a value for which no significant amounts of the intermediate **HA** were observed (k_2 was at least $1000 \times$ higher than k_1 , k_3), based on experimental observations. For each combination of rate constants k_1 and k_3 , the goodness of fit between experimental and numerical data was determined as the sum of mean square errors in the concentrations of **A**, **HA₂** and **HA₃** (Supplementary Figure 10). The rate constants k_1 and k_3 that gave the smallest error are summarized in Supplementary Table 2 for two values of the pH, and are within one order of magnitude as the rate constant for the one-step reaction $k_{\mathbf{H}'\mathbf{A}}$. The corresponding concentration data is in good agreement with the experimental data, suggesting the validity of the model assumptions.

Based on the linear dependence between $-\log k_{\mathbf{H}'\mathbf{A}}$ and pH found for the one-step reaction, we assume that $-\log k_1$, $-\log k_2$ and $-\log k_3$ also linearly depend on pH as the **HA₃** reaction involves the same type of bond, but three times instead of once. Using the data in Supplementary Table 2 for k_1 and k_3 , we find

$$k_1 = 10^{-(0.74\text{pH}+0.42)} \quad (1.6)$$

$$k_3 = 10^{-(0.87\text{pH}-0.45)}. \quad (1.7)$$

Reaction-diffusion model for 1D pattern formation. Having determined the rate constants and their dependency on pH, we developed a reaction-diffusion model to describe the formation of a 1D pattern in the basic experiment shown in Figure 2a. We hereby used the experimentally measured 1D pattern widths (Supplementary Section 6) to validate the model and to find the values of the diffusion coefficients. The reaction-diffusion model is based on Fickian diffusion and described by the following set of partial differential equations.

$$\frac{\partial c_H(x,t)}{\partial t} = D_H \frac{\partial^2 c_H(x,t)}{\partial x^2} - k_1 c_H(x,t) c_A(x,t) \quad (1.8)$$

$$\frac{\partial c_A(x,t)}{\partial t} = D_A \frac{\partial^2 c_A(x,t)}{\partial x^2} - k_1 c_H(x,t) c_A(x,t) - k_2 c_{HA}(x,t) c_A(x,t) - k_3 c_{HA_2}(x,t) c_A(x,t) \quad (1.9)$$

$$\frac{\partial c_{HA}(x,t)}{\partial t} = D_{HA} \frac{\partial^2 c_{HA}(x,t)}{\partial x^2} + k_1 c_H(x,t) c_A(x,t) - k_2 c_{HA}(x,t) c_A(x,t) \quad (1.10)$$

$$\frac{\partial c_{HA_2}(x,t)}{\partial t} = D_{HA_2} \frac{\partial^2 c_{HA_2}(x,t)}{\partial x^2} + k_2 c_{HA}(x,t) c_A(x,t) - k_3 c_{HA_2}(x,t) c_A(x,t) \quad (1.11)$$

$$\frac{\partial c_{HA_3}(x,t)}{\partial t} = D_{HA_3} \frac{\partial^2 c_{HA_3}(x,t)}{\partial x^2} + k_3 c_{HA_2}(x,t) c_A(x,t). \quad (1.12)$$

The gel was considered as a one-dimensional (1D) domain, with edges at $x = 0$ and $x = L$ in contact with the **H** and **A** reservoir, respectively. Initially, concentrations of **HA**, **HA₂**, and **HA₃** are zero everywhere. Similar is valid for **A** and **H**, except at the edges of the domain where we used (in the notation $c(x, t)$): $c_H(0, 0) = 40$ mM and $c_A(L, 0) = 160$ mM. The edges of the domain were considered perfect sinks for the products ($c_{HA_3}(0, t) = c_{HA_3}(L, t) = 0$ mM, alike for **HA** and **HA₂**), while the concentrations of **A** and **H** at the edges were updated each time step, accounting for depletion of reactants in the reservoirs. The set of equations, together with the initial and boundary conditions, was solved numerically using a MATLAB code. The output gives the spatiotemporal concentration profiles of all species, which can be used to calculate the evolution of the width of the 1D pattern. We determined the width from the time-dependent concentration profile of **HA₃** as the horizontal distance between the points where the concentration of **HA₃** equals 1 mM. To determine the diffusion coefficients of all species (except for **HA₃**, which is virtually 0), we performed a set of simulations in which we varied their values over a wide range. From this set, we determined the best fit to the experimental data of the width of the 1D pattern formed at pH = 4.0 to find their values (Supplementary Table 3). Comparing the resulting pattern predicted by the model with that observed in experiments at pH=4, we observed that the simulated 1D pattern keeps increasing in width, while the experimental pattern reaches a plateau, as shown in Supplementary Figure 11a. By taking samples from the reservoirs, we excluded depletion of reactants as the underlying reason for the plateau. We hypothesized that the difference in dynamics is due to the gelation of **HA₃**, which makes it harder for the

reactants and intermediates to diffuse through the domain. We took into account the local dependence of diffusion coefficients on the local \mathbf{HA}_3 concentration using a stretched exponential function of the form

$$D_g = D_0 \exp(-a\varphi^\nu) \quad (1.13)$$

with φ the volume fraction of \mathbf{HA}_3 in the agar gel matrix modeled as⁴

$$\varphi = \frac{W_{\mathbf{HA}_3 \text{ in } 1\% \text{ agar}}}{1.025} = \frac{c_{\mathbf{HA}_3} M_{\mathbf{HA}_3} V_{\mathbf{HA}_3}}{1.025 \times (c_{\mathbf{HA}_3} M_{\mathbf{HA}_3} V_{\mathbf{HA}_3} + m_{1\% \text{ agar}})}. \quad (1.14)$$

We assumed negligible volume changes upon gelation of solutions, i.e. a certain volume of solution gives the same volume of gel. For simplicity, we set the parameter $\nu = 1$ and used the values in Supplementary Table 3 for D_0 . Using the approach similar to the one described before for the determination of D_0 , we analyzed the ranges of constant a for reactants and intermediates to determine the values that gave the best fit with experimental data. The best fit was found for $a = 30$ for \mathbf{H} , and $a = 34$ for \mathbf{A} . We noted that the wide range of values around $a = 30$ for \mathbf{HA} and \mathbf{HA}_2 does not show any influence on the outcome of the model so we set it to $a = 34$, the same as for \mathbf{A} . With all parameters optimized at $\text{pH} = 4.0$, we obtained good agreement between model and experiment, as shown in Supplementary Figure 11b, showing the importance of taking into account the dependence of the diffusion coefficients on local gelation.

Finally, we used the optimized model to investigate how changes of different experimentally controllable parameters influence the width of 1D pattern. The results of these simulations are shown in Supplementary Figure 12.

Supplementary Discussion

When comparing the width of the 1D pattern for different concentrations of \mathbf{H} at a fixed ratio of \mathbf{H} and \mathbf{A} concentrations, low concentrations yield wider structures than high concentrations when compared at the same point in time (except for very short times (<20 hours)). This is understood, as higher concentrations yield tougher \mathbf{HA}_3 gels such that it takes longer for reactants and intermediates to diffuse through. This same effect is seen for a decreasing distance between the reservoirs, which yields tougher gels earlier on, slowing down the formation of the 1D pattern. The effect of pH was studied by varying the reaction rate constants in the model. We hereby used the experiment at $\text{pH} = 4.0$ as a benchmark, such that a 200-fold increase in reaction rates corresponds to a decrease in pH to 0.9. Although the pH in our experiments cannot be decreased below 3.3 (as gelation does not occur for the agar and alginate/ CaCO_3 / \mathbf{GDL} systems) resulting in about 2 mm wide lines, the model does enable exploring how the width of the 1D pattern further decreases with pH. As can be seen in Supplementary Figure 12c, pH strongly influenced the line width, reaching 1.0 mm at $\text{pH} = 0.9$. In summary, the model

demonstrates that the smallest patterns could be made using the highest concentrations of reactants possible, keeping the smallest feasible distances between reservoirs, while taking care that reaction rate constants are the highest possible (controlled by pH). Additionally, by knowing only the reaction rates and the diffusion coefficients of participating species, the model can be used to estimate minimum and maximum sizes of produced patterns and is not limited to the reaction used in this research. In our case, the minimum size estimated using the model was in the order of 2 mm, and maximum size was in the order of 15 mm, thus spanning over approximately one order of magnitude.

Supplementary References

- 1 Jimenez, F. *et al.* Aryloxyacetic esters structurally related to alpha-asarone as potential antifungal agents. *Med. Chem. Res.* **19**, 33-57 (2010).
- 2 Neises, B. & Steglich, W. 4-Dialkylaminopyridines as acylation catalysts .5. Simple method for esterification of carboxylic-acids. *Angew. Chem. Int. Ed.* **17**, 522-524 (1978).
- 3 Dirksen, A., Dirksen, S., Hackeng, T. M. & Dawson, P. E. Nucleophilic catalysis of hydrazone formation and transimination: Implications for dynamic covalent chemistry. *J. Am. Chem. Soc.* **128**, 15602-15603 (2006).
- 4 Johnson, E. M., Berk, D. A., Jain, R. K. & Deen, W. M. Diffusion and partitioning of proteins in charged agarose gels. *Biophys. J.* **68**, 1561-1568 (1995).

Control over the Formation of Supramolecular Patterns Using Reaction-Diffusion

Abstract

Reaction-diffusion is a promising approach for the formation of soft structured materials. In this chapter we show that 1D structure formation can be influenced and controlled by reaction kinetics and concentration gradients. Additionally, we outline methodology for *a priori* estimation of desired structure dimension from known experimental parameters.

Introduction

Control over structure formation is an important requirement in the fields of micro- and nanofabrication. Techniques for controlling the size and/or shapes of structures include various photolithographic techniques, 3D printing and microfluidic devices. Contrary to artificially made structures, natural structures are often created in response to dynamic environment. The dynamic environment creates chemical gradients which are a key factor defining natural structures. The resulting inhomogeneities cause spontaneous transport of matter which is exploited in nature for delivering matter to specific locations, for example specific organelles in cells, without additional input of energy. However, diffusive transport alone is often not sufficient because it requires significantly steep concentration gradients. Therefore, to facilitate transport when gradients are shallow, a series of transport enzymes separated by small distances is employed. Although enzymatic transport is active because it is facilitated by a series of chemical reactions, molecules cross short distances between enzymes purely by diffusion. Since diffusion is coupled to a series of enzymatic chemical reactions, the overall process is called reaction-diffusion (RD) and it is essential for various cellular mechanisms. Examples from nature include calcium waves^{1,2}, glucose-induced oscillations³, transport of ATP to ATP-deficient sites⁴⁻⁶, and building and maintaining of microtubules⁷. First evidence that links RD to pattern formation in living systems was provided by Alan Turing⁸ and Boris Belusov⁹. Both Turing's and Belousov's systems contain nonlinear coupling between reactions and feedback loops which are abundantly employed mechanisms in nature for various regulatory processes and spatial organization. For example, their discoveries provide a suggestion to explain skin pattern formation on animals.¹⁰⁻¹² Therefore, using concentration gradients coupled to chemical reactions in dynamic system should enable the production of novel and diverse artificial materials. Although abundantly present in nature, approaches to use dynamic conditions for the design of structured materials are still rare. Some recent examples include gradients of carbon dioxide¹³ and oxygen¹⁴ to control the growth of complex structures. Recently, we reported a self-assembling system capable of forming macroscopic patterns with varying shape and composition using an RD approach.¹⁵ Concentration gradients and reaction rates controlled by acid catalysis were explored to control the spatial distribution of soft matter structure formation. We also verified the observed behavior with an RD model. In general, the major drawback of experimental exploration of such large parameter space is that it is often time-consuming. Numerical simulations can facilitate this process since they can execute the same task in matter of hours. On the other hand, writing a custom code for the specific set of RD equations might still require significant time. Therefore, to fully benefit from RD approach as a tool for pattern formation, one would ideally want a simple, *e.g.* linear, relation between experimental conditions and desired pattern characteristics, *e.g.* pattern size.

Results and discussion

In this work we derive a simple equation for quick order-of-magnitude estimates of pattern size from experimental conditions. Initially, we we briefly explore experimentally the effect of concentration gradient steepness and reaction rate on supramolecular pattern size, and compare the results with the established RD model. Most notably, the model indicates that the formation of supramolecular structures hampers diffusion of reactants, thereby further reducing pattern dimensions. Next, we further simplify the RD model to obtain the relation between pattern size and experimental parameters. We anticipate that the methodology developed herein outlines general approach towards rational design of RD experiments, eliminating laborious experimental investigation of big set of parameters.

In our approach towards control of supramolecular pattern formation by RD we made use of the reactive formation of supramolecular hydrogels from hydrazide (**H**) and aldehyde (**A**) derived compounds.¹⁵ In the RD setup, these water soluble precursors **H** and **A** are spatially separated by a hydrogel matrix. Over time, **H** and **A** diffuse through the matrix forming concentration gradients within. Eventually, a reaction between **H** and **A** to give hydrogelator **HA**₃ occurred at locations where their gradients coincided leading to different patterns of hydrogelator **HA**₃ with varying dimensions, depending on the initial geometry of the system. To understand the relation between the pattern size and control parameters, we explored three parameters in this work: pH, the initial concentration of **H** ($c_{H,0}$), and the diffusion distance (L). These parameters determine the steepness of the concentration gradient ($c_{H,0}$ and L) and reaction rate constant (pH). In general, the concentration gradient becomes steeper as $c_{H,0}$ increases and d decreases, and the reaction rate constant becomes higher with decreasing pH.

Firstly, we investigated experimentally how the width of the supramolecular pattern (w_{HA3}) depends on pH while keeping all other parameters constant ($L = 2$ cm; $c_{H,0} = 40$ mM; $c_{H,0}:c_{A,0} = 1:4$). The width w_{HA3} was defined as the distance between the edges of the pattern.¹⁵ We observed that in the pH range between 3.3 and 7.0 w_{HA3} varied from 2.6 to 16.7 mm. It can be seen in Figure 1a that, with increasing pH, pattern formation started later and became wider. Secondly, we investigated the effect of $c_{H,0}$ while keeping $L = 20$ mm, pH = 4.0, and $c_{H,0}:c_{A,0} = 1:4$. As can be seen in Figure 2a, the effect is much less dramatic over the investigated interval of concentrations with the width varying between 2.8 and 3.2 mm. It can be noticed that in all cases pattern formation started at comparable time. Finally, the effect of L was investigated by varying the distance between reservoirs of **H** and **A** from 5 to 20 mm, while keeping reactant concentrations and pH constant ($c_{H,0} = 40$ mM, $c_{H,0}:c_{A,0} = 1:4$, pH = 4.0). As can be seen in Figure 3a, L shows a minor influence on w_{HA3} . The obtained w_{HA3} was between 1.5 and 2.7 mm. Also, the pattern started forming earlier when L was smaller.

To understand the formation of supramolecular pattern, we developed an RD model.¹⁵ The model was discussed in full detail in our previous work, but we briefly mention its main characteristics herein. Due to experimental design, where **H** and **A**

were allowed to diffuse in only one direction, we described RD process as a 1D mathematical problem (along the x axis). The supramolecular gelator \mathbf{HA}_3 (with diffusion coefficient $D_{\mathbf{HA}_3}$) forms from \mathbf{H} and \mathbf{A} through a 3-step reaction via intermediates \mathbf{HA} and \mathbf{HA}_2 (with diffusion coefficients $D_{\mathbf{HA}}$ and $D_{\mathbf{HA}_2}$). The following system of differential equations containing diffusion and reaction terms describes the concentration variations of all species:

$$\frac{\partial c_{\mathbf{H}}(x,t)}{\partial t} = D_{\mathbf{H}} \frac{\partial^2 c_{\mathbf{H}}(x,t)}{\partial x^2} - k_1 c_{\mathbf{H}}(x,t) c_{\mathbf{A}}(x,t) \quad (3.1)$$

$$\frac{\partial c_{\mathbf{A}}(x,t)}{\partial t} = D_{\mathbf{A}} \frac{\partial^2 c_{\mathbf{A}}(x,t)}{\partial x^2} - k_1 c_{\mathbf{H}}(x,t) c_{\mathbf{A}}(x,t) - k_2 c_{\mathbf{HA}}(x,t) c_{\mathbf{A}}(x,t) - k_3 c_{\mathbf{HA}_2}(x,t) c_{\mathbf{A}}(x,t) \quad (3.2)$$

$$\frac{\partial c_{\mathbf{HA}}(x,t)}{\partial t} = D_{\mathbf{HA}} \frac{\partial^2 c_{\mathbf{HA}}(x,t)}{\partial x^2} + k_1 c_{\mathbf{H}}(x,t) c_{\mathbf{A}}(x,t) - k_2 c_{\mathbf{HA}}(x,t) c_{\mathbf{A}}(x,t) \quad (3.3)$$

$$\frac{\partial c_{\mathbf{HA}_2}(x,t)}{\partial t} = D_{\mathbf{HA}_2} \frac{\partial^2 c_{\mathbf{HA}_2}(x,t)}{\partial x^2} + k_2 c_{\mathbf{HA}}(x,t) c_{\mathbf{A}}(x,t) - k_3 c_{\mathbf{HA}_2}(x,t) c_{\mathbf{A}}(x,t) \quad (3.4)$$

$$\frac{\partial c_{\mathbf{HA}_3}(x,t)}{\partial t} = D_{\mathbf{HA}_3} \frac{\partial^2 c_{\mathbf{HA}_3}(x,t)}{\partial x^2} + k_3 c_{\mathbf{HA}_2}(x,t) c_{\mathbf{A}}(x,t). \quad (3.5)$$

The model contains several parameters that can be varied: $D_{\mathbf{H}}$, $D_{\mathbf{A}}$, $D_{\mathbf{HA}}$, $D_{\mathbf{HA}_2}$, $D_{\mathbf{HA}_3}$, $c_{\mathbf{H},0}$, $c_{\mathbf{A},0}$, k_1 , k_2 and k_3 (rate constants being defined by pH). Initial values, *i.e.* at $t = 0$, of $D_{\mathbf{H}}$, $D_{\mathbf{A}}$, $D_{\mathbf{HA}}$, $D_{\mathbf{HA}_2}$, $D_{\mathbf{HA}_3}$ were kept the same throughout all simulations.¹⁵ The other parameters were varied, similar as in aforementioned experiments. For simplicity, the gelation of \mathbf{HA}_3 was simulated by setting $D_{\mathbf{HA}_3}$ to a very low value (around 5×10^5 smaller than the other diffusion coefficients). The RD model was solved for a concentration profile of \mathbf{HA}_3 over a given L as a function of time. To allow comparison with experimental data $w_{\mathbf{HA}_3}$ was determined from this concentration profile.¹⁵ The goodness of fit between the experimental data and the model was defined as mean square error (MSE). Our first simulations showed that significant discrepancies between the experimental data and the model occur at later stages of pattern development. Whereas in experiments $w_{\mathbf{HA}_3}$ reached a constant value after initial growth, the model showed a constant increase of $w_{\mathbf{HA}_3}$. Based on this observation we anticipated that after initial formation, the \mathbf{HA}_3 structure blocks further diffusion of \mathbf{H} and \mathbf{A} . To test this hypothesis, we let a dye of unknown chemical composition diffuse through a blank agar matrix and an agar matrix with a preformed structure. We observed that the diffusion of the dye was slower in the region with the supramolecular structure (see Supplementary Figure 1 for details). Based on this finding, we introduced dependency of $D_{\mathbf{H}}$, $D_{\mathbf{A}}$, $D_{\mathbf{HA}}$ and $D_{\mathbf{HA}_2}$ on the local concentration of \mathbf{HA}_3 . The decrease was defined using the stretched exponential function

$$D_g = D_0 \exp(-a\phi^v) \quad (3.6)$$

with D_g and D_0 being the diffusion coefficients of certain species in gel and water solution (diffusion in 1% agar is negligibly different from pure water), respectively, and ϕ is the volume fraction of \mathbf{HA}_3 . Parameter ν was set to 1 for simplicity and parameter a was determined by fitting the model to the experimental data.¹⁵ With this correction included, we were able to reproduce the experimentally observed behavior using the model.

In general, the model showed good agreement with experimental data for all investigated parameters. Figure 1b shows that $w_{\mathbf{HA}_3}$ can be predicted with a high level of precision by the RD model for different values of the pH. MSE for pHs below 5.5 was below 0.1 (the ideal fit gives MSE = 0). Above pH = 5.5, larger discrepancies between the experimental data and the model occurred, as can be seen from less defined edges of the experimental supramolecular pattern due to smearing. This smearing caused larger errors in determination of width from experimental data, especially in the beginning of the pattern formation, which led to higher MSEs (between 2.0 and 3.0 for pHs between 6.0 and 6.5 and around 6.5 for pH = 7.0). The model confirmed the experimental observation that with higher pH (slower reaction kinetics) the pattern becomes wider. In this way, reactants \mathbf{H} and \mathbf{A} cross-diffuse much further before starting to form gelator \mathbf{HA}_3 . Additionally, since \mathbf{HA}_3 is not formed fast, decrease of $D_{g,\mathbf{H}}$, $D_{g,\mathbf{A}}$, $D_{g,\mathbf{HA}}$ and D_{g,\mathbf{HA}_2} is smaller. Therefore, the reaction kinetics combined with a decrease of diffusion coefficient determines $w_{\mathbf{HA}_3}$.

For different $c_{\mathbf{H},0}$, the model shows again good agreement with the experimental data (Figure 2b). For $c_{\mathbf{H},0}$ higher than 25 mM, MSE values were below 0.1. Larger discrepancies, with MSE values between 1.0 and 3.0, can be observed for $c_{\mathbf{H},0}$ smaller than 25 mM. There, reaction times become longer, indicating that the model is not able to accurately describe the behavior of the system on long time scales. In that situation, the modelled $w_{\mathbf{HA}_3}$ were usually slightly larger than the experimental ones. The hindering of diffusion might be higher in reality than predicted by the model due to intermolecular interactions. Still, the model confirmed again the experimentally observed behavior that higher reaction rates lead to smaller $w_{\mathbf{HA}_3}$. Also, it can be seen from Figure 2 that the effect of $c_{\mathbf{H},0}$ variation has a much smaller influence on $w_{\mathbf{HA}_3}$ than pH. As mentioned, the local concentration gradient becomes steeper as $c_{\mathbf{H},0}$ increases, which leads, in turn, to higher local concentration of \mathbf{H} along L (see Supplementary Figure 2). Since the reaction rate is first order with respect to $c_{\mathbf{H}}$ and $c_{\mathbf{A}}$ ^{16,17}, changing $c_{\mathbf{H},0}$ from 10 mM to 40 mM increases the local reaction rate up to four times with respect to \mathbf{H} . As before, higher reaction rate means faster accumulation of \mathbf{HA}_3 , which leads to a more pronounced decrease of $D_{g,\mathbf{H}}$, $D_{g,\mathbf{A}}$, $D_{g,\mathbf{HA}}$ and D_{g,\mathbf{HA}_2} .

Finally, comparing the RD model to the experimental data for different L also shows a good fit (Figure 3b), confirming once more that the model has good predictive power. The highest MSE was 0.12 with the majority of them being less than 0.1. The model confirmed that lower L leads to smaller $w_{\mathbf{HA}_3}$ and that the effect is not as dramatic as with pH. Since L determines how quickly \mathbf{H} and \mathbf{A} are brought to the reaction site (Figure 3a), shorter L means faster delivery of \mathbf{H} and \mathbf{A} leading to higher local

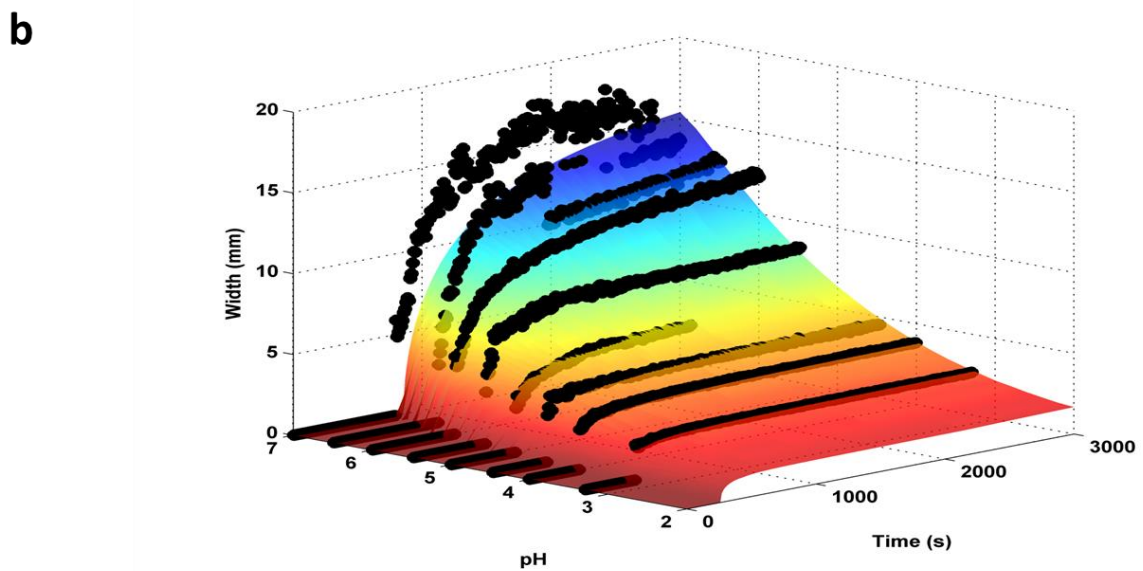
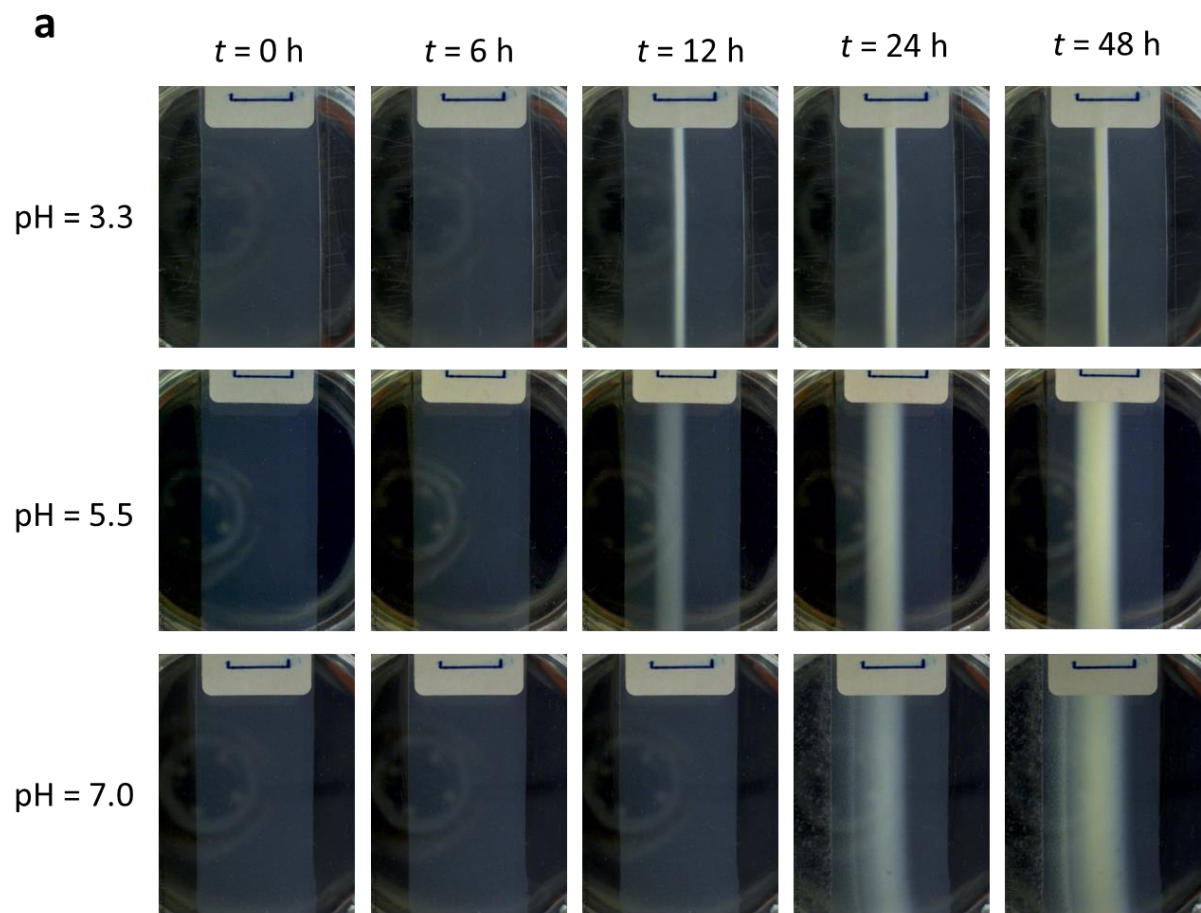


Figure 1. Controlling the dimension of 1D pattern by pH. **a)** Time snapshots of experiments conducted at pH of 3.3, 5.5 and 7.0. **b)** Comparison between the RD model (colored surface) and experiment (black dots). The reaction rate in the experiments was controlled by varying the pH between 3.3 (fast reaction) and 7.0 (slow reaction).

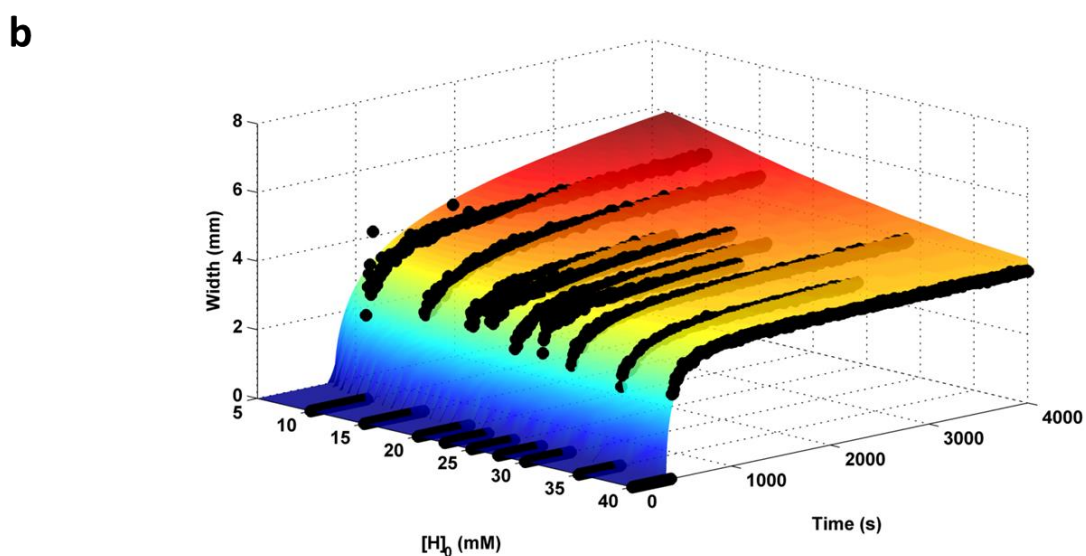
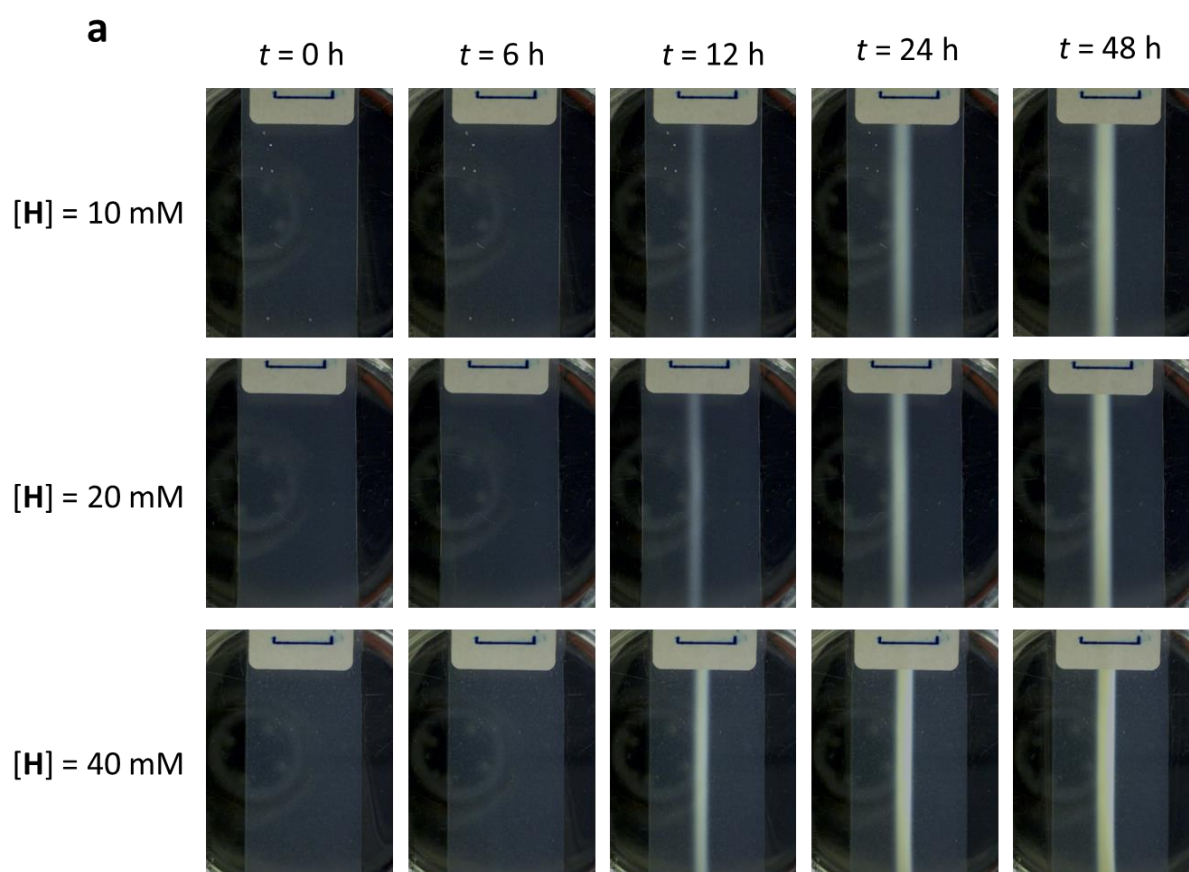


Figure 2. Controlling the dimension of 1D pattern by the concentration of H. a) Time snapshots of experiments conducted at 10 mM, 20 mM, and 40 mM H. b) Comparison between the RD model (colored surface) and experiment (black dots). The concentration of H in the experiments was varied between 10 and 40 mM.

concentration of H and A, and a steeper local concentration gradient (Supplementary Figure 3). Hence, local reaction rates are higher, causing a faster accumulation of HA_3 which dictates the decrease of $D_{g,H}$, $D_{g,A}$, $D_{g,HA}$ and D_{g,HA_2} . Also, H and A depleted by

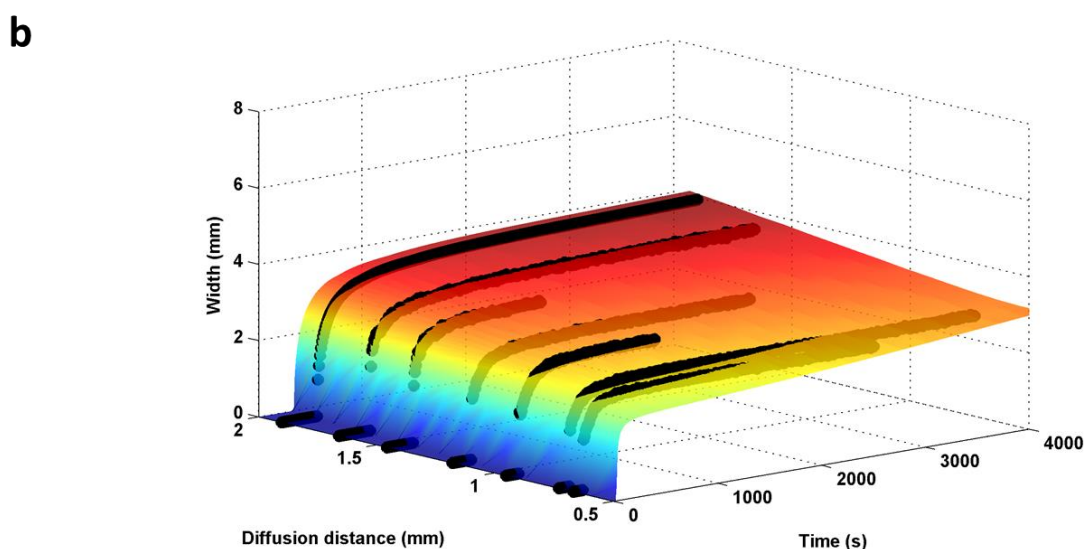
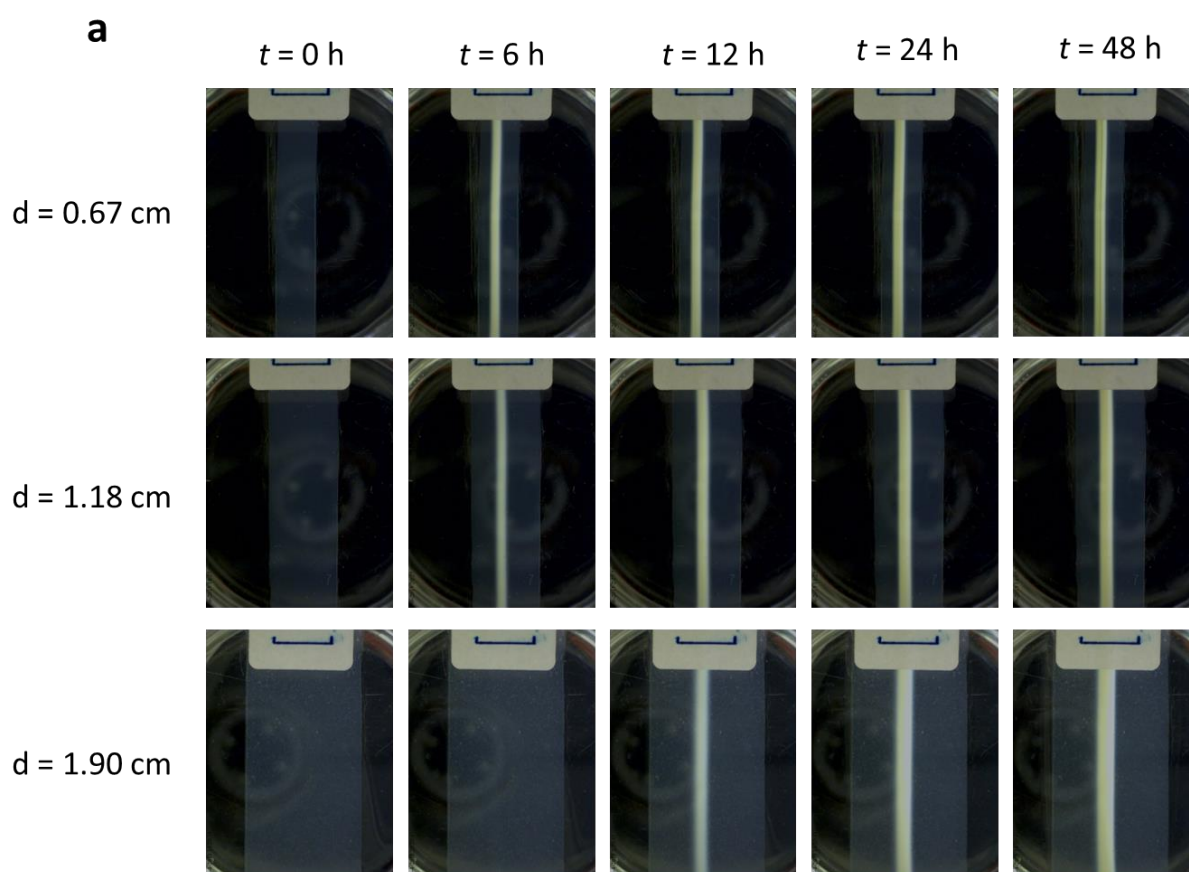


Figure 3. Controlling the dimension of 1D pattern by distance between reservoirs. a) Time snapshots of experiments conducted at distances of 0.67 cm, 1.18 cm, and 1.90 cm **H. b)** Comparison between the RD model (colored surface) and experiment (black dots). The distance between containers in the experiments was varied between 0.5 cm and 2.0 cm.

reaction are replenished faster (due to higher influx caused by steeper concentration gradient). In this way, further widening of the pattern is prevented by the sudden formation of HA_3 . Overall, the concentration gradient steepness ($c_{\text{H},0}$ and L) has a

relatively small effect on w_{HA3} , compared to the more pronounced effect of reaction rate on w_{HA3} as controlled by the pH. The major difference between these two approaches is the accessible range of reaction rates. While local reaction rates vary less than 10-fold depending on chosen $c_{\text{H},0}$ and L , they can be varied over several orders of magnitude by changing the pH.

To further our understanding, we investigated the relation between w_{HA3} and experimental parameters such as $c_{\text{H},0}$, L and k (determined by pH in this case) in more detail. Such understanding would allow quick order-of-magnitude estimates of achievable pattern dimensions from known experimental parameters. Since RD is an interplay between reaction and diffusion, we start our analysis by quantifying reaction and diffusion times, and relate them later to w_{HA3} . Reaction and diffusion times are generally related by dimensionless quantity called the Damköhler number (Da):

$$\text{Da} = \frac{\tau_{\text{D}}}{\tau_{\text{R}}}. \quad (3.7)$$

The Damköhler number gives us insight in whether the RD process is in a reaction-limited regime when the diffusion time scale is much smaller than the reaction time scale ($\text{Da} \ll 1$), a diffusion-limited regime when the diffusion time scale is much larger than reaction time scale ($\text{Da} \gg 1$) or in a regime where reaction and diffusion time scales are similar ($\text{Da} \approx 1$). The expression relating Da to k , L and $c_{\text{H},0}$ can be derived from the set of RD equations defining the system. Since **H** and **A** are reactants in our system, and their diffusion drives the formation of the supramolecular pattern, we chose **H** as a relevant species for the determination of Da. **A** was discarded because its concentration was in stoichiometric excess meaning that the concentration of **H** defines the concentration of **HA**₃. Also, for simplicity, we approximated the overall process with only one reaction between **H** and **A** setting $c_{\text{H},0} = c_{\text{A},0} = c_0$ leading to a single differential equation. The following expression describes spatio-temporal variation of the concentration of **H**:

$$\frac{\partial c_{\text{H}}(x,t)}{\partial t} = D_{\text{H}} \frac{\partial^2 c_{\text{H}}(x,t)}{\partial x^2} - k c_{\text{H}} c_{\text{A}}. \quad (3.8)$$

To relate reaction and diffusion time scales, the RD equation (3.8) was turned non-dimensional using the steady-state approximation and rescaling the variables $\bar{c}_{\text{H}} = c_{\text{H}} / c_0$, $\bar{c}_{\text{A}} = c_{\text{A}} / c_0$ and yielding $\bar{x} = x / L$ to give

$$\frac{\partial^2 \bar{c}_{\text{H}}(\bar{x}, t)}{\partial \bar{x}^2} - \text{Da} \bar{c}_{\text{H}} \bar{c}_{\text{A}} = 0 \quad (3.9)$$

where

$$Da = \frac{\tau_D}{\tau_R} = \frac{c_0 k L^2}{D_H} \quad (3.10)$$

The equation (3.10) shows that the reaction and diffusion times can be estimated as $\tau_D \sim \frac{L^2}{D_H}$ and $\tau_R \sim \frac{1}{kc_0}$. Next, we related the Damköhler number to w_{HA3} . Figure 4. shows a schematic representation of the 1D RD geometry discussed before. At $x = 0$ and $x = L$, concentration is maintained at $c_{H,0} = c_{A,0} = c_0$. In the reaction zone of width w_{HA3} , the concentration is unknown and indicated by $c_H^* = c_A^* = c^*$. The rate in the reaction zone is of the order $R \approx kc_H^* c_A^* \approx kc^{*2}$ and zero elsewhere. Inside the reaction zone we can estimate the concentration of **H** from equation (3.8) using the steady-state approximation giving

$$D \frac{d^2 c_H}{dx^2} - kc_H c_A = 0. \quad (3.11)$$

The terms in the equation (3.11) can be estimated as $D \frac{d^2 c_H}{dx^2} \sim D \frac{c^*}{w_{HA3}^2}$ and $kc_H c_A \sim kc^{*2}$.

Applying these approximations equation (3.11) becomes

$$D \frac{c^*}{w_{HA3}^2} \sim kc^{*2} \quad (3.12)$$

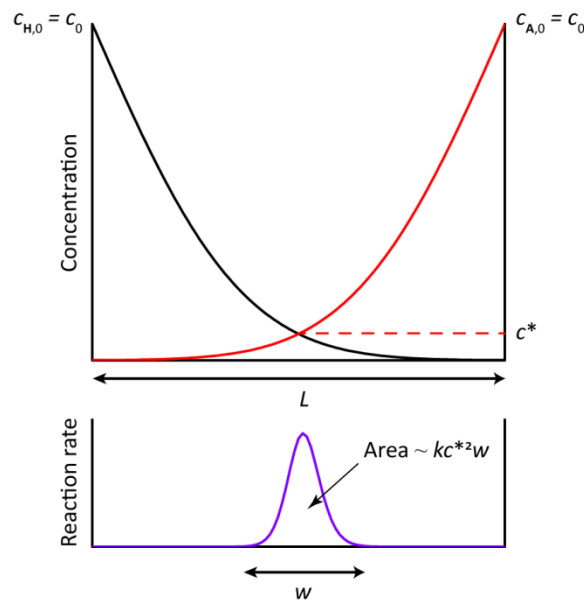


Figure 4. Schematic representation of 1D RD setup.

which can be rearranged to

$$\frac{D}{kc_0L^2} \sim \left(\frac{c^*}{c_0}\right) \left(\frac{w_{\text{HA}_3}}{L}\right)^2. \quad (3.13)$$

Further, the flux into the reaction zone can be approximated as

$$J = D \frac{c_0 - c^*}{L/2} \sim \frac{Dc_0}{L} \quad (3.14)$$

if $c^* \ll c_0$. This flux becomes the total amount reacted

$$R = \int_{-\infty}^{\infty} kc_{\text{H}^+}c_{\text{A}} dx \sim kc^*w_{\text{HA}_3}. \quad (3.15)$$

Combining equations (3.14) and (3.15) give

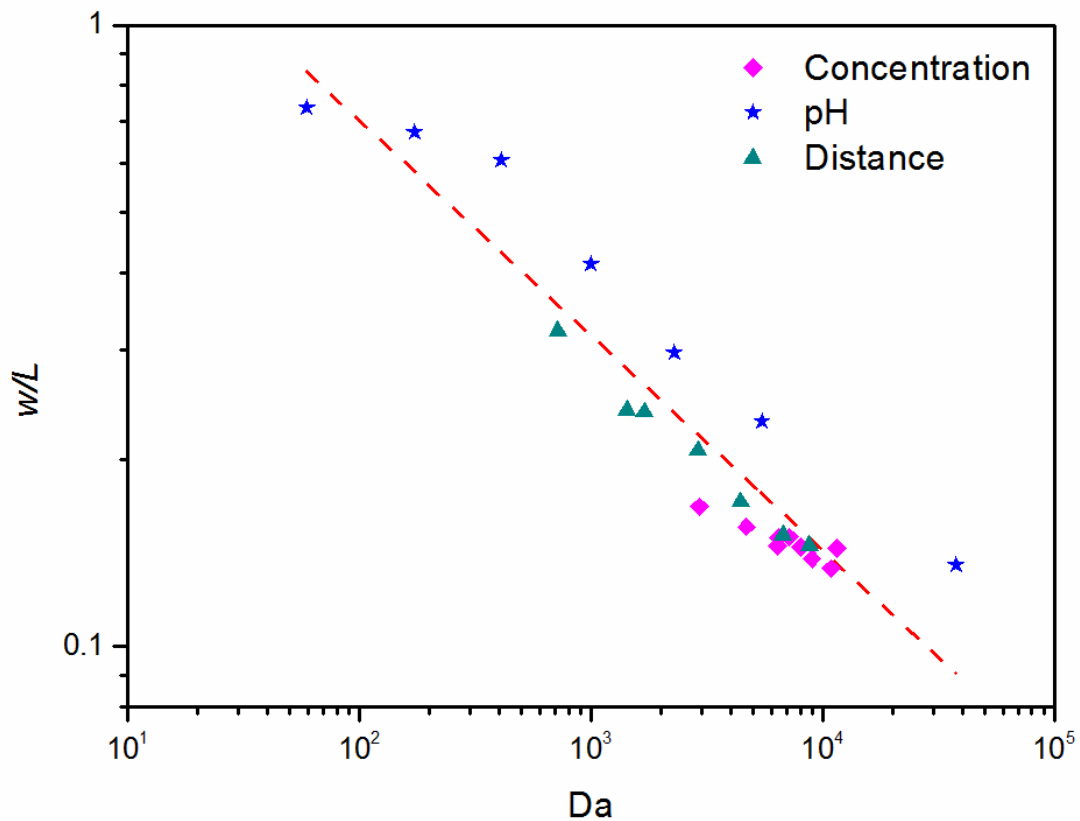


Figure 5. Control of width represented in terms of Damköhler number. The experimental data (shaped points) shows good agreement with the theory (red dotted line). The theoretical line has the slope of -0.35 ± 0.03 which is in agreement with the theoretical slope of $-1/3$.

$$\frac{D}{kc_0L^2} \sim \left(\frac{c^*}{c_0}\right)^2 \left(\frac{w_{\text{HA}_3}}{L}\right). \quad (3.16)$$

Solving equations (3.13) and (3.16) for $\left(\frac{w_{\text{HA}_3}}{L}\right)$ yields

$$\frac{w_{\text{HA}_3}}{L} \sim \text{Da}^{-\frac{1}{3}} \quad (3.17)$$

which indicates that plotting w_{HA_3} against the Damköhler number on a logarithmic scale should give a slope of $-1/3$. As can be seen in Figure 5, the slope of the plot is -0.35 ± 0.03 which is in agreement with the theory. This result indicates that knowing the experimental parameters of RD system, one can estimate the outcome through the use of the Damköhler number. For example, if experimental parameters are such that Damköhler number is relatively small (e.g. of the order of 10^2), it can be estimated using equation (3.17) that w_{HA_3} will be roughly 21.5% of L . In contrast, when Damköhler number is high (e.g. 10^4), w_{HA_3} will be 4.6% of L . As can be noted, the estimated values deviate from the values obtained experimentally (w_{HA_3} was 70% of L for $\text{Da} = 10^2$, and 15% of L for $\text{Da} = 10^4$) possibly due to approximations in the derivation of equation (3.17). However, both experimental findings and equation (3.17) show that the pattern is 4.7 times wider for $\text{Da} = 10^2$ than for $\text{Da} = 10^4$. Therefore, derived equation provides a tool for quick order-of-magnitude estimates of the resulting pattern dimensions based purely on readily known experimental parameters. Similarly, Grzybowski showed that a comparable expression can be derived for different types of systems, suggesting that similar analysis can be done for other types of RD systems.¹⁸ Therefore, the rational experimental design should include this type of analysis followed by experimental confirmation. Then, if desired, the full RD model can be used to explore large parameter space.

Conclusion

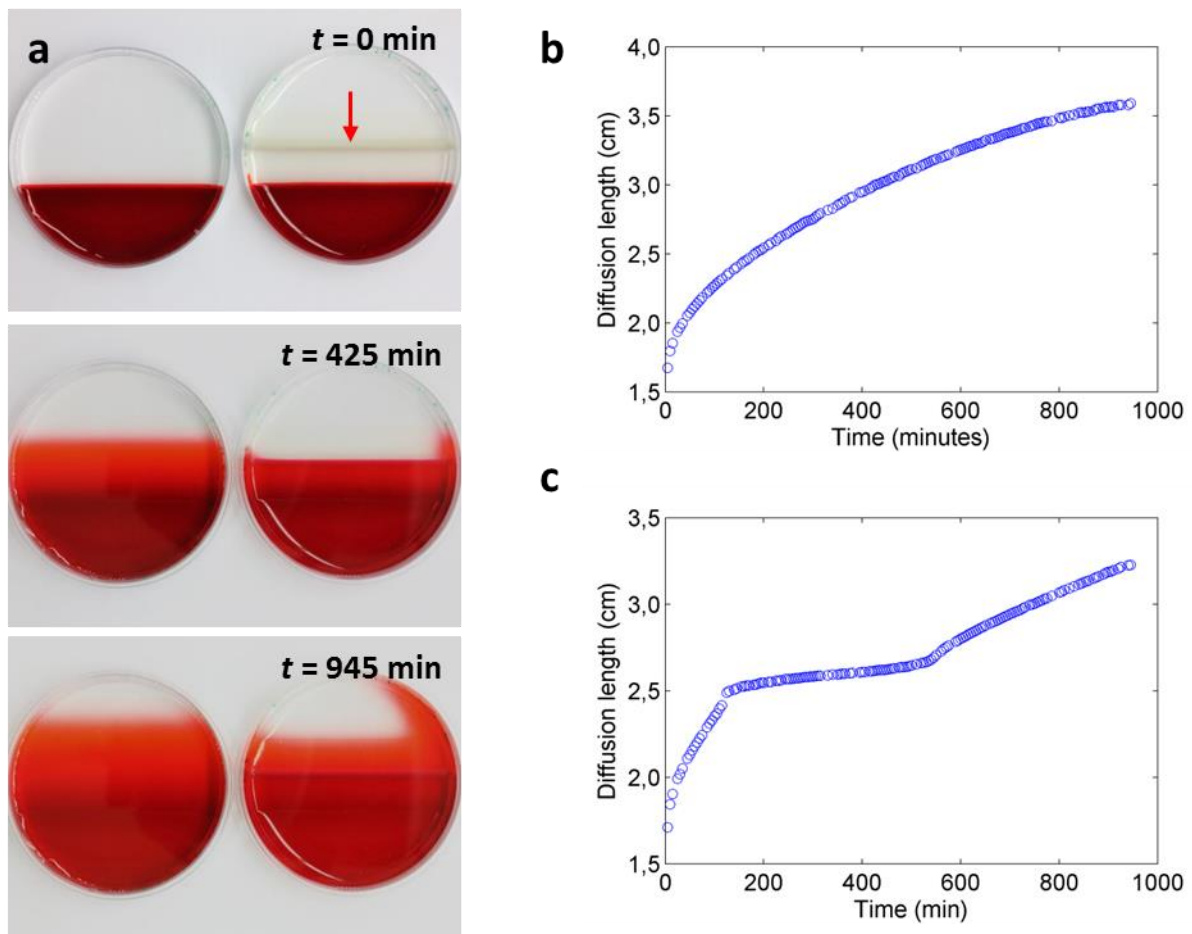
In conclusion, this study finds that controlling local reaction kinetics by means of pH, diffusion length and the concentrations of reactants allows control over the dimensions of formed supramolecular patterns. Furthermore, it is shown that all these control parameters can be unified using the Damköhler number which can be related to the structure width, thus providing a simple relation between experimental parameters and structure dimensions. This relation can be used as a tool for quick order-of-magnitude estimates of structure dimensions for chosen experimental conditions. Finally, our study suggests that control over steepness of concentration gradients in

combination with supramolecular chemistry can offer promising platform for design of materials of defined sizes, which has not been fully developed so far.

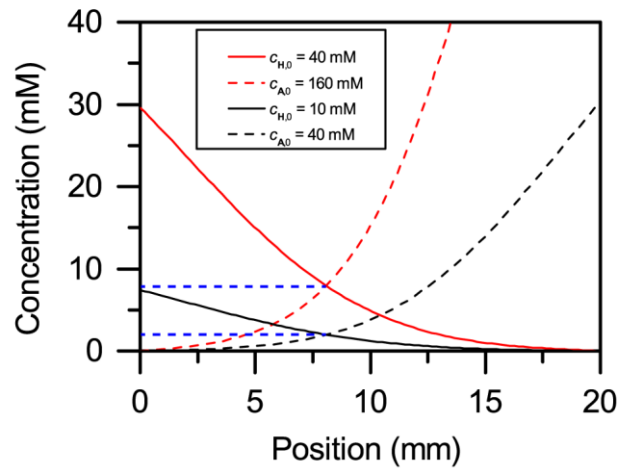
References

- 1 Newman, E. A. & Zahs, K. R. Calcium waves in retinal glial cells. *Science* **275**, 844-847 (1997).
- 2 Straub, S. V., Giovannucci, D. R. & Yule, D. I. Calcium wave propagation in pancreatic acinar cells - functional interaction of inositol 1,4,5-trisphosphate receptors, ryanodine receptors, and mitochondria. *J. Gen. Physiol.* **116**, 547-559 (2000).
- 3 Mair, T., Warnke, C., Tsuji, K. & Muller, S. C. Control of glycolytic oscillations by temperature. *Biophys. J.* **88**, 639-646 (2005).
- 4 Reich, J. G. & Sel'kov, E. E. *Energy metabolism of the cell: A theoretical treatise.* (Academic Press, 1981).
- 5 Dzeja, P. P. & Terzic, A. Phosphotransfer reactions in the regulation of atp-sensitive k⁺ channels. *FASEB J.* **12**, 523-529 (1998).
- 6 Dzeja, P. P. & Terzic, A. Phosphotransfer networks and cellular energetics. *J. Exp. Biol.* **206**, 2039-2047 (2003).
- 7 Tabony, J., Glade, N., Demongeot, J. & Papaseit, C. Biological self-organization by way of microtubule reaction-diffusion processes. *Langmuir* **18**, 7196-7207 (2002).
- 8 Turing, A. M. The chemical basis of morphogenesis. *Philos. Trans. R. Soc. London, Ser. B* **237**, 37-72 (1952).
- 9 Zaikin, A. N. & Zhabotinsky, A. M. Concentration wave propagation in two-dimensional liquid-phase self-oscillating system. *Nature* **225**, 535-537 (1970).
- 10 Kondo, S. & Asai, R. A reaction-diffusion wave on the skin of the marine angelfish pomacanthus. *Nature* **376**, 765-768 (1995).
- 11 Kondo, S. The reaction-diffusion system: A mechanism for autonomous pattern formation in the animal skin. *Genes Cells* **7**, 535-541 (2002).
- 12 Jiang, T. X. *et al.* Integument pattern formation involves genetic and epigenetic controls: Feather arrays simulated by digital hormone models. *Int. J. Dev. Biol.* **48**, 117-135 (2004).
- 13 Noorduyn, W. L., Grinthal, A., Mahadevan, L. & Aizenberg, J. Rationally designed complex, hierarchical microarchitectures. *Science* **340**, 832-837 (2013).
- 14 Shim, T. S., Yang, S. M. & Kim, S. H. Dynamic designing of microstructures by chemical gradient-mediated growth. *Nat. Commun.* **6**, 6584 (2015).
- 15 Lovrak, M. *et al.* Free-standing supramolecular hydrogel objects by reaction-diffusion. *Nat. Commun.* **8**, 15317 (2017).
- 16 Dirksen, A., Dirksen, S., Hackeng, T. M. & Dawson, P. E. Nucleophilic catalysis of hydrazone formation and transimination: Implications for dynamic covalent chemistry. *J. Am. Chem. Soc.* **128**, 15602-15603 (2006).
- 17 Larsen, D., Pittelkow, M., Karmakar, S. & Kool, E. T. New organocatalyst scaffolds with high activity in promoting hydrazone and oxime formation at neutral ph. *Org. Lett.* **17**, 274-277 (2015).
- 18 Grzybowski, B. A. *Chemistry in motion: Reaction-diffusion systems for micro- and nanotechnology.* (Wiley, 2009).

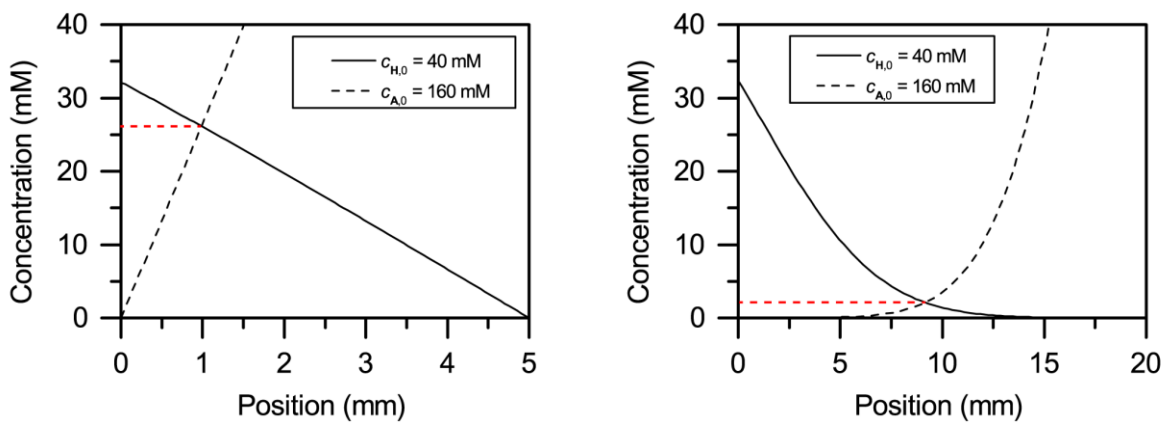
Supplementary Information



Supplementary Figure 1. Effect of a supramolecular pattern on the diffusion of a food-grade dye (chemical composition unknown) through 1% agar. a) Photographs of diffusion at different time points. The red arrow indicates the location of the supramolecular pattern in agar. **b)** Distance traveled in 1% agar. **c)** Distance diffused in 1% agar with the supramolecular patter. The food-grade dye used was purchased in a supermarket and diluted 4 times.



Supplementary Figure 2. Effect of initial concentration of H and A on their respective concentration profiles after 12 hours of diffusion. The initial concentration of H and A were denoted as $c_{H,0}$ and $c_{A,0}$. The blue dashed line indicates the point in the reaction zone where $c_H^* = c_A^* = c^*$. The reaction between **H** and **A** was not taken into account to demonstrate pure diffusional effects.



Supplementary Figure 3. Effect of diffusion distance on concentration profiles of H and A after 6 hours of diffusion. The initial concentrations of **H** and **A** were denoted as $c_{H,0}$ and $c_{A,0}$. The blue dashed line indicates the point in the reaction zone where $c_H^* = c_A^* = c^*$. The reaction between **H** and **A** was not taken into account to demonstrate pure diffusional effects.



4

Supramolecular Gluing of Polymeric Hydrogels

Abstract

We report a simple method for gluing hydrogels together, based on supramolecular chemistry. The gluing is achieved by reactive self-assembly of a low molecular weight gelator at the interface of the two hydrogels.

Introduction

Connecting pieces of solid material for the purpose of construction or repair has been a human need since the dawn of mankind, and today we can easily attach pieces of solid material, such as wood, metal or even bone, simply by mechanical connection (e.g. using screws), gluing or welding (in the case of metals and thermoplastics). In contrast, soft biological tissues and hydrogels require different techniques for connecting.^{1, 2} Strategies for connecting hydrogels include *in situ* polymerization³, polymer-based adhesives⁴, self-healing⁵, polymer interdiffusion⁶, employment of electrolytic polymer liquid⁷, ultraviolet irradiation³, pH change⁸, wrinkle formation⁹, or an electrophoretic transport of polymers to the interface^{10, 11}. However, most of these approaches require additional equipment and are often highly specific for certain materials. Only recently a rare example of a generic and simple solution for gluing hydrogels and biological tissues has been reported, in which a solution of nanoparticles acts as a glue.^{12, 13} In this work we report a novel and simple way for gluing polymeric gels that is based on the reactive self-assembly of a supramolecular gelator at the interface of two hydrogels.

Results and discussion

Recently, we have reported a supramolecular gelator that is formed by an acid catalyzed chemical reaction between hydrazide (**H**) and aldehyde (**A**) leading to the formation of trishydrazone **HA₃** (Figure 1a).^{14, 15} This two-component reaction proved highly versatile to a range of different conditions^{16, 17} and setups including reaction-diffusion.¹⁸ Therefore, we envisioned that this reaction could be used for gluing different types of hydrogels. In our method, when two pieces of polymer hydrogel are to be connected, one is first loaded with **H** and the other with **A**. They are then manually brought in contact with each other, and left standing to allow the formation of **HA₃** supramolecular fibrils to take place. Because the contact area between two polymer hydrogels is also the interface between **H** and **A**, we anticipated that the reaction between **H** and **A** would occur across the interface resulting in the formation and local deposition of fibrous **HA₃** aggregates. In this way, the resulting supramolecular hydrogel **HA₃** connects the other two pieces of hydrogel by crossing the interface between them. The general approach is shown in Figure 1.

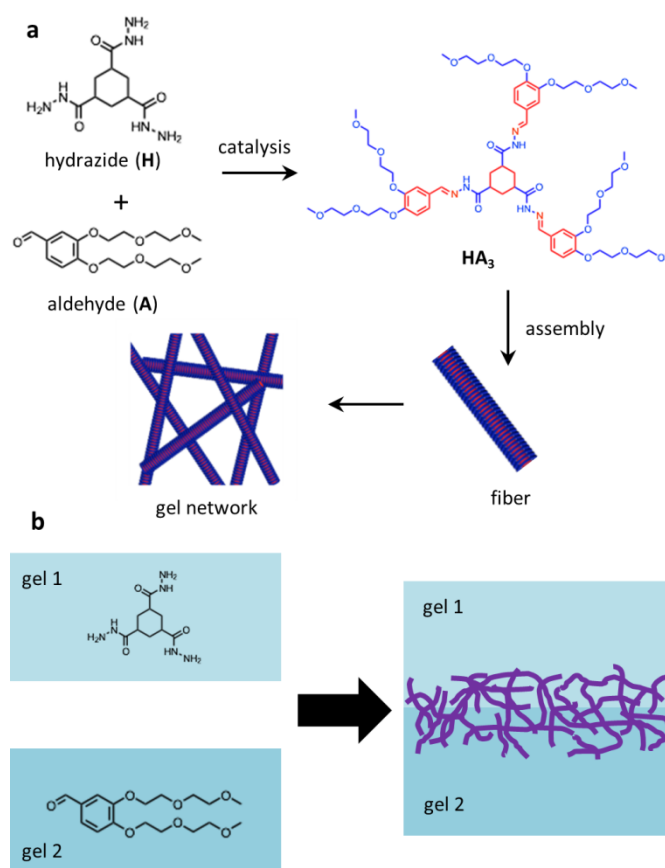


Figure 1. The concept of gluing gels using a supramolecular hydrogel. a) The formation of supramolecular hydrogel. Water soluble molecules **H** and **A** react to form a gelator HA_3 which subsequently stacks into fibers and forms a supramolecular hydrogel. b) Two pieces of polymer gel were loaded with **H** and **A**, respectively. Upon bringing the pieces into contact, supramolecular fibrils of HA_3 are formed at the interface resulting attachment of two pieces.

To investigate this hypothesis, we soaked two strips of polymer hydrogel made from the same or different crosslinked polymers in solutions of 40 mM **H** and 160 mM **A** at pH = 4.0 overnight (each piece in one of the solutions). Subsequently, the gels were taken out of the solutions, placed on a glass slide, connected, and left standing in a humid atmosphere. After standing overnight the interface between two gels was not clearly visible anymore. Instead, a white, non-transparent band was created around the contact point. This band was an indication of HA_3 formation.¹⁸ When the gel construct was carefully taken off the glass slide, the two gel pieces remained connected and could be clamped as one piece in a hanging position for imaging (Figure 2a-c). When we tried to repeat the procedure with polymer gels that were not loaded with any reactants, the gels disconnected upon lifting from the glass slide. Also, simply applying several drops of **H** and **A** solution to the respective gel surfaces and bringing them into contact after several minutes of sorption did not yield any white band and gels were easily disconnected. To test the universality of our approach, we glued together different types of polymer hydrogels, such as agar, alginate, and polyacrylamide. For all types, both

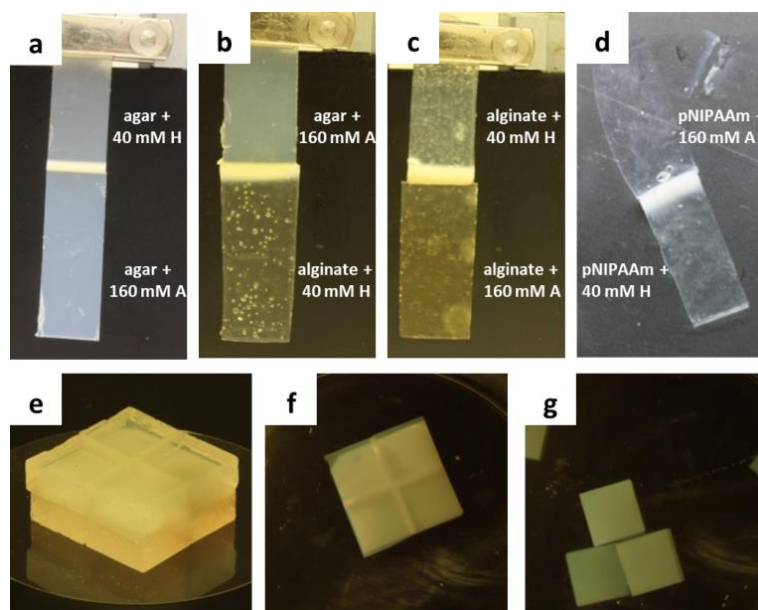


Figure 2. Gluing gels using the trishydrazone gelation reaction. a) Two separate pieces of 3 % agar glued together. **b)** 3 % agar (top) and 3% alginate (bottom) glued together. **c)** Two pieces of 3% alginate glued together. **d)** Two pieces of polyacrylamide (PAAm) gel glued together floating in water. **e)** The cuboid consisting of 8 agar pieces glued together. **f)** The cuboid in water did not disassemble into the constituent pieces. **g)** The cuboid consisting of 8 non-glued pieces disassembled when immersed in water (not all are visible in the image).

homo and hetero combinations would form a permanent bond using this approach (Figure 2a-d).

Interestingly, this method of gluing can also be used to fabricate new gel objects from multiple gel pieces. To demonstrate this, we soaked four pieces of agar in a solution containing **H**, and four pieces of agar in a solution containing **A**, and assembled them subsequently into a $2 \times 2 \times 2$ cube (using an alternating **H** and **A** loading pattern). We left the assembled cube standing overnight for gluing to take place (Figure 2e). To test whether the assembly of the object was successful using our gluing method, we immersed the $2 \times 2 \times 2$ cube in water and subsequently agitated the container for roughly 20 seconds. As can be seen in Figure 2f, the glued object remained in one piece. In contrast, when we assembled a similar cube from pure agar gel blocks, the cube fell apart into constituent pieces immediately after immersing it into water and shaking the container (Figure 2g). This result indicates that this gluing method can be used even in somewhat more complex situations than simply attaching two pieces of gel together.

To evaluate the mechanism of gluing, we took a closer look at the interface of two glued gels. We compared the appearance of the interface in the state when the gels were glued and when they were carefully separated. As can be seen in Figure 3a, the interface of two gels (marked with a red dotted line) cannot be very clearly distinguished after the gels were glued. However, after carefully separating them by manually pulling them apart, **HA**₃ aggregates were clearly visible on both sides of the interface (marked with yellow rectangles). This result indicates that the supramolecular gelator **HA**₃ connects two polymer gels by spanning over the interface. Additionally, we confirmed our

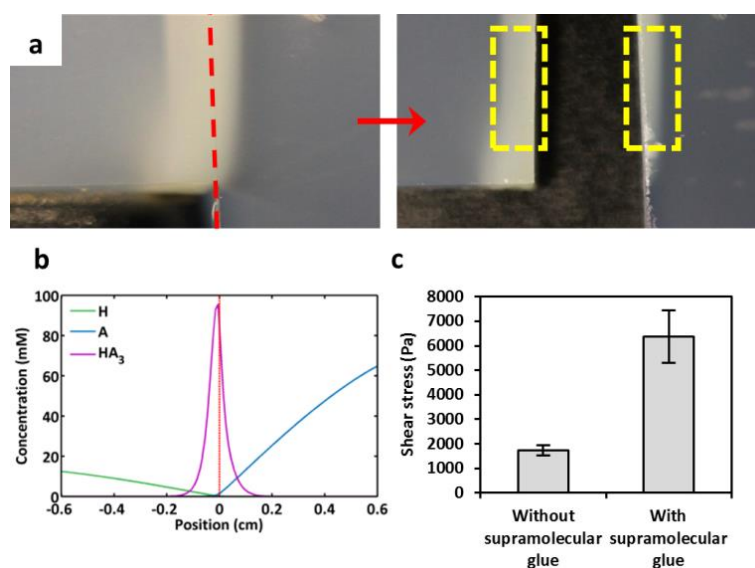


Figure 3. The interface of two pieces of 3% agar glued using HA₃ supramolecular glue. a) The left piece was loaded with **H** (40 mM), and the right piece was loaded with **A** (160 mM). The red dotted line indicates the interface. Two yellow rectangles indicate the presence of **HA₃** on both sides of the interface after the separation of pieces. b) Concentration profiles (from RD model) of **H**, **A** and **HA₃** in the gels and at the interface (red dotted line) after 24 hours of gluing. The initial concentrations of **H** and **A** were 40 and 160 mM, respectively. c) Detachment stress of glued and non-glued pieces of agar determined using a shear test plotted as mean \pm s.d. ($n = 3$). Two pieces of 3% agar loaded with **H** and **A**, respectively, were attached to the top and bottom plate of rheometer. They were brought into contact by slowly lowering the top plate. After 2 hours of contact, the top plate was rotated at a constant shear rate of 0.001 s^{-1} until fracture was observed.

hypothesis using a reaction diffusion model for this system.¹⁸ The model showed that, indeed, if two compartments with **H** and **A** are in direct contact, the gelator **HA₃** will form supramolecular fibrils across the interface (Figure 3b).

One of the important properties of a glue to effectively attach two parts of a material is the strength of the connection. Therefore, we measured the shear stress (see Supplementary Information for details) needed to separate two pieces of agar kept in contact for 2 hours with and without supramolecular gelator **HA₃** acting as a glue. As can be seen in Figure 3c, a higher shear stress had to be applied to separate glued gels ($6.4 \pm 1.1 \text{ kPa}$) compared to non-glued gels ($1.7 \pm 0.2 \text{ kPa}$). This result clearly indicates that the supramolecular gel of **HA₃** acts as a glue. Applying only several drops of **H** and **A** to the respective gel surfaces, as mentioned before, did not show any difference in shear stress compared to non-glued gels.

Conclusion

In conclusion, we have developed a novel and simple approach for gluing polymer gels based on supramolecular gel formation. Prior to gluing, polymer gels do not have to be chemically modified nor treated in any other way, except being soaked into the constituents of the supramolecular glue. This implies that polymer gels can be

used in their native state and unreacted compounds can be easily washed off by soaking the glued gels in water afterwards. Although loading polymer gels with reactants that have to be washed off later implies impracticalities in preparation gels for gluing, our approach shows how simple and modular supramolecular chemistry can be used as a solution to problems such as gluing of soft matter.

References

- 1 Bochynska, A. I., Hannink, G., Grijpma, D. W. & Buma, P. Tissue adhesives for meniscus tear repair: An overview of current advances and prospects for future clinical solutions. *J. Mater. Sci.: Mater. Med.* **27**, 85 (2016).
- 2 Spotnitz, W. D. & Burks, S. Hemostats, sealants, and adhesives iii: A new update as well as cost and regulatory considerations for components of the surgical toolbox. *Transfusion* **52**, 2243-2255 (2012).
- 3 Saito, J. *et al.* Robust bonding and one-step facile synthesis of tough hydrogels with desirable shape by virtue of the double network structure. *Polym. Chem.* **2**, 575-580 (2011).
- 4 Duarte, A. P., Coelho, J. F., Bordado, J. C., Cidade, M. T. & Gil, M. H. Surgical adhesives: Systematic review of the main types and development forecast. *Prog. Polym. Sci.* **37**, 1031-1050 (2012).
- 5 Faghihnejad, A. *et al.* Adhesion and surface interactions of a self-healing polymer with multiple hydrogen-bonding groups. *Adv. Funct. Mater.* **24**, 2322-2333 (2014).
- 6 Sahlin, J. J. & Peppas, N. A. Enhanced hydrogel adhesion by polymer interdiffusion: Use of linear poly(ethylene glycol) as an adhesion promoter. *J. Biomater. Sci., Polym. Ed.* **8**, 421-436 (1997).
- 7 Tamagawa, H. & Takahashi, Y. Adhesion force behavior between two gels attached with an electrolytic polymer liquid. *Mater. Chem. Phys.* **107**, 164-170 (2008).
- 8 Alfhaid, L., Seddon, W. D., Williams, N. H. & Geoghegan, M. Double-network hydrogels improve ph-switchable adhesion. *Soft Matter* **12**, 5022-5028 (2016).
- 9 Kato, M., Tsuboi, Y., Kikuchi, A. & Asoh, T.-A. Hydrogel adhesion with wrinkle formation by spatial control of polymer networks. *J. Phys. Chem. B* **120**, 5042-5046 (2016).
- 10 Asoh, T.-A. & Kikuchi, A. Electrophoretic adhesion of stimuli-responsive hydrogels. *Chem. Commun.* **46**, 7793-7795 (2010).
- 11 Techawanitchai, P. *et al.* Photo-switchable control of ph-responsive actuators via ph jump reaction. *Soft Matter* **8**, 2844-2851 (2012).
- 12 Rose, S. *et al.* Nanoparticle solutions as adhesives for gels and biological tissues. *Nature* **505**, 382-385 (2014).
- 13 Meddahi-Pelle, A. *et al.* Organ repair, hemostasis, and in vivo bonding of medical devices by aqueous solutions of nanoparticles. *Angew. Chem., Int. Ed.* **53**, 6369-6373 (2014).
- 14 Boekhoven, J. *et al.* Catalytic control over supramolecular gel formation. *Nat. Chem.* **5**, 433-437 (2013).
- 15 Poolman, J. M. *et al.* Variable gelation time and stiffness of low-molecular-weight hydrogels through catalytic control over self-assembly. *Nat. Protoc.* **9**, 977-988 (2014).
- 16 Maity, C., Hendriksen, W. E., van Esch, J. H. & Eelkema, R. Spatial structuring of a supramolecular hydrogel by using a visible-light triggered catalyst. *Angew. Chem., Int. Ed.* **54**, 998-1001 (2015).
- 17 Versluis, F. *et al.* Negatively charged lipid membranes catalyze supramolecular hydrogel formation. *J. Am. Chem. Soc.* **138**, 8670-8673 (2016).
- 18 Lovrak, M. *et al.* Free-standing supramolecular hydrogel objects by reaction-diffusion. *Nat. Commun.* **8**, 15317 (2017).

Supplementary Information

Materials. Agar, alginate, solution of acrylamide (40%) and solution of *N,N'*-methylenebisacrylamide (2%) were purchased from commercial sources and used as provided. Hydrazide (**H**) and aldehyde (**A**) were synthesized as described in our earlier work.¹ All stock solutions of **H**, **A**, and polymers were prepared in 100 mM phosphate buffer (pH = 4.0) unless stated otherwise.

Preparation of agar. 3% agar (mass fraction, *w*) was prepared by dissolving agar in the appropriate amount of phosphate buffer. To completely dissolve the agar, the mixture was heated and stirred at ~100 °C until the solution turned transparent. The solution was subsequently allowed to cool down and left to solidify.

Preparation of alginate. Alginate gels were prepared according to the procedure proposed by Draget et al.² Briefly, a powder of CaCO₃ was dispersed in water. Then, dry sodium alginate was added and this dispersion was heated at 100 °C in a closed vial until all alginate was dissolved. The solution was subsequently allowed to cool to room temperature. Finally, an aqueous solution of glucono- δ -lactone (GDL) was added, and the resulting solution was stirred briefly. The alginate gel was formed by leaving the solution standing overnight. Unless otherwise stated, final concentrations of CaCO₃, alginate, and GDL were 12.5 mM, 1.5 % (mass fraction, *w*), and 40 mM, respectively, giving Ca²⁺ crosslinked alginate gels with pH = 4.5.

Preparation of poly(*N*-isopropylacrylamide) gel. Solution of acrylamide (40%, 2.5 mL) and solution of *N,N'*-methylenebisacrylamide (2%, 1.5 mL) were mixed with water (6 mL). The mixture was degassed for 15 minutes and the solution of ammonium persulfate (75 mg mL⁻¹, 100 μ L) was added subsequently. Finally, 10 μ L of tetramethylethylenediamine (TEMED) was added and the resulting mixture was briefly stirred and left standing for 1 hour to form a gel. Unreacted compounds were removed by immersing gel in water for 3 hours while exchanging water every 30 minutes.

Gluing pieces of polymeric gel. Alginate, agar and polyacrylamide gels were prepared in a Teflon mold (10 \times 5 \times 0.3 cm³) as described above. Two rectangular pieces were cut out of the mold and soaked separately in the solutions of **H** (40 mM) and **A** (120 mM) overnight. Next, they were taken out of the solutions, blotted with a blotting paper to remove the excess of the solutions, brought into contact with their shortest sides, and left standing overnight again. The following day they were clamped using a Hoffman clamp in hanging position for imaging by camera.

A gel cube was assembled in a similar way, but using 8 cube shaped pieces of agar. 4 of them were soaked in the solution of **H**, and 4 in the solution of **A**. After soaking the pieces overnight and blotting with a blotting paper to remove the excess of the

solutions, they were assembled in an alternating manner into a cube. The cube was then left standing overnight for gluing to take place.

Measuring the detachment stress of glued gels using a rheometer. To measure detachment stress of glued gels we used an AR G2 rheometer (TA Instruments) in constant shear-rate mode (“Hold Peak” step in the software). The plate-plate configuration was used with the top plate being 25 mm in diameter. First, a textile plaster was glued to the top plate of the rheometer using double-sided adhesive tape, to completely cover its surface, and any pieces of plaster sticking outside the plate were carefully cut away with a razor blade, after which the top plate was mounted to the rheometer. A plastic rim 5 cm in diameter and *ca.* 5 mm in height was glued to the bottom plate using adhesive tape. The rim was centered relative to the top plate. Care should be taken that the connection between the rim and the bottom plate of the rheometer is properly sealed to avoid leakage of liquid gel-precursor solution in later steps. A circular piece of Kapton® polyimide film slightly smaller in diameter than the rim was inserted inside the rim. The top plate was lowered to 3500 μm from the surface of the bottom plate, 10 mL of hot 3% agar solution was poured inside the rim, and everything was left to cool down for 30 minutes. The rim was then removed, and the excess of agar was removed by cutting around the top plate leaving the cylinder of gel attached to the top plate. The top plate was carefully lifted off from the bottom plate and removed from the rheometer, as well as the Kapton® polyimide film. Next, the double-sided adhesive tape was glued to the bottom plate and a textile plaster was glued on top of it. The area covered with the textile plaster should be somewhat bigger than the plastic rim. A new plastic rim 5 cm in diameter was glued on top of the area covered with the textile plaster, 10 mL of hot 3% agar solution was poured inside the rim, and everything was left to cool down for 30 minutes. Again, the rim was removed. A Kapton® polyimide film was placed on top of the gel. The 40 mm in diameter top plate was mounted to the rheometer, and it was lowered until it pressed gently against the gel with the Kapton® polyimide film (the detected normal force should not exceed 1 N). This step was done to ensure that the surface of the gel is flat. The plate was kept in contact with the gel for 10 minutes. Afterwards, the top plate was lifted off, while keeping the Kapton® polyimide film on the gel, and removed from the rheometer. The 25 mm plate with the previously formed cylinder was mounted again into the rheometer, and it was carefully brought into contact with the Kapton® polyimide film on the bottom gel. From this contact point, the top plate with the gel was raised 500 μm . The Kapton® polyimide film was removed, and the measurement program was started. The program consisted of the following steps: the top plate with the gel was lowered by 600 μm (at rate 5 $\mu\text{m s}^{-1}$) causing the top gel and the bottom gel to get into the contact, waiting for 2 hours, and, finally, applying constant shear of 10^{-3} s^{-1} until the contact between gels is broken. From the resulting shear stress vs. strain curves, we determined the stress required for these two pieces of gels to be separated.

The procedure was the same for hydrogels loaded with **H** and **A**. Loading was achieved by adding the appropriate amounts of **H** and **A**, respectively, into the initial mixture of agar and phosphate buffer.

Supplementary references

- 1 Boekhoven, J. *et al.* Catalytic control over supramolecular gel formation. *Nat. Chem.* **5**, 433-437 (2013).
- 2 Draget, K. I., Ostgaard, K. & Smidsrod, O. Alginate-based solid media for plant-tissue culture. *Appl. Microbiol. Biotechnol.* **31**, 79-83 (1989).

The Effect of Supramolecular Hydrogel on Cell Viability and Proliferation

Abstract

Supramolecular hydrogels show a great potential as an artificial extracellular matrix since they can be relatively easily functionalized with various signaling cues for cell attachment. This study shows the influence of precursor molecules for the formation of trishydrazone supramolecular gel on cell viability. Additionally, we report the cytotoxicity of gel itself.

Introduction

In the last few decades hydrogels have emerged as a promising material for mimicking extracellular matrix (ECM) due to their physical and chemical properties.^{1,2} So far, researchers have developed a wide range of nature-inspired synthetic hydrogels that can support cell attachment, proliferation, and differentiation.^{3,4} However, the morphological/structural homogeneity of synthetic hydrogels does not match the natural ECM which is structured at all scales. Hierarchical organization in the natural ECM regulates cellular adhesion, migration, proliferation, differentiation and morphogenesis. Therefore, significant efforts have been made to produce gels with well-defined structural organization ranging from micrometer scale to nanometer scale.⁵ Apart from single- and double-network⁶⁻⁸ polymeric hydrogels that are usually used as ECM, one more class of hydrogels have gained attention as a potential candidate for mimicking ECM – supramolecular gels.⁹ Supramolecular gels are gels made out of small molecules (also called low molecular weight gelators, LMWGs) which are held together by non-covalent interactions. These gels can be easily tailored according to wanted functionalities due to the relative simplicity of the organic synthesis of small molecules. Considering this advantage of supramolecular gels, combining supramolecular gels with polymeric gels might lead to a new class of double-network materials for mimicking natural ECM. In our previous work we have developed a hybrid gel consisting of alginate and a supramolecular gel, and used this system to make gels with defined structure. The modular nature of our supramolecular system combined with the possibilities of spatial structuring might offer a promising platform for the development of structured artificial ECMs. Taking into account that structured gels have an impact on cell attachment, proliferation, and differentiation, we envisioned that the system that we have developed could provide good artificial ECM.^{4,5,10,11} Additionally, our gel system contains only physical cross links compared to most other double-network gels whose networks are chemically cross-linked, either one or both. Despite similar possibilities being reported before¹², the potential of these kind of systems for cell related applications has not been investigated.

In this chapter we investigate the potential of hybrid alginate/supramolecular hydrogel network as ECM for 2D cell cultures. First, we investigate the cytotoxicity of different gel components. Next, we analyze how to prevent potential cytotoxicity. Finally, we explore cell viability on hybrid alginate/supramolecular hydrogel network and discuss design requirements for future development of similar ECMs.

Results and discussion

As previously reported, we prepared hybrid alginate/supramolecular hydrogel objects from small molecular self-assembling building blocks using reaction-diffusion approach.¹³ Briefly, diffusion of hydrazide **H** and aldehyde **A** through alginate gel matrix

leads to the localized formation of the trishydrazone gelator **HA**₃ which then assembles into fibers and, finally, forms a fibrous network within the alginate matrix.¹⁴ The obtained alginate/**HA**₃ hydrogel objects ranged in size from micro- to millimeter scale. To be suitable as artificial ECM, the alginate/**HA**₃ hydrogel materials should not exhibit any toxic effects to cells. Because of the known biocompatibility of alginate, we focused on the potential cytotoxicity of **HA**₃. We also investigated the effect of pure **H** and **A** on the viability of cells since these precursor molecules for the formation of **HA**₃ might remain in alginate/**HA**₃ hydrogel in unreacted form. To investigate their cytotoxicity, we used two adherent cell lines – mouse embryonic fibroblasts (3T3) and human embryonic kidney (HEK 293) cells. We cultured 3T3 and HEK 293 cells in cell culture plates for 18-20 hours following standard procedure (see Supplementary Information). Afterwards, we replaced initial cell culture medium (DMEM supplemented with 10% Fetal Bovine Serum and 1% Penicilin/Streptomycin) with cell culture medium containing **H** (2.5-10 mM), and **A** (25-100 mM), respectively. The investigated concentration ranges were chosen based on the preparation procedure for alginate/**HA**₃ hydrogel (10-40 mM for **H**, and 100-400 mM for **A**; see Supplementary Information for details), and decreased 4 times due to dissolution limitations in cell culture medium. We chose to use 1:10 ratio of concentrations of **H** to **A** to increase influx of **A** into alginate thereby leading to faster formation of **HA**₃ in alginate, and preventing significant diffusion of **H** out of alginate. This was important to ensure that the final concentration of **HA**₃ in alginate is comparable to the initial concentration of **H** in alginate. It can be seen from Figure 1a and b that both cell lines cultured on medium with **H** had a stretched morphology, similar to the morphology in the control experiment, while both cell lines cultured on medium with **A** had a spherical morphology. The tests of metabolic activity (for experimental details see Supplementary Information) showed that the viability of cells was significantly lower in the cell culture medium with **H** compared to the control experiment, whereas the metabolic activity of cells cultured in the medium with **A** was negligible (Figure 1c). This result suggests that **A** exhibits higher cytotoxicity than **H** in the concentration ranges that were used for the preparation of alginate/**HA**₃ hydrogel. Therefore, its concentration in ECM for use with mammalian cells should be kept as low as possible. However, we did not investigate what is the highest concentration allowed. The cytotoxicity of benzaldehyde for different cell lines has been also confirmed by other researchers.^{15,16} To prepare alginate/**HA**₃ hydrogels with negligible content of **A**, we considered two approaches: the ratio of **H** to **A** in preparation procedure could be decreased to 1:3 (which might lead to decreased final concentration of **HA**₃ in alginate due to increased diffusion of **H** out of alginate), or the samples of alginate/**HA**₃ hydrogel have to be thoroughly washed. In the end, we decided to proceed with washing of alginate/**HA**₃ hydrogels to remove residual **H** and **A**. Moreover, since **H** was in stoichiometric deficiency, its remaining concentration in alginate/**HA**₃ hydrogel before washing should be negligible (assuming full conversion), thus posing no significant cytotoxic effects. Here, we assumed that dissociation of **HA**₃ is negligible

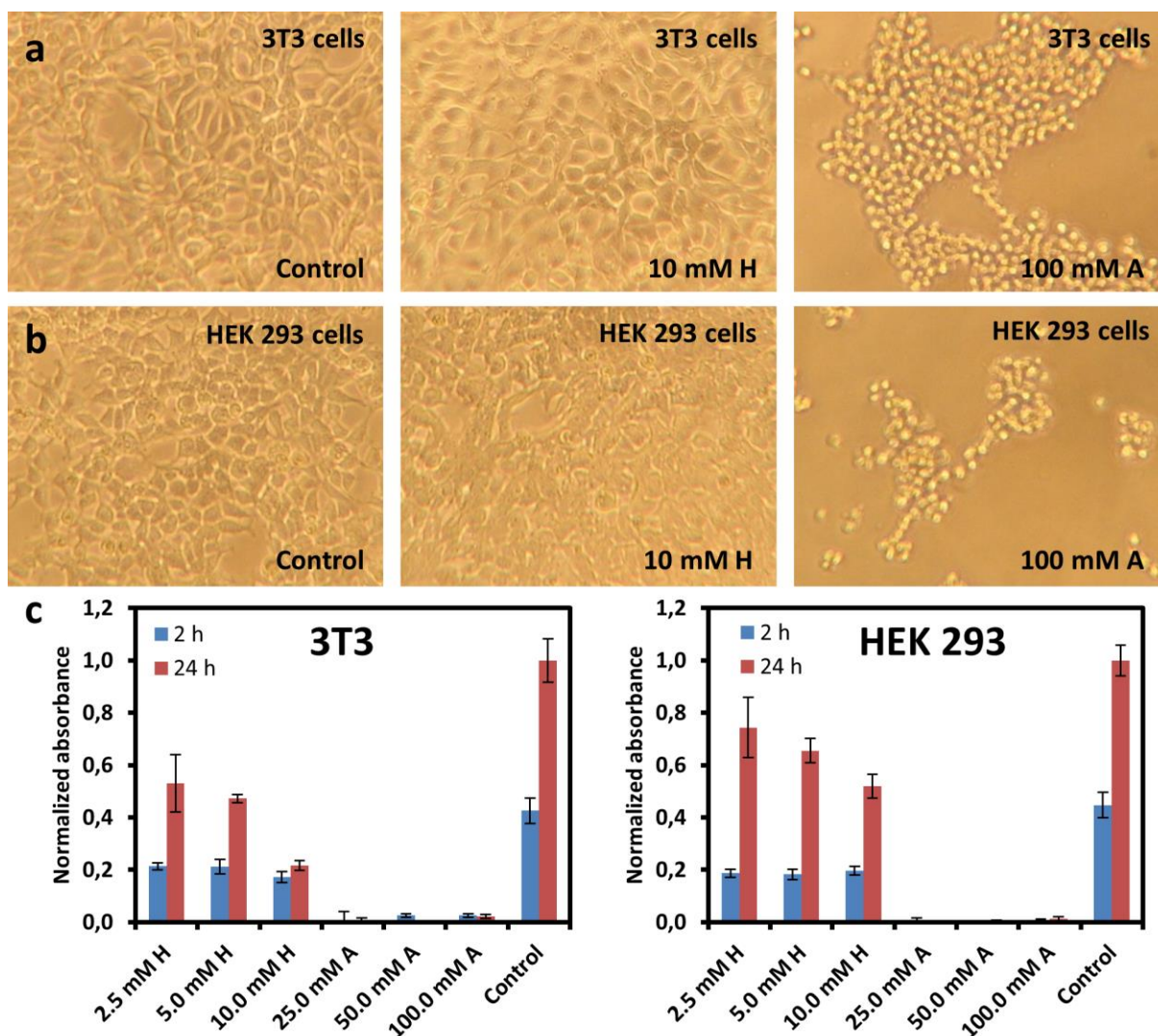


Figure 1. The cytotoxicity of H and A. a) The morphology of 3T3 cells after 24 hours of incubation on the surface of a well in cell culture medium, cell culture medium with 10 mM H, and cell culture medium with 100 mM A. b) The morphology of HEK 293 cells after 24 hours of incubation on the surface of a well in cell culture medium, cell culture medium with 10 mM H, and cell culture medium with 100 mM A. c) The metabolic activity tests conducted on 3T3 and HEK 293 cells after 2 and 24 hours of incubation. Images were taken with 10× magnification objective.

since we observed previously that alginate/HA₃ hydrogel can be stored for months in water without visible degradation.

Following the cytotoxicity tests, we briefly investigated how thoroughly alginate/HA₃ hydrogels have to be washed to remove residual A before dispensing cells. We prepared alginate/HA₃ hydrogels as described before and washed them several times with cell culture medium (see Supplementary Information for details of preparation and washing procedure). After each washing step the washing medium (WM) was collected and analyzed for its effect on cell morphology and viability. As can be seen in Figure 2 and Supplementary Figure 1, the general observation for both cell lines was that the cells were not able to proliferate significantly in any sample of WM compared to the control experiment, most likely due to high concentration of A in WM.

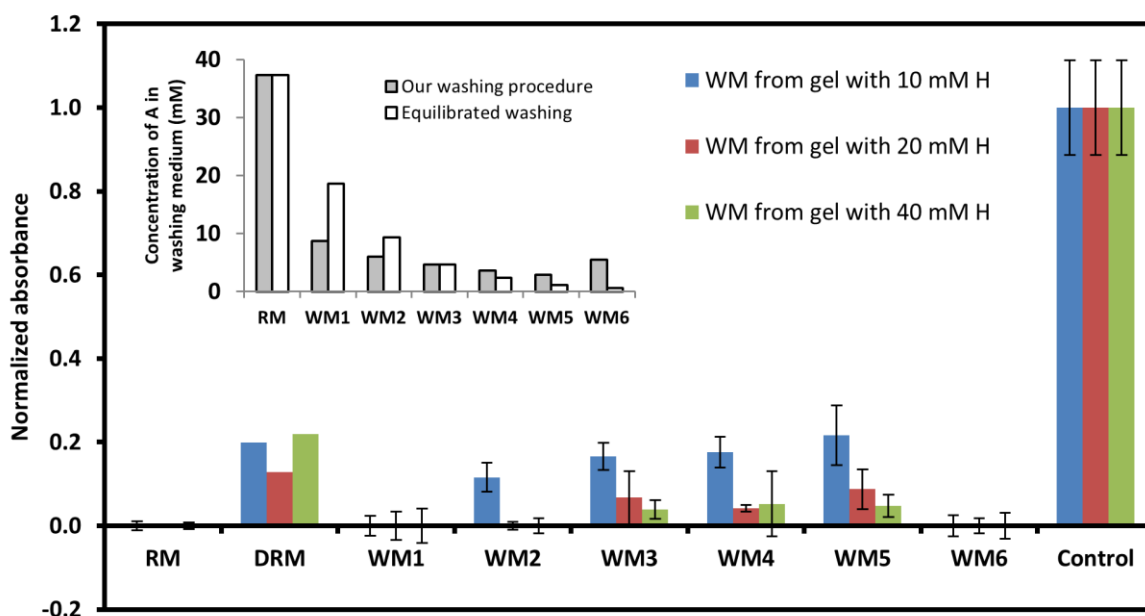


Figure 2. Metabolic activity of 3T3 cells cultured for 2 hours in cell culture medium (DMEM supplemented with 10% Fetal Bovine Serum and 1% Penicillin/Streptomycin) used previously for washing alginate/HA₃ hydrogels (called washing medium, WM). RM – the reaction mixture after the formation of gels collected from the top of the gels; DRM – the reaction mixture diluted with cell culture medium (25 μ L of RM with 75 μ L of cell culture medium); WM1 to WM5 – cell culture medium exchanged each hour; WM6 – cell culture medium left overnight on top of the gel. Inset shows the variation of the concentration of **A in WM obtained from numerical simulations. Comparison between the washing procedure that we used (exchanging WM each 1 hour) against the procedure in which gels would equilibrate with WM for at least 4 hours in each step is given. Calculations are based on equal volumes of gel and WM ($V_{\text{gel}}:V_{\text{wm}} = 1:1$) for alginate/HA₃ hydrogel with 37 mM **A** remaining initially (corresponding to alginate with 10 mM **H** initially). The similar volume ratio ($V_{\text{gel}}:V_{\text{wm}} = 1.2:1$) was used in our experiments due to the limited volume of a well.**

Although the metabolic activity of 3T3 cells in WM1-5 showed systematic increase, the metabolic activity suddenly dropped in WM6. This result indicates that diffusion of unreacted compounds, predominantly **A**, from alginate/HA₃ hydrogel to WM takes longer than we originally anticipated. Therefore, we simulated washing of alginate/HA₃ hydrogel using the model¹³ developed before to confirm our experimental observation. Indeed, the simulations showed good correlation with our experiments. First five washing steps showed systematic decrease of **A** in WM leading to increased viability of cells. However, the concentration of **A** increased in WM6, and it was around 5 mM (inset in Figure 2). On the other hand, the model predicts that the remaining concentration of **A** in WM6 would be around 0.5 mM if concentration of **A** equilibrated throughout the system in each washing step. Although optimization of washing might seem a trivial task, time-consuming preparation of this type of ECM might hinder its application potential considering that faster solutions are usually preferred.

Finally, we investigated whether alginate/HA₃ hydrogel is a viable ECM. Based on the previous findings, we prepared 4.8 \times smaller volume of alginate/HA₃ hydrogels to increase the efficiency of washing, and washed them with Dulbecco's phosphate

buffered saline (DPBS) the same way as before to remove residual **A** before dispensing cells on top of the them (2D environment, see Supplementary Information for details). We observed that gels started to fragment during washing procedure, probably due to their small volume. However, fragmentation was not so severe to cause complete degradation. As can be seen in Figure 3a and 3b, the cells on gels had spherical morphology compared to the control experiment in which the cells had stretched morphology (the surface of wells is properly treated to obtain optimized cell adhesion). This result indicates that after one day of incubation the cells were not able to adhere to the alginate/**HA**₃ hydrogel surface. Since non-adhered cells do not exert optimal metabolic activity, we tested the metabolic activity of cells after one and four days of incubation. It can be clearly seen from Figure 3c that both cell lines show negligible metabolic activity on the alginate/**HA**₃ hydrogels compared to the metabolic activity of cells in the control experiment. This result confirms the visual observation that the cells were not able to adhere and survive on the surface of alginate/**HA**₃ hydrogels. Due to decreased volume of alginate/**HA**₃ hydrogel and increased volume ratio of WM to alginate/**HA**₃ ($V_{\text{gel}}:V_{\text{wm}} = 1:4$), we assumed that the amount of **A** left in the gel was insufficient to pose severe cytotoxic effects to cells. Therefore, this finding indicates that the nature of alginate/**HA**₃ hydrogel cannot promote cell adhesion due to the lack of chemical cues.^{17,18}

Based on the obtained results, we propose several solutions to the current problems with cytotoxicity. First, the alginate/**HA**₃ hydrogels were prepared by using **H** and **A** in the molar ratio of 1:10.¹⁴ Since the formation of **HA**₃ proceeds with the molar ratio of 1:3, **A** will always be in excess meaning that extensive washing is necessary to remove all unreacted **A**. Therefore, the smallest possible excess of **A** (or no excess) should be used in the preparation of **HA**₃ to allow direct use of alginate/**HA**₃ hydrogels. Secondly, when the preparation step is optimized, it is possible, as previously mentioned, that alginate/**HA**₃ gels cannot support the cell proliferation due to the lack of chemical cues on alginate and PEG that promote the attachment of adherent cells.^{17,18} The solution for this problem may be rather simple. It has been shown that multiple types of functional groups, such as fluorophores or sugars, can be coupled to **A**.¹⁹ In this way the groups that would signal cells to attach, such as RGD, could be potentially incorporated into alginate/**HA**₃ hydrogel. Thus, the alginate/**HA**₃ gels functionalized with signaling motifs could be easily prepared using the same procedure as described in this work.

Conclusion

In conclusion, our study shows that **A** is the constituent of alginate/**HA**₃ hydrogel which exhibits the highest level of cytotoxicity in the relevant concentration range. The main reason for such high concentrations of **A** in alginate/**HA**₃ is the excess of **A** used in the preparation procedure. Although this study does not clearly show the potential of

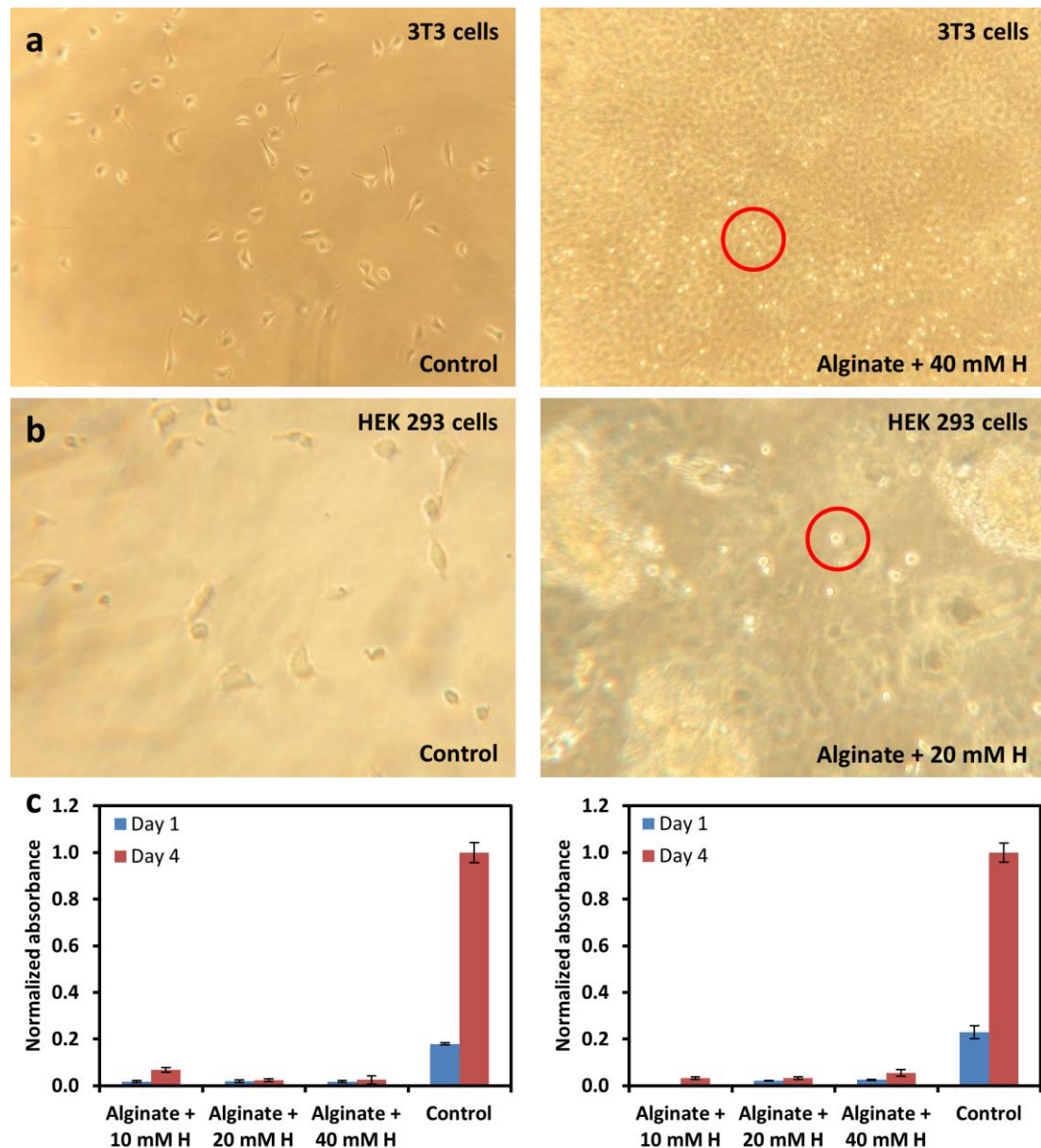


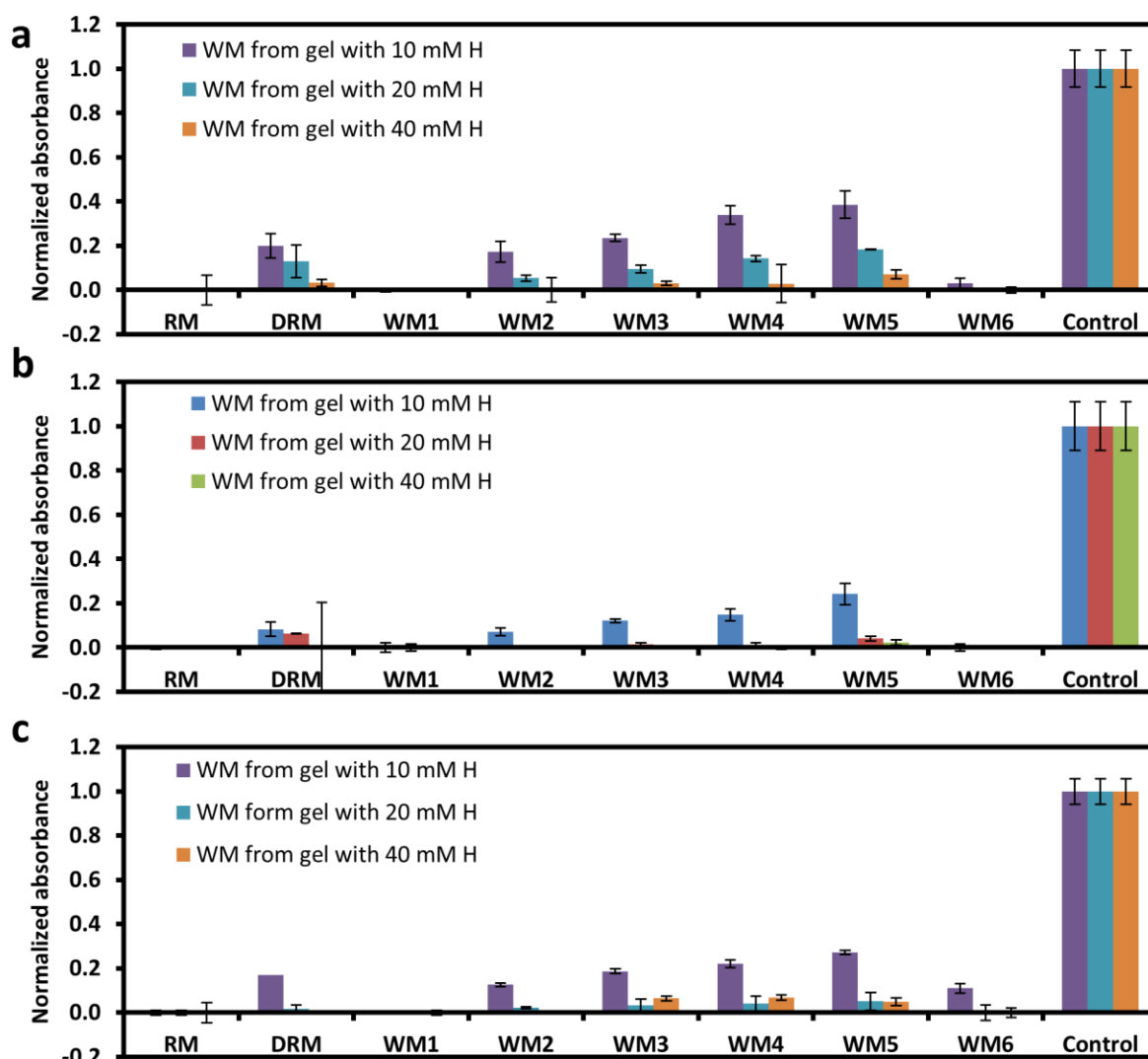
Figure 3. Cells seeded on top of alginate/HA₃ hydrogels. **a)** The comparison of the morphology between 3T3 cells seeded on a commercial cell culture plate optimized for cell proliferation used as a control (left), and the cells seeded on top of alginate/HA₃ hydrogel (right) after one day of incubation. Several 3T3 cells, visible as bright dots, are marked with the red circle for clarity. Their circular morphology indicates the lack of cell adhesion and stretching. **b)** The comparison of the morphology between HEK 293 cells seeded on treated cell culture plate (left) and the cells seeded on alginate/HA₃ hydrogel (right) after one day of incubation. A HEK 293 cell, visible as a bright dot, is marked with the red circle for clarity. Similarly to 3T3 cells, HEK 293 cells also did not adhere and stretch. **c)** The results of metabolic activity tests for 3T3 cells (left) and HEK 293 cells (right).

alginate/HA₃ hydrogel for cell related applications, it identifies problems and suggests steps towards its potential use as an artificial extracellular matrix. Following our suggestions could direct future research towards development of novel types of ECMs.

References

- 1 Park, S. & Park, K. M. Engineered polymeric hydrogels for 3d tissue models. *Polymers* **8** (2016).
- 2 Lowe, S. B., Tan, V. T. G., Soeriyadi, A. H., Davis, T. P. & Gooding, J. J. Synthesis and high-throughput processing of polymeric hydrogels for 3d cell culture. *Bioconjugate Chem.* **25**, 1581-1601 (2014).
- 3 Magin, C. M., Alge, D. L. & Anseth, K. S. Bio-inspired 3d microenvironments: A new dimension in tissue engineering. *Biomedical Materials* **11** (2016).
- 4 Whang, M. & Kim, J. Synthetic hydrogels with stiffness gradients for durotaxis study and tissue engineering scaffolds. *Tissue Engineering and Regenerative Medicine* **13**, 126-139 (2016).
- 5 Ma, S., Yu, B., Pei, X. & Zhou, F. Structural hydrogels. *Polymer* **98**, 516-535 (2016).
- 6 Liang, Z. *et al.* Double-network hydrogel with tunable mechanical performance and biocompatibility for the fabrication of stem cells-encapsulated fibers and 3d assemble. *Scientific Reports* **6** (2016).
- 7 Zhang, Y., Heher, P., Hilborn, J., Redl, H. & Ossipov, D. A. Hyaluronic acid-fibrin interpenetrating double network hydrogel prepared in situ by orthogonal disulfide cross-linking reaction for biomedical applications. *Acta Biomaterialia* **38**, 23-32 (2016).
- 8 Skaalure, S. C., Dimson, S. O., Pennington, A. M. & Bryant, S. J. Semi-interpenetrating networks of hyaluronic acid in degradable peg hydrogels for cartilage tissue engineering. *Acta Biomaterialia* **10**, 3409-3420 (2014).
- 9 Pape, A. C. H. & Dankers, P. Y. W. in *Supramolecular polymer networks and gels* Vol. 268 *Advances in polymer science* (ed S. Seiffert) 253-279 (Springer-Verlag Berlin, 2015).
- 10 Aubin, H. *et al.* Directed 3d cell alignment and elongation in microengineered hydrogels. *Biomaterials* **31**, 6941-6951 (2010).
- 11 Branco da Cunha, C. *et al.* Influence of the stiffness of three-dimensional alginate/collagen-i interpenetrating networks on fibroblast biology. *Biomaterials* **35**, 8927-8936 (2014).
- 12 Draper, E. R., Eden, E. G. B., McDonald, T. O. & Adams, D. J. Spatially resolved multicomponent gels. *Nat Chem* **7**, 848-852 (2015).
- 13 Lovrak, M. *et al.* Free-standing supramolecular hydrogel objects by reaction-diffusion. *Nat. Commun.* **8**, 15317 (2017).
- 14 Boekhoven, J. *et al.* Catalytic control over supramolecular gel formation. *Nat. Chem.* **5**, 433-437 (2013).
- 15 Ulker, Z., Alpsoy, L. & Mihmanli, A. Assessment of cytotoxic and apoptotic effects of benzaldehyde using different assays. *Human & Experimental Toxicology* **32**, 858-864 (2013).
- 16 Bassi, A. M., Penco, S., Canuto, R. A., Muzio, G. & Ferro, M. Comparative evaluation of cytotoxicity and metabolism of four aldehydes in two hepatoma cell lines. *Drug Chem. Toxicol.* **20**, 173-187 (1997).
- 17 Lin, C.-C. & Anseth, K. S. Glucagon-like peptide-1 functionalized peg hydrogels promote survival and function of encapsulated pancreatic β -cells. *Biomacromolecules* **10**, 2460-2467 (2009).
- 18 Sarker, B. *et al.* Evaluation of fibroblasts adhesion and proliferation on alginate-gelatin crosslinked hydrogel. *PLoS ONE* **9**, e107952 (2014).
- 19 Poolman, J. M. *et al.* A toolbox for controlling the properties and functionalisation of hydrazone-based supramolecular hydrogels. *J. Mat. Chem. B* **4**, 852-858 (2016).

Supplementary Information



Supplementary Figure 1. Metabolic activity of cells cultured in cell culture medium (DMEM supplemented with 10% Fetal Bovine Serum and 1% Penicilin/Streptomycin) used previously for washing alginate/HA₃ gels (called washing medium, WM). a) 3T3 cells cultured for 24 hours. b) HEK 293 cells cultured for 2 hours. c) HEK 293 cells culture for 24 hours. RM – the reaction mixture after the formation of gels collected from the top of the gels; DRM – the reaction mixture diluted with cell culture medium (25 uL of RM with 75 uL of cell culture medium); WM1 to WM5 – cell culture medium exchanged each hour; WM6 – cell culture medium left overnight on top of the gel.

Materials. All materials and reagents were purchased from commercial sources and used as provided, unless stated otherwise. Hydrazide **H** and aldehyde **A** were synthesized according to reported methods.¹

Cell culture - 3T3 and HEK 293 cells. 3T3 or HEK 293 cells were expanded in T75 flasks, with DMEM + 10% Fetal Bovine Serum (FBS) + 1% Penicilin/Streptomycin (P/S).

To obtain a pellet of cells the medium was removed from the T75 flask, the cells were washed with 10 mL of DPBS pre warmed at 37 °C, and 1.5 mL of trypsin/EDTA was added and the T75 flask was incubated at 37 °C. After 3-4 min it was checked using a microscope whether the cells are detaching. Then, the trypsin was neutralized with 8.5 mL of DMEM + 10% FBS + 1% P/S, and the cell suspension was collected to a 50 mL tube. The cells were counted in the Neubauer chamber by mixing 50 µl of cell suspension + 150 µl of trypan blue (4× dilution).

The cell suspension obtained previously was diluted into the volume required to put on the top of the all gels, and 0.5 mL/well was dispensed into 24 well plates (cells on the top of the gels). The plates were incubated at 37 °C, in the atmosphere containing 5% CO₂ with 95% humidity. Density of 3T3 cells was 5000 cells/gel, and density of HEK293 cells was 10000 cells/gel.

Cytotoxicity of H and A. The cell suspension obtained previously was diluted to the required cell concentration. In 96 well plates HEK 293 and 3T3 cells were seeded with densities 20000 cells/well and 4000 cells/well, respectively (100 µl of suspension/well). Approximately after 18-20 hours, the normal cell culture medium was replaced by 100 µl dilution of **H** and **A**, respectively (75 µL of washing medium + 25 µL of **H** or **A** stock solution). **H** and **A** were dissolved in DPBS to prepare stock solutions. The concentrations of stock solutions were 10, 20 and 40 mM for **H**, and 100, 200 and 400 mM for **A**. Afterwards, the metabolic activity of cells was tested.

Metabolic Activity: WST-1. The WST-1 reagent was thawed and x µl of WST-1 was added to each well ($x = 10\%$ of the total volume in the well). The plate was incubated at 37°C for 3h. The medium of each well was collected into 1.5mL Eppendorf tubes, and the samples were frozen. For the analysis, the samples were thawed (protecting them from the light), homogenized in the vortex, and centrifuged at maximum speed (13200 rpm) at 4 °C for 5 min. 70-100 µl of the supernatant was collected and put it in a new 96 well plate. The absorbance was measured on microplate reader at 440 nm. WST-1 was performed at day 1 and day 4.

Preparation of alginate/HA₃ hybrid hydrogel and subsequent washing. Powder of CaCO₃, **H** and alginate were dispersed in water and heated at 100 °C until all **H** and alginate were dissolved. The solution was cooled down to room temperature. Glucono-δ-lactone (GDL) was dissolved in water and the solution was added to the solution of CaCO₃, **H** and alginate. This solution was then dispensed into cell culturing plates. The final concentration of **H** was 10, 20 and 40 mM, and the final concentration of alginate was 1% (weight/volume). The concentrations of CaCO₃ and GDL depend on the concentration of alginate and desired pH (12.5 mM and 40 mM, respectively for 1% alginate at pH ≈ 4.5).

The gels were prepared in 12 well plates (1.5% alginate with 10, 20 and 40 mM hydrazide, 1.2 ml/well). Next day 1.0 mL of the solution of **A** was added on top of prepared gels. The concentration of the solution of **A** should be 10 times higher than the concentration of **H** in alginate. Then, the remaining liquid part was removed and each of these gels was washed with 1.0 ml of cell culture medium (the same medium used to expand the cells in the T75 flasks) which was then collected and filtered (0.45 μ m filters) to test the cytotoxicity. Medium was exchanged each hour. The last washing was overnight.

To decrease the volume of gels, they were prepared in 24 well plates (250 μ L/well). The plate with solution was left standing overnight to form a gel. Next day 0.5 mL of the solution of **A** was added on top of prepared gels. The concentration of the solution of **A** should be 10 times higher than the concentration of **H** in alginate. The plate was left standing overnight. Then, the remaining liquid part was removed and 1.0 mL of DPBS buffer was added. Buffer was exchanged every hour. At the end of the day 1.5 ml of PBS buffer was added and left standing overnight. The gels were washed once more with 1.0 mL PBS buffer the next day.

Cytotoxicity of gel washing media. The cell suspension obtained previously was diluted to the required cell concentration. In 96 well plates HEK 293 and 3T3 cells were seeded with densities 20000 cells/well and 4000 cells/well, respectively (100 μ l of suspension/well). Approximately after 18-20 hours, the normal cell culture medium was replaced by 100 μ l of washing media. Afterwards, the metabolic activity of cells was tested.

Supplementary references

- 1 Boekhoven, J. *et al.* Catalytic control over supramolecular gel formation. *Nat. Chem.* **5**, 433-437 (2013).

Implantable Artificial Plaque as an Alternative to Atherosclerotic Animal Models

Abstract

Atherosclerotic arteries are commonly re-opened using drug eluting stents, but it remains unclear how plaque properties affect drug transport. The lack of control over plaque location and structure limits the utility of experimental animal models. We therefore created an implantable and biocompatible artificial atherosclerotic plaque of reproducible and controllable complexity, ultimately aimed at incorporation in the arterial wall at a prespecified location. We demonstrate proof-of-principle of *in vivo* implantability and its potential use for drug transport studies.

Introduction

Heart disease is the main cause of death in the modern world. In 2012 alone, 17.5 million people died as a result of the disease, with coronary artery disease (CAD) accounting for nearly half of the victims. Atherosclerosis, the root cause of CAD, is characterized by a build-up of cholesterol and other materials inside the artery wall, referred to as a plaque, ultimately causing the artery to narrow or the plaque to rupture.

The primary choice for treatment of symptomatic CAD is the implantation of a stent, with drug eluting stents (DES) generally being favored over bare metal stents to reduce the build-up of excessive scar tissue⁴. Preclinical research on DES is focused on vascular healing, which depends on drug transport from the stent to the artery wall. The majority of these studies are based on porcine arteries due to their close resemblance to human arteries⁵. Although most research is done using healthy animals without coronary atherosclerotic plaques, modelling work suggests that the presence of plaque strongly influences the transport of drugs through the arterial wall.⁶ Only a few studies report the use of large atherosclerotic animals due to the immense costs and time associated with natural plaque development^{2,7,8}. In addition, natural evolution of plaque leads to plaque of uncontrollable compositions at unpredictable locations within the coronary tree. The lack of well controlled and readily available experimental models for atherosclerotic plaque with a predictable and reproducible composition and location hampers a systematic study of treatment options for specific types of atherosclerotic plaque.

A fast and low cost model yielding predictable atherosclerotic lesions of controllable composition and location could have tremendous impact on vascular research as has been recognised in literature⁹⁻¹¹. Pharmacokinetic and pharmacodynamic studies of DES and other forms of local drug delivery such as drug eluting balloons, or even systemic pharmacotherapy aimed at plaque regression, would be more efficient, accessible, and clinically relevant. Such a model would reveal crucial information on drug transport in these well characterized and reproducible types of atherosclerotic plaque. In addition, it could be used to validate new imaging modalities aimed to visualize atherosclerotic plaque¹².

The aim of this research is, therefore, to create a flexible platform for making implantable artificial plaque for pre-clinical or *ex vivo* studies, allowing a designable plaque composition and thickness, mimicking those reported for humans. In our approach we combined gelatin and alginate hydrogels to carry the most common plaque lipids in concentrations reported for human atherosclerotic plaque. We chose this hydrogel type because of its proven biocompatibility¹³, the ease to incorporate lipids and other components of human atherosclerotic plaque, and the possibility for implantation at prespecified locations and subsequent incorporation of the plaque into the arterial wall.

Methods

Hydrogel and lipid blend preparation. Lipid composition in the gelatin/alginate hydrogels to create the artificial plaque was determined from literature ^{14,15} as shown in Table 1. Liposome solutions were prepared as follows: powdered lipids (cholesterol, cholesterol palmitate, cholesterol oleate, cholesterol linoleate (all from Sigma-Aldrich, St. Louis, MO) and 1,2-dipalmitoyl-*sn*-glycero-3-phosphocholine (DPPC) (Tokyo Chemical Industry Co., Tokyo, Japan)) were first dissolved in chloroform (VWR International, the Netherlands) in a round-bottom glass flask in a 1:10 mass ratio for full lipid dissolution. The flask was placed on a rotary evaporator (Buchi Rotovapor R-215) until chloroform had fully evaporated. This resulted in a thin lipid film on the walls of the flask. This film was then soaked in water (MilliQ grade) (also in 1:10 mass ratio) and the flask was left in a sonication bath (Bransonic 2510E-MTH) for 30 minutes at 35°C.

Table 2. Most abundant atherosclerotic plaque lipids for artificial plaque composition. Atherosclerotic plaque lipid composition as based on endarterectomy samples (excluding healthy arterial wall) taken from carotid and femoral artery plaques and the percentage of the most abundant cholesterol esters. Dry weight is calculated from mg/g wet weight with the assumption that ~79% of tissue is water. This composition is used for incorporation in the artificial plaque.

	Wet weight		Dry weight	
	mg/g	weight %	mg/g	weight %
Cholesterol ¹⁴	13.1	1.30	62.4	6.24
Cholesterol Ester ¹⁴	9.50	0.95	45.2	4.52
Cholesterol Palmitate (C16:0) ¹⁵	16.7%	0.16	16.7%	0.75
Cholesterol Oleate (C18:1) ¹⁵	33.3%	0.32	33.3%	1.51
Cholesterol Linoleate (C18:2) ¹⁵	50.0%	0.48	50.0%	2.26
Phospholipid ¹⁴	9.70	0.97	46.2	4.62

Preparation of the artificial plaque is illustrated in Figure 1. Gelatin/alginate hydrogels of different composition (mass ratios of 1:1, 1:2, and 1:3) were prepared as follows: typically 100 mg gelatin (Type B, Sigma-Aldrich) was added to 5 mL of water at 40°C at constant stirring. Once gelatin had fully dissolved, sodium alginate (Sigma-Aldrich) was added to the solution and stirred until dissolved. The prepared liposome solutions were subsequently mixed with gelatin/alginate solutions under constant stirring at 40°C until homogenization (observed visually). The resulting uniform mixture was poured into plastic Petri dishes (inner diameter 5 cm) and left in the oven overnight at 40°C to form thin, dry gel films. The films were then soaked at room temperature in an aqueous 100 mM CaCl₂ (Sigma-Aldrich) solution for 24 hours to crosslink the sodium alginate.

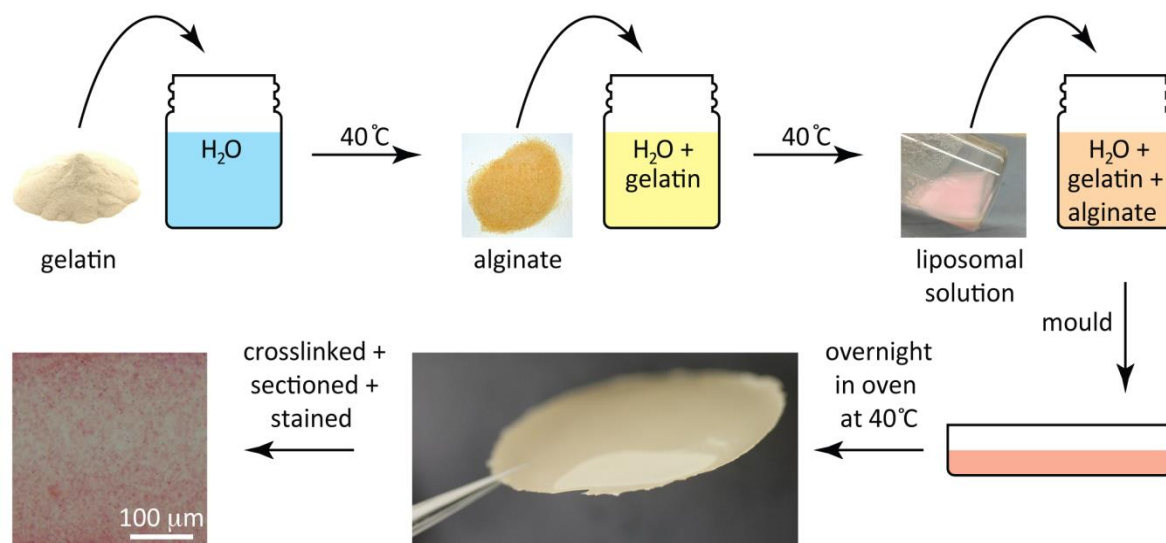


Figure 1. Production of artificial plaque. Artificial plaque is created by making a gelatin/alginate/liposome solution that is moulded overnight and crosslinked by CaCl_2 . Sectioning and staining by Oil-red-O illustrates the homogeneous lipid distribution in the gel.

Lipid dispersion within artificial plaque. Confocal microscopy (Zeiss LSM 710) was used to examine lipid dispersion within the hydrogels. For this, 1,2-dioleoyl-sn-glycero-3-phosphoethanolamine-N-(lissamine rhodamine B sulfonyl) (DOPE-Rhodamine B) (supplied in chloroform, Avanti Lipids, Inc., Alabama, USA) was added to the lipid solution in chloroform during liposome preparation (final DOPE-Rhodamine B concentration in water not exceeding $4 \mu\text{M}$ for imaging). Confocal microscopy analysis was performed to track any changes in lipid dispersion. ImageJ (version 1.5i) color threshold analysis was performed to quantify the lipid fraction relative to the imaged hydrogel area. In addition, and for comparison to swine coronary plaque, we also stained the artificial plaque with Oil-Red-O.

Lipid retention in artificial plaque. Lipid retention in the hydrogels was investigated by incubating hydrogels for 17 days in water at room temperature. Crosslinked hydrogels were left in 3 mL of water (MilliQ grade) in tightly sealed Petri dishes. After incubation, water was transferred into glass vials and placed in the oven at 45°C to evaporate. The residue layer was then soaked with chloroform until a clear solution was obtained. The resulting chloroform mixture was analysed using fluorescence spectroscopy (Jasco J-815 CD). It was assumed that all of the lipids assembled into liposomes, i.e. any trace of DOPE-Rhodamine B, would be a direct indication for the presence of lipids. Hydrogels were also imaged with confocal microscopy to investigate changes during the incubation period. Color threshold analysis was performed to compare incubated and freshly crosslinked hydrogels.

Diffusion coefficient measurements in artificial plaque. A two-compartment diffusion cell was used to measure the diffusion coefficient of the hydrogels. The setup was adapted from Pal et al ¹⁶ and optimized in-house. The dye Lucifer Yellow CH (potassium salt, M_w 521.56 Da, Sigma-Aldrich) was used as a model molecule. The top compartment was filled with 5 mL of solution of a known starting concentration of the

dye. This compartment was separated from the bottom compartment by a circular piece of hydrogel (artificial plaque). A glass beaker filled with 25 mL of pure water (MilliQ grade) was used as the bottom compartment. The solutions in the compartments were thoroughly mixed at 50 rpm. The experiment started by lowering the top compartment into the glass beaker so that liquid levels in both tanks were equal to avoid effects of hydrostatic pressure.

Samples were periodically drawn from the glass beaker and analysed using a UV-vis spectrophotometer (Shimadzu UV-1800) to measure the concentration of the dye as a function of time. The diffusion coefficient D was obtained by fitting this data against a standard diffusion model given in equation 6.1¹⁷

$$c_2(t) = \frac{c_1^0 [1 - \exp(-D\beta t)] + c_2^0 \left[\exp(-D\beta t) + \frac{V_2}{V_1} \right]}{1 + \frac{V_2}{V_1}}. \quad (6.1)$$

where c_2 is the dye concentration in the glass beaker, c_1^0 (3.8 ± 0.2 mM) is the initial dye concentration in the syringe, c_2^0 (0 mM) is the initial dye concentration in the glass beaker, V_1 is the volume of the solution in the syringe, V_2 is the volume of the solution in the glass beaker, A_H (0.5 cm²) is the surface area of the hydrogel, W_H is the thickness of the hydrogel (between 220 and 700 μ m, depending on the hydrogel composition), $\beta = \left(\frac{A_H}{W_H}\right)\left(\frac{1}{V_1} + \frac{1}{V_2}\right)$ and t is time. Thickness of each hydrogel was measured using a dynamic mechanical analyzer (DMA) (DMA 7e, Perkin Elmer Instruments).

Mounting artificial plaque on stents. Two thin strips of hydrogel, one strip of hydrogel with lipids (artificial plaque) and one without (control), were cut to size and mounted onto a Everolimus DES using polypropylene suture (8-0 Prolene Blue 2X18" BV130-5 Double Armed, Ethicon, USA). Alternatively, to create stent-free segments of artificial plaque for stent-free plaque imaging, the gel ends were clamped between two segments (rings) of a stent. The stent-mounted hydrogels were tested for implantability by advancing them through 8F guiding catheters and by inflating and deflating the balloon-stent-hydrogel system and ascertaining that the stent or double stent-ends could be fully deployed whilst the hydrogel remained attached to the stent.

Ex vivo artificial plaque implantation and perfusion in porcine coronary arteries. Porcine hearts were supplied from a local slaughterhouse and transported to Erasmus MC in ice cold KREBS buffer within two hours post-excision. The left anterior descending (LAD) coronary artery together with approximately 1 cm of myocardial tissue was dissected from the hearts in KREBS buffer immersed in ice, mounted in a perfusion chamber, and large side branches were tied off to maintain as much flow through the LAD as possible.

The plaque-mounted stent-balloon system, containing both a control (proximal) and a lipid rich plaque (distal), was inserted into the artery and inflated for at least 20

seconds to ensure full stent expansion. After deflation, the catheter was removed and the perfusion chamber was connected to a heart - lung machine. The perfusion chamber was placed on a heating plate that was kept at 37°C. The chamber was perfused with HEPES buffer mix (325mL 1x HEPES saline buffer, 40 mL phosphate buffer containing 62 mg/ml sucrose and 8.2 mg/ml mannitol). After experiments, arteries were removed from the chamber and embedded for cryosectioning in preparation for histology and MALDI and stored at -80°C until further analysis.

***In vivo* artificial plaque implantation in porcine coronary arteries.** An *in vivo* procedure, approved by the Erasmus MC Animal Ethics committee and performed in accordance with the Guide for Care and Use of Laboratory Animals ¹⁸ was executed in a swine coronary artery (sex, age and weight not taken into account) as described before ¹⁹. Following quantitative coronary angiography to determine the size of the LAD, an appropriate stent size was selected and the artificial plaque was mounted on the stent-balloon system. The stent-mounted plaque was implanted and imaged with optical coherence tomography (OCT) ¹² to visualize the plaque inside the artery directly upon implantation.

Cryosectioning of stented arteries. Arteries were cut into 3 mm thick blocks starting at the distal end, labelled and cryosectioned (Microm HM560, Germany) starting at the distal end of each block. Sections of 12 µm thickness were mounted and stored at -80°C until further analysis. Blocks containing control or lipid rich plaque were selected for sectioning. A total of 7 slides were cut per block containing plaque, with multiple sections per slide.

Matrix assisted laser desorption/ionization mass spectrometry (MALDI MS). Matrix was prepared by dissolving 50 mg of 2,5-dihydroxybenzoic acid (DHB) (Sigma-Aldrich) in 10 mL acetone. The solution was pipetted on the sublimation device (designed and manufactured in-house, Erasmus MC) and heated to 50°C until acetone was evaporated. Glass slides were mounted onto the sample holder and subjected to vacuum. At 5 mbar, the matrix table was heated to 125°C (10 minutes) to sublimate the DHB and then immediately analyzed by MALDI MS imaging (MALDI Synapt ® G2-Si; Waters, Wilmslow UK) with a step size of 75 µm and laser energy of 150 (arbitrary units). Polarity was positive with target enhancement at 980 Da for Everolimus (*m/z* 980.5).

Arterial tissue histology. Two histology methods were used. Oil Red-O stain was used to visualize lipids and haematoxylin-eosin (HE) stain to visualize the artery wall.

Drug distribution following *ex vivo* artificial plaque implantation. Once MALDI MS analysis was completed, raw data was processed with HD Imaging and Masslynx (version 4.1; Waters, Wilmslow UK) for *m/z* values of 980.5 or 980.6 for Everolimus (preference given to 980.5). Then the ROI tool was used to analyse the sections. Everolimus intensity in a selected region of the arterial wall behind the hydrogel was measured. Same size region in the arterial wall opposite the hydrogel was chosen to calculate the Everolimus intensity. Twenty regions of interest (ROI) were analyzed behind the gel and an additional 20 ROI were measured opposite the gel in the normal artery wall for each plaque type per experiment. Intensities reported were all

normalised within each section or artery to the highest intensity in the arterial wall (specifically excluding the stent struts themselves) to allow relative intensities or intensity ratios within sections and arteries.

Statistical analysis. Results are presented as a mean \pm SD or median [min, max, and interquartile range] using SPSS 24 (IBM SPSS statistics). A paired t-test was performed to compare arterial wall regions for the blank hydrogel and no hydrogel arterial wall regions within the same section. An independent samples t-test based on unequal variance was performed to compare arterial wall regions behind blank and lipid hydrogels because they originated from different sections within the same artery. All data sets were tested for normality taking into account Shapiro-Wilk test as well as Q-Q plots.

Results

Lipid dispersion within artificial plaque. Similar to the distribution of lipids in porcine atherosclerotic plaque (Fig. 2a-c), lipids in the artificial plaque were homogeneously dispersed (Fig. 2d).

Lipid retention in artificial plaque. Visual inspection of the confocal micrographs indicated that the dispersion of lipids in the 1:2 and 1:3 gel images remained unchanged over a period of 17 days. Color threshold analysis of the gels indicated no difference between the freshly prepared gels and the gels after 17 days of incubation for all tested compositions. This is in agreement with the analysis of the incubation extract, which showed that less than 0.1% of lipids had leached from the gels, indicating suitability of both 1:2 and 1:3 gels for further analysis. Lipid dispersion in the 1:1 gel did seem to change upon visual inspection during the 17 day incubation period (Fig. 2e) and was not chosen for further analysis.

Diffusion coefficient measurements in artificial plaque. The comparison between the diffusion coefficients for gels with and without lipids is shown in Fig. 3. All diffusion coefficients are of the same order of magnitude as the diffusion coefficient reported by Carlyle *et al*¹ for Sirolimus (same drug family as Everolimus) in a healthy arterial wall. While the diffusion coefficient in the lipid-rich hydrogel was lower for the 1:1 and 1:3 samples, no significant difference was observed for the 1:2 sample. The diffusion coefficient of the 1:3 gel best reflected diffusion properties reported for human coronary artery¹ and was chosen for further analysis by *ex vivo* and *in vivo* implantation.

Mounting artificial plaque. Artificial plaque was either mounted by sutures or by clamping plaque between stent segments, as illustrated in Fig. 4a/b. Both techniques were feasible as judged by the plaque remaining on the stent after passing the guiding catheter and following inflation and deflation of the stent delivery balloon. This sequence of mounting, passage, and inflation, was tested several times (not counted) until results were stable. This was performed before *in vivo* implantation was executed. For stent-free implantation using the double stent-end technique, care had to be taken

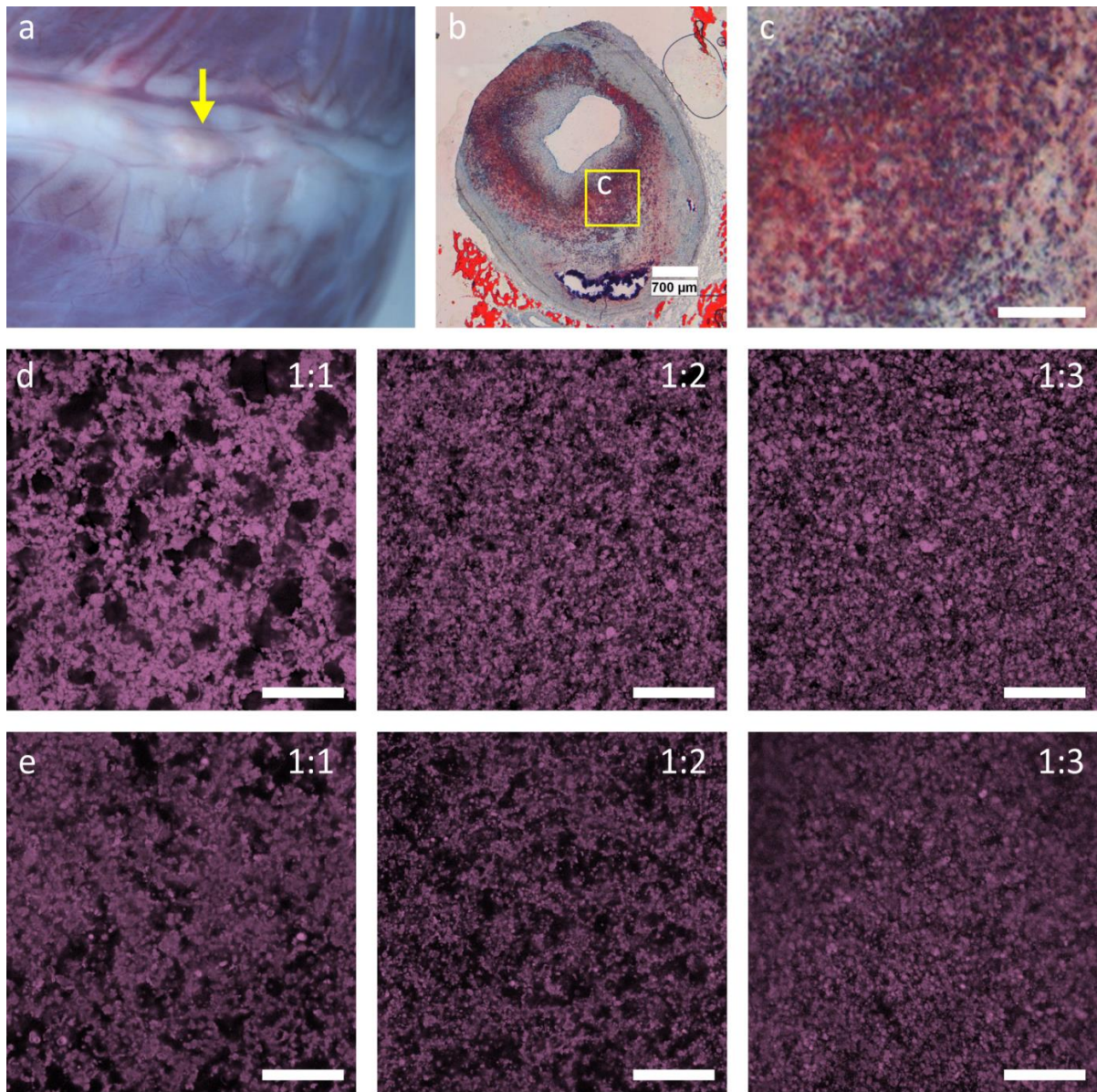


Figure 2. Plaque lipid dispersion. Macroscopy and microscopy of swine atherosclerotic plaque (a-c), and confocal micrographs of three different compositions of artificial plaque (d-e). In a swine coronary atherosclerosis model, 12 months of high cholesterol diet after induction of Diabetes Mellitus by streptozotocin leads to focal atherosclerotic plaque as illustrated in a macroscopic image of a swine heart (a, arrow). Histology (b, Oil-red-O stain, ²) shows a lipid-rich intima with a nearly circumferential accumulation of lipid droplets (c, detail). In Oil-red-O, lipids are stained red, nuclei are stained blue. The confocal micrographs (d-e) show the distribution of liposomes throughout artificial plaque. Liposomes were labelled with DOPE-Rhodamine B. Color threshold analysis (CTA) was used to determine the percentage of area covered with lipids. d) Dry gel films before crosslinking. The results from TA (from left to right): 73%, 80%, and 81%. e) Crosslinked hydrogel films after 17 days of incubation in water. The results from TA (from left to right): 79%, 85%, and 89%. Scale bars b: 700 μ m; c: 200 μ m; d-e: 50 μ m.

to connect the leading and trailing stent-ends with a suture opposite the plaque to ascertain even expansion of the stent segments without them gliding off the balloon ends. For drug distribution studies, suture mounted plaque was used for further analysis.

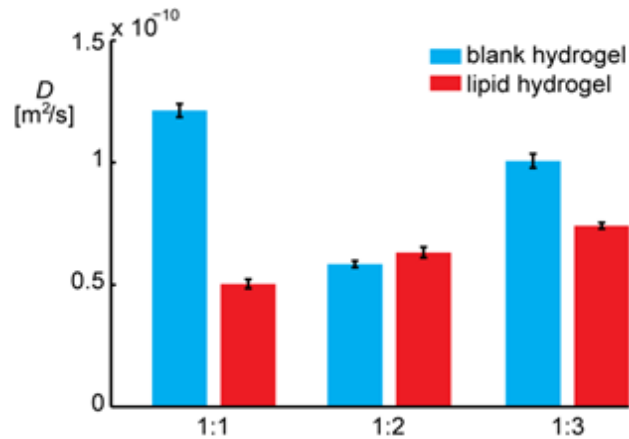


Figure 3. Diffusion through artificial plaque. Diffusion coefficient of Lucifer Yellow CH through gelatin/alginate hydrogels with and without lipids. The composition corresponds to mass ratio of gelatin and alginate. All diffusion coefficients are of the same order of magnitude as the diffusion coefficient of drugs through arterial wall.¹ For the 1:1 and 1:3 samples, the diffusion through the lipid-rich hydrogels is somewhat lower than for the hydrogels without lipids, except for the 1:2 sample. Error bars represent the 95% confidence interval of the fit of the experimental data against Eq. 1.

Drug distribution in stented porcine coronary arteries. An example of one of the perfusion results is shown in Fig. 4c-e. MALDI MS images were laid alongside histology (HE, Oil-red-O) to determine hydrogel location in MALDI MS images. A quantitative comparison of the region of interest analysis of Everolimus in the arterial wall behind the artificial plaque and blank gels (data combined for perfusions of 30 and 300 minutes) is illustrated in Fig. 5. Data indicate that the intensities of Everolimus in the arterial wall behind the lipid-rich artificial plaque and the blank hydrogel were significantly lower ($p < 0.05$). The abundance of Everolimus in the arterial wall behind the blank gel was also significantly lower compared to free wall ($p < 0.05$). It remains to be determined whether this is simply the result of an increased wall thickness.

***In vivo* artificial plaque implantation.** Stents carrying the artificial lipid-rich plaque were deployed in the coronary artery. Imaging by OCT was performed within 15 minutes of introduction and revealed successful coronary implantation (Fig. 6).

Discussion

We aimed to create an artificial lipid-rich plaque of reproducible and tuneable composition implantable at a specified location in the arterial tree. This offers an alternative to costly and time-consuming animal models of atherosclerosis that are generally unpredictable in terms of plaque location and severity. Our report is the first example of implanting artificial atherosclerotic plaque in arteries. While previous studies reported artificial hydrogel plaque to study drug transport *in vitro*, none of these studies explicitly aimed at the creation of an implantable artificial plaque platform²⁰⁻²².

Microscopy demonstrated a homogeneous lipid distribution in our artificial plaque, similar to porcine plaque. OCT imaging confirmed the implantability of such plaque in the coronary artery. *Ex vivo* perfusion experiments demonstrated that this lipid-rich

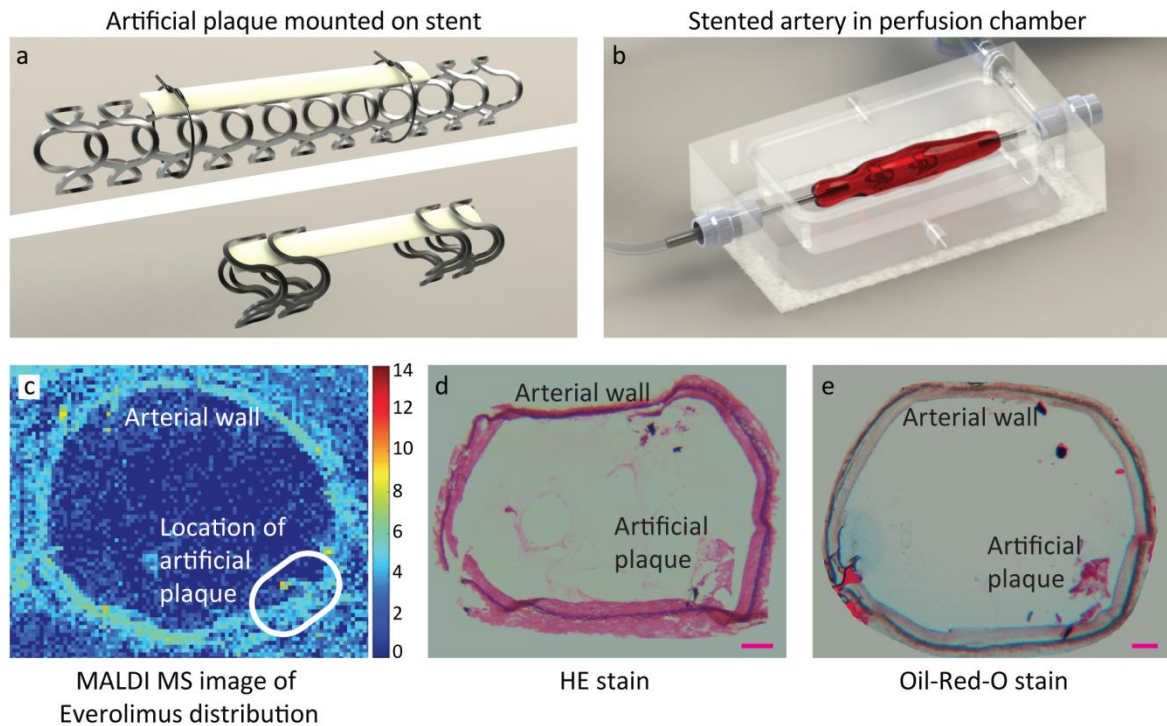


Figure 4. Artificial plaque model. Artists impression of artificial plaque mounted on an Everolimus eluting stent using 8.0 prolene sutures (a, top), and double stent segments (a, bottom) to clamp the plaque extremities in preparation for implantation of stent-free artificial plaque. Artists impression of the perfusion chamber mounted with a stented porcine coronary artery (b). Serial cryosections after 30 minutes of perfusion were interrogated by MALDI MS Imaging for Everolimus (m/z 980.5) with a rainbow scale bar representing the total ion count for Everolimus (c) with adjacent sections stained by hematoxylin eosin as an overview stain (d) and Oil-red-O (e) as a lipid stain to visualize the location of the artificial plaque. The highlighted region in (c) shows the arterial wall segment behind the hydrogel as indicated by histology (d, e). Scale bars: 250 μ m. Of note, stent struts tend to get lost during preparation for MALDI imaging and hence only few are detected.

artificial atherosclerotic plaque represents a barrier for drug diffusion from DES, illustrating its use for preclinical studies.

Preparation and characterization of artificial plaque. Hydrogels made from biopolymers such as gelatin and alginate, and combinations thereof have proven their use as implantable (cardiac) tissue¹³. Based on this work, we hypothesized that gelatin/alginate gels would form a good basis for making an artificial lipid rich plaque. Two important criteria in this study were: the ability to incorporate physiologically relevant lipid levels in the gels, and to match the diffusive properties of the gels to those in tissue. A third important criterium was the ability to handle the gels such that they could be implanted. Although a detailed study of the mechanical properties was beyond the scope of the present study, we started this work by selecting gelatin/alginate compositions in the range 3:1 to 1:3 yielding firm, yet pliable films. The primary criteria considered for this selection was the mechanical resistance towards manual manipulation (ability to handle the films with tweezers, stretching them slightly), and the stability of films in water (resistance towards degradation when left in water for a prolonged period). 1:1 – 1:3 compositions met these properties.

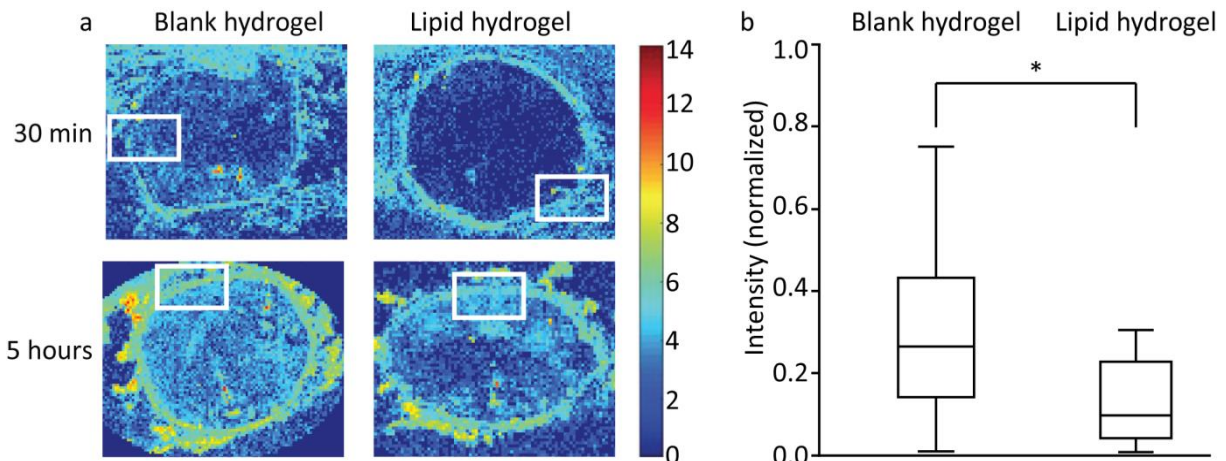


Figure 5. MALDI MS of Everolimus distribution. MALDI MS of Everolimus distribution across the arterial wall in gelatin/alginate and gelatin/alginate/lipid hydrogels. a) The distribution of Everolimus after 30 minutes and 5 hours of perfusion. The boxed regions indicate the location of the artificial plaque as indicated by HE (not shown). Rainbow scale shows an Ln scale of the total ion count for Everolimus. b) Analysis of the 30 minute and 5 hour perfusion shows a difference between Everolimus intensities in arterial wall regions behind the blank and lipid hydrogel (artificial plaque). Intensities for this analysis were normalised with respect to the highest intensity within the media (excluding stent struts), i.e. intensity ratios between two investigated areas from the media in the same section are compared. Data are given as a boxplot illustrating the median and interquartile range, with the ends of the whiskers indicating the minimum and maximum observed values. $*=p<0.05$

Drug and lipid transport through artificial plaque. Due to complexity of the composition of a diseased artery, drug transport studies prove to be truly challenging. Even though the composition of a healthy artery is rather well known, the effects of each

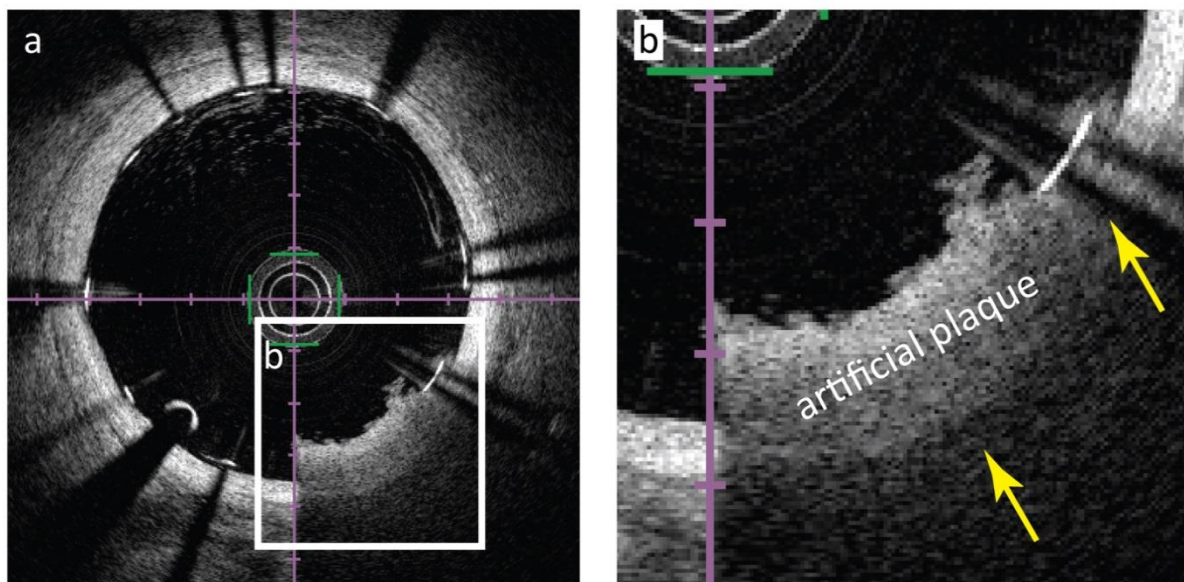


Figure 6. In vivo artificial plaque implantation. OCT image of a coronary artery following implantation of a stent with artificial plaque (a). The detail illustrates the presence of the artificial plaque (b) successfully implanted in the coronary artery, with a relevant thickness of at least twice the medial thickness. Stent struts give shadowing (arrow) in the image since no light can pass through the metal. Also, shadowing is seen behind the plaque (arrow) which is commonly known to be a property of lipids. ³

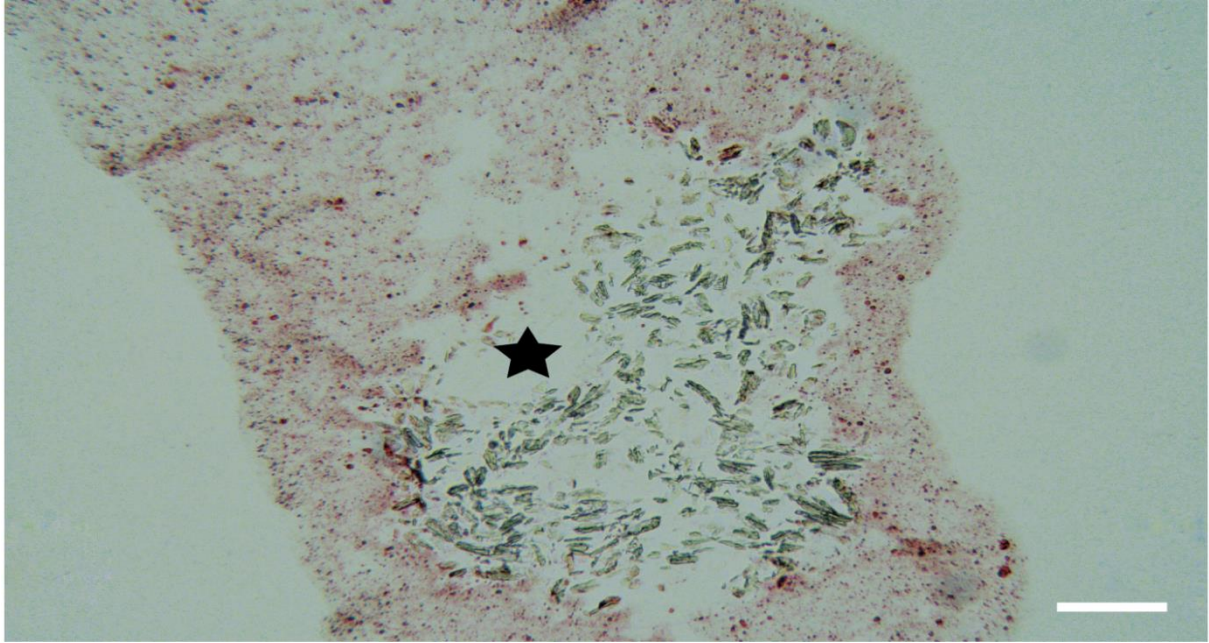


Figure 7. Complex atherosclerotic plaque. Artificial plaque containing crystals (*) incorporated in the lipid-rich gel to illustrate the feasibility of incorporating complex plaque constituents. Oil-red-O staining. Scale bar: 100 μ m.

of the constituents of atherosclerotic plaque on the drug transport remain a complex task to unravel ⁹. The creation of an artificial plaque allows the controlled addition of each of the constituents. This proof-of-principle study indicates that lipids in this artificial plaque significantly affect drug transport. This corroborates current models for mathematical modeling ⁶. Hence, this type of artificial plaque might be useful for detailed studies towards drug transport properties through lipid-rich tissues. It can be used to validate computational models and to develop strategies to improve drug transport through lipid-rich plaque both for local and systemic pharmacotherapeutic approaches. Besides drug transport phenomena, an artificial plaque would further allow assessment and quantitation of lipid transport properties through plaque once the artificial plaque is incorporated in the arterial wall.

Current platform for artificial plaque implantation. The artificial plaque can be mounted both on whole stents or scaffolds as well as clamped between two segments as illustrated in Figure 4a. This allows for the creation of stent-free segments of atherosclerotic plaque which, once incorporated in the arterial wall, can be used as a marker of the original plaque location. The added benefit of this strategy is that the precise positioning enables image overlay during longitudinal and/or multimodality monitoring such as optical coherence tomography (OCT), intravascular ultrasound (IVUS), near infrared spectroscopy (NIRS), photoacoustics or other novel imaging technology ^{12,23,24}. Moreover, a model system with known lipid composition might also facilitate validation and development of minimally invasive imaging techniques. Using non-radioopaque scaffolds with a small metallic marker may, for example, allow for MRI and CT safe artificial plaque implantation.

Complex atheromatous plaque and plaque regression. While the current paper pursued the creation of a type IV atherosclerotic plaque according to the modified AHA classification ²⁵, our approach of an implantable artificial plaque also allows the incorporation of more complex materials such as cholesterol crystals (Fig. 7) and calcifications, typically observed in advanced atherosclerosis. This allows the creation of plaques of specific, well documented, and reproducible complexity to study different strategies geared towards plaque specific pharmacotherapy, with plaque regression as an interesting area of application.

Limitations. We tested the stability of artificial plaque in blood and found that it desintegrates within an hour after incubation. While the current hydrogel is suitable for testing in *ex vivo* experiments using buffers, and allowed *in vivo* proof-of-principle, permanent *in vivo* implantation requires the addition of covalent cross linking methods, such as adipic acid dihydrazide (AAD), which can even be used to tailor the degradation rate of the artificial plaque ¹³. Pilot experiments (data not shown) indicate that AAD indeed creates a plaque that is stable in blood for several hours.

Conclusions

We showed that a gelatin/alginate/lipid hydrogel provides a versatile platform for making implantable artificial atherosclerotic plaque with known properties and composition. This artificial plaque will allow the creation of different types of plaques with the potential for *in vivo* evaluation of drug-coated endovascular technologies as well as systemic pharmacotherapy for the treatment of atherosclerosis.

References.

- 1 Carlyle, W. C. *et al.* Enhanced drug delivery capabilities from stents coated with absorbable polymer and crystalline drug. *Journal of Controlled Release* **162**, 561-567 (2012).
- 2 van Ditzhuijzen, N. S. *et al.* Invasive coronary imaging in animal models of atherosclerosis. *Netherlands Heart Journal* **19**, 442-446 (2011).
- 3 Jang, I.-K. *et al.* Visualization of coronary atherosclerotic plaques in patients using optical coherence tomography: Comparison with intravascular ultrasound. *Journal of the American College of Cardiology* **39**, 604-609 (2002).
- 4 Kassimis, G. & Banning, A. P. Is it time to take bare metal stents off the catheter laboratory shelf? *Eur Heart J* **37**, 3372-3375 (2016).
- 5 Schwartz, R. S. *et al.* Drug-eluting stents in preclinical studies: Recommended evaluation from a consensus group. *Circulation* **106**, 1867-1873 (2002).
- 6 Karanasiou, G. S. *et al.* Stents: Biomechanics, biomaterials, and insights from computational modeling. *Ann Biomed Eng* (2017).
- 7 Hampton, T. High-cholesterol pigs. *Jama-J Am Med Assoc* **309**, 431-431 (2013).
- 8 Iqbal, J., Chamberlain, J., Francis, S. E. & Gunn, J. Role of animal models in coronary stenting. *Ann Biomed Eng* **44**, 453-465 (2016).
- 9 Levin, A. D., Vukmirovic, N., Hwang, C. W. & Edelman, E. R. Specific binding to intracellular proteins determines arterial transport properties for rapamycin and paclitaxel. *Proc. Natl. Acad. Sci. U. S. A.* **101**, 9463-9467 (2004).
- 10 Mongrain, R. *et al.* Effects of diffusion coefficients and struts apposition using numerical simulations for drug eluting coronary stents. *J Biomech Eng-T Asme* **129**, 733-742 (2007).
- 11 Cunnane, E. M. & Walsh, M. T. Towards the development of an in vitro model of atherosclerotic peripheral vessels for evaluating drug-coated endovascular technologies. *Drug Discovery Today* **21**, 1512-1520 (2016).
- 12 Wu, M. *et al.* Real-time volumetric lipid imaging in vivo by intravascular photoacoustics at 20 frames per second. *Biomed Opt Express* **8**, 943-953 (2017).
- 13 Lee, K. Y. & Mooney, D. J. Alginate: Properties and biomedical applications. *Prog Polym Sci* **37**, 106-126 (2012).
- 14 Marinello, E. *et al.* Lipid composition in atheromatous plaque: Evaluation of the lipid three-phase percentage. *Life Sci.* **72**, 2689-2694 (2003).
- 15 Rapp, J. H., Connor, W. E., Lin, D. S., Inahara, T. & Porter, J. M. Lipids of human atherosclerotic plaques and xanthomas - clues to the mechanism of plaque progression. *J. Lipid Res.* **24**, 1329-1335 (1983).
- 16 Pal, K., Bantia, A. K. & Majumdar, D. K. Biomedical evaluation of polyvinyl alcohol-gelatin esterified hydrogel for wound dressing. *J Mater Sci: Mater Med* **18**, 1889-1894 (2007).
- 17 Cussler, E. L. *Diffusion: Mass transfer in fluid systems*. 3rd ed. edn, 23-25 (Cambridge Univ. Press, 2009).
- 18 National Research Council Committee for the Update of the Guide for the, C. & Use of Laboratory, A. (2011).
- 19 van der Giessen, W. J., Sorop, O., Serruys, P. W., Peters-Krabbendam, I. & van Beusekom, H. M. Lowering the dose of sirolimus, released from a nonpolymeric hydroxyapatite coated coronary stent, reduces signs of delayed healing. *JACC Cardiovasc Interv* **2**, 284-290 (2009).
- 20 Sirianni, R. W. *et al.* Effect of extracellular matrix elements on the transport of paclitaxel through an arterial wall tissue mimic. *Biomacromolecules* **9**, 2792-2798 (2008).
- 21 Guo, J., Saylor, D. M., Glaser, E. P. & Patwardhan, D. V. Impact of artificial plaque composition on drug transport. *J. Pharm. Sci.* **102**, 1905-1914 (2013).

- 22 Semmling, B., Nagel, S., Sternberg, K., Weitschies, W. & Seidlitz, A. Development of hydrophobized alginate hydrogels for the vessel-simulating flow-through cell and their usage for biorelevant drug-eluting stent testing. *AAPS PharmSciTech* **14**, 1209-1218 (2013).
- 23 Waxman, S. *et al.* In vivo validation of a catheter-based near-infrared spectroscopy system for detection of lipid core coronary plaques: Initial results of the spectacl study. *JACC Cardiovasc Imaging* **2**, 858-868 (2009).
- 24 Garcia-Garcia, H. M., Gogas, B. D., Serruys, P. W. & Bruining, N. Ivus-based imaging modalities for tissue characterization: Similarities and differences. *Int J Cardiovasc Imaging* **27**, 215-224 (2011).
- 25 Sary, H. C. *et al.* A definition of advanced types of atherosclerotic lesions and a histological classification of atherosclerosis - a report from the committee on vascular-lesions of the council on arteriosclerosis, american-heart-association. *Circulation* **92**, 1355-1374 (1995).

Summary

Nature is full of life, which is driven by the numerous biochemical processes that occur in living organisms. Many motifs are universal regardless of species, such as enzymatic networks, self-assembly and reaction-diffusion. Furthermore, living organisms are mostly soft. Their skin, their organs, and even single cells are soft, and therefore living organisms are referred to as soft matter. Scientists try to replicate these motifs by observing nature and implement the same principles into artificial materials. In the area of soft matter, the efforts of mimicking nature range from making different types of responsive and dynamic hydrogels to the development of artificial organs and organs-on-a-chip.

This work examines the development of novel soft functional materials via self-assembly and reaction-diffusion approaches. The combination of these two principles from nature offers new possibilities for the development and structuring of soft matter.

Chapter 1 introduces the concepts of self-assembly and reaction-diffusion and presents a brief literature overview. In chapter 2, the application of the reaction-diffusion self-assembly approach to make patterned hydrogels and hydrogel objects is described. The dimensions of the patterns and objects that have been made range from centimeter scale to microscale. Also, we demonstrated various possibilities of chemical functionalization of patterns and objects. Finally, our findings were supported with a numerical model which gives additional insight into the pattern formation and parameters that control pattern dimensions.

The parameters that control the size of a supramolecular pattern are further described in chapter 3. The correlation between the experimental data and the theoretical model was explored. It was shown that a simple reaction-diffusion model can be used to explain the effect of a variety of parameters on the size of the pattern. Additionally, it was demonstrated that a simple power function, instead of the set of differential equations, can be used to estimate the size of the pattern by only knowing the experimental conditions.

Chapter 4 presents a novel strategy for gluing polymeric gels. We showed that self-assembly combined with reaction-diffusion at the interface of two gels can be used to glue pieces of gel by forming a self-assembled fibrous network across the interface. While non-glued pieces were easily separated, the glued pieces required four times higher stress for separation. This approach worked for different biological and polymeric gels and was supported with a numerical model.

The potential of hybrid alginate/supramolecular hydrogel network as extracellular matrix for 2D cell cultures was described in chapter 5. We studied the cytotoxicity of different gel components and then investigated the effect of this kind of extracellular matrix on viability and proliferation of two cell types. Both cell types showed limited ability to proliferate on this kind of extracellular matrix. One of the components of the supramolecular gel proved to be toxic for cells. Despite limitations

associated with this type of extracellular matrix, we gave recommendations for further improvements by addressing each of the discovered issues.

Finally, in chapter 6 a new strategy to make an *in vitro* model of artificial plaque is discussed. An artificial plaque was made by loading gelatin/alginate polymeric film with liposomes. The prepared films showed similar liposomal distribution as porcine plaque. Also, the plaque was implantable as demonstrated in *ex-vivo* and *in-vivo* experiments.

In conclusion, the research in this thesis presents new strategies towards the development of functional soft materials based on self-assembly and reaction-diffusion. These types of materials are important in areas ranging from cell related research and tissue engineering towards biomedical applications. The research presented herein represents the first steps in combining nature-inspired principles such as self-assembly and reaction-diffusion for the purpose of development of new soft materials.

Samenvatting

De natuur zit vol leven, wat gedreven is door talrijke biochemische processen die voorkomen in levende organismen. Veel patronen zijn universeel, onafhankelijk van het soort, zoals enzymatische netwerken, zelf-assemblage en reactie-diffusie. Verder zijn levende organismen vaak zacht. Hun huid, organen en zelfs individuele cellen zijn zacht, en daarom worden levende organismen ook wel zachte materie genoemd. Wetenschappers proberen deze patronen te repliceren door de natuur te observeren en deze principes uit te voeren in kunstmatige materialen. In het onderzoeksgebied van zachte materie wordt de natuur op verschillende manieren nagebootst, variërend van verschillende soorten responsieve en dynamisch hydrogels tot de ontwikkeling van kunstmatige organen en organen-op-een-chip.

Dit werk onderzoekt de ontwikkeling van nieuwe zachte, functionele materialen via zelf-assemblage en reactie-diffusie methoden. The combinatie van deze twee principes uit de natuur geven nieuwe mogelijkheden voor de ontwikkeling en het structureren van zachte materie.

Hoofdstuk 1 introduceert de concepten van zelf-assemblage en reactie-diffusie en presenteert een kort literatuuroverzicht. In hoofdstuk 2 worden de toepassingen van de reactie-diffusie zelf-assemblage methode om hydrogels met een patroon en hydrogelobjecten te maken, beschreven. De dimensies van de gemaakte patronen en objecten variëren van de centimeter tot de micrometer schaal. Bovendien hebben we gedemonstreerd dat het mogelijk is om verscheidene chemische functies van patronen en objecten te introduceren. Tot slot zijn onze resultaten ondersteund met een numeriek model dat extra inzicht geeft in de patroonvorming en parameters die de patroondimensies controleren.

De parameters die de grootte van het supramoleculaire patroon controleren zijn verder beschreven in hoofdstuk 3. De correlatie tussen de experimentele data en het theoretisch model is onderzocht. Er is aangetoond dat een simpel reactie-diffusie model gebruikt kan worden om het effect van een aantal parameters op de patroongrootte te verklaren. Bovendien is er gedemonstreerd dat een simpele machtsfunctie, in plaats van een reeks differentiaalvergelijkingen, gebruikt kan worden om de grootte van het patroon te schatten waarbij alleen de kennis van de experimentele condities een vereiste is.

Hoofdstuk 4 presenteert een nieuwe strategie voor het lijmen van polymeergels. We hebben laten zien dat zelf-assemblage gecombineerd met reactie-diffusie op het grensvlak van twee gels gebruikt kan worden om stukjes gel aan elkaar te lijmen door een zelf-geassembleerd netwerk van vezels op het grensvlak te vormen. Terwijl niet-gelijmde stukjes makkelijk gescheiden konden worden, hadden de gelijmde stukjes vier keer zo veel kracht nodig om gescheiden te worden. Deze methode werkte voor verschillende biologische en polymeergels en werd ondersteund met een numeriek model.

Het potentieel van een hybride alginaat/supramoleculaire hydrogel netwerk als extracellulaire matrix voor 2D celculturen wordt besproken in hoofdstuk 5. We hebben de cytotoxiciteit van verschillende gelcomponenten bestudeerd en we hebben het effect van dit soort extracellulaire matrix op de levensvatbaarheid en proliferatie van twee verschillende celtypen onderzocht. Beide celtypen vertonen een beperkt vermogen om te prolifereren op dit soort extracellulaire matrix. Een van de componenten van de supramoleculaire gel bleek toxisch voor cellen. Ondanks de beperkingen van dit type extracellulaire matrix geven we aanbevelingen voor verdere verbeteringen door ieder van de ontdekte kwesties te adresseren.

Tenslotte wordt er in hoofdstuk 6 een nieuwe strategie besproken om een *in vitro* model van kunstmatige plaque te maken. Een kunstmatige plaque is gemaakt door liposomen toe te voegen aan een polymeerfilm van gelatine/alginaat. De bereide films vertoonden een vergelijkbare liposomale verdeling als varkensplaque. De plaque was ook implanteerbaar zoals gedemonstreerd in *ex-vivo* en in *in-vivo* experimenten.

Concluderend, het onderzoek in deze thesis toont nieuwe strategieën voor de ontwikkeling van functionele zachte materialen gebaseerd op zelf-assemblage en reactie-diffusie. Deze types materialen zijn belangrijk in gebieden variërend van celonderzoek en weefseltechniek tot biomedische toepassingen. Het onderzoek dat hier gepresenteerd is vertegenwoordigt de eerste stappen in het combineren van op de natuur geïnspireerde principes, zoals zelf-assemblage en reactie-diffusie met als doel de ontwikkeling van nieuwe zachte materialen.

About the author

Matija Lovrak was born on 7 April 1988 in Bjelovar, Croatia. He obtained his BSc degree in chemistry from University of Zagreb in 2010. The same year he continued his education at the same university where he graduated in 2012 obtaining MSc degree in chemistry. His master project was focused on developing a novel method for determination of zeta potential of gas/liquid interfaces. This project resulted in two scientific publications. After his graduation he worked shortly as a chemistry teacher at a local primary school, before starting his PhD research in Advanced Soft Matter group at Delft University of Technology under supervision of prof. dr. Jan H. van Esch and dr. Rienk Eelkema. The focus of his research was development of novel soft materials, namely hydrogels, based on reaction-diffusion and self-assembly approaches. This research resulted in the thesis you are holding in your hands.

List of publications

- 1 M. Lovrak, W. E. J. Hendriksen, C. Maity, S. Mytnyk, V. van Steijn, R. Eelkema, J. H. van Esch, Free-standing supramolecular hydrogel objects by reaction-diffusion. *Nat. Commun.*, **8**, 15317 (2017).
- 2 M. Wu, G. Springeling, M. Lovrak, F. Mastik, S. Iskander-Rizk, T. Wang, H. M. M. van Beusekom, A. F. W. van der Steen, G. van Soest, Real-time volumetric lipid imaging in vivo by intravascular photoacoustics at 20 frames per second. *Biomed. Opt. Express* **8**, 943 (2017).
- 3 F. Trausel, F. Versluis, C. Maity, J. M. Poolman, M. Lovrak, J. H. van Esch, R. Eelkema, Catalysis of Supramolecular Hydrogelation. *Acc. Chem. Res.* **49**, 1440 (2016).
- 4 T. Preočanin, F. Šupljika, M. Lovrak, J. Barun, N. Kallay, Bubbling potential as a measure of the charge of gas bubbles in aqueous environment. *Colloids Surf. A: Physicochem. Eng. Asp.* **443**, 129 (2014).
- 5 N. Kallay, M. Lovrak, T. Preočanin, F. Šupljika, Effect of Bubbling on the Potential of Reference Electrode. *Croat. Chem. Acta* **86**, 103 (2013).

Acknowledgements

As all things come to their end, this PhD journey has also finished. Now it's time to look back and to remember all the people that made it possible and were part of it, in one way or another. First, I would like to thank all the staff members who helped me in various aspects of my daily activities.

Jan, thank you for the given opportunity to be a member of ASM group and to do research on such interesting topic as reaction-diffusion. You have always challenged me to reach new horizons and to go one step further. Also, thank you for organizing the workshop in Bad Gastein which I really enjoyed attending. I hope you will keep organizing it in coming years and wish you a lot of success with it. Finally, I should not forget Sinterklaas dinners at your place which have always been evenings full of fun and good food.

Rienk, thank you for taking the role of my daily supervisor and copromotor. I appreciate a lot your help during the preparation of manuscripts for submission. Also, whenever I had a question regarding experiments or writing you have been available.

Stephen, thank you for the idea that led to the manuscript which will, hopefully, get published soon. Good luck in the future with „Elektrisch kabinet“ and with all other events that you are helping to organize.

Eduardo, we have not collaborated scientifically, but our collaboration on a football field resulted in numerous goals and left opponents in tears.

Ger, thank you for the invitation to your 60th birthday party. It was a nice experience in my early days in the Netherlands.

Volkert, I appreciate your help with simulations. Discussions with you were always productive and I am glad that we worked together on more than one project.

Heleen, thank you for involving me in the cross-disciplinary project. This was new and insightful experience for me. I hope that our manuscript will be accepted soon.

Lars, it is amazing to have a technician who is also a DJ, biker, traveler and who knows what more. I wish you success with all your future hobbies.

Marcel, master of AFM and volleyball player. I enjoyed our numerous conversations and discussions during group drinks. You always had an interesting story to tell, either scientific one or from general life. I wish you success in all future volleyball matches.

Ben, another master, but this time of rheometer and DMA. Thank you very much for numerous advices regarding the use of instruments. Congratulations on 40 years at TU Delft. This is a quite impressive achievement.

Louw, thanks for arranging hardware that I needed for my experiments. Without it, I would not get so far.

Mieke, thank you for all the help with administrative questions.

But what would PhD be without all the amazing colleagues and friends. Honestly, it was not easy to remember all of you without help of old group meetings list. I am still afraid that I might have forgot some people. I apologize in advance for that.

Alex, the only person who I worked with twice in the same group. It was nice have beers and partying with you on multiple occasions.

Alexandra, it is fun how world is small sometimes. ASM is not our only connection. It was fun to chat with you in the lab to disrupt daily routine.

Angie, I still sometimes think that you have started recently, but it has been quite some time already. I hope we can repeat our Friday parties at some point.

Benjamin, listening to your poster presentation late in the night after who knows how many drinks was priceless experience. Let's have more of Friday parties in the future.

Bowen, although you are one of the newest members of the group, I already had more Friday drinks with you than with some older members. Let's continue this tradition with more stories about football.

Çansel, it is always fun to hear your stories and gossips. I do not have chance to party often with you, but when I do it's always good. Keep it this way.

Chandan, whatever compound I needed I could come to you and you would synthesize it. I think this is quite an amazing skill. Thank you for all those dyes that I used in my research.

Dainius, since you were already a group member for long time when I arrived, I have always listened to your stories and advices with curiosity. In the end, I managed to spend all my holidays during my PhD.

Emanuela, thank you for arranging dinner at your place with a few other ASM members on one of my first weekends in Delft.

Emma, your life changed quite some during my PhD – you became mom twice. I wish luck to you and your family in the future.

Elena, I liked a lot when you surprised us with flan during coffee breaks or when you prepared it for some other occasions. Also, partying with you has always been fun, although learning random expressions in Spanish did not work out in late hours.

Frank, you have quite a unique style – a tennis match on one screen and work on the other. It was fun to hear your jokes in various appropriate and inappropriate situations.

Fanny, I have enjoyed barbecues and dinners at your place a lot. I will especially remember that one evening in the sports center.

Jos, I have not attended birthday parties with so many people before I met you. I am already looking forward to the next one. Since you were around during my whole PhD we also had a lot of fun during all kinds of other events. Your ability to come up with jokes in almost any situation does not stop to amaze me. And not to forget, I appreciate a lot your help with moving.

Kai, it has been fun to drink with you and to listen about all adventures that you had when you drank on different occasions. Thanks for preparing Chinese food for me at your place.

Karolis, it was pleasure to have occasional chat and drinks with you.

Katarzyna, although you stayed shortly in ASM, it was nice to have you around. Those Polish sweets were amazing.

Marta, I did not know anything about hydrogels when I came to ASM, but I was happy that I partially understood at least someone's research, particularly, zeta potential of your particles.

Piotr, I appreciate advices that you gave me about making images in PowerPoint. It was and still is useful on many occasions. It was also fun to play football together. I hope we will still play sometimes. And last, but not least, I should thank you once more for help with moving.

Qian, that Chinese lunch at your place was amazing. I am glad that you also contributed to group drinks with your presence.

Roman, instead of a PhD in chemistry you should get a PhD in partying. I can barely remember contacting you to go out and getting a negative answer. It was nice partying with you all night long and hearing about all those crazy experiences that you had.

Saida, my former office mate. I really enjoyed our numerous discussions about all kinds of topics. This was a perfect way to spend (a part of) a working day.

Sander, although we did not manage to make some gels, at least we partied well on CHAINS. I have never thought that I will know someone whose job is to investigate crime scenes.

Serhii, we had a lot of fun moments since you were first PhD who started after me. Various parties, conferences and meetings, drinks and dinners. I am also glad that we were both also SMARTNET members. It was especially fun to get lost in Delft in our early days in the Netherlands, and to party with Juan in Austria.

Simge, too bad that I do not drink coffee. I am sure that I would enjoy the coffee that you used to make during our group coffee breaks. Nevertheless, I enjoyed very much the food that you prepared on several occasions.

Susan, although I didn't have chance to have drinks with you so often, it has been always pleasant to chat with you.

Tomasz, we have been through so much on many places, both as ASM members and SMARTNET members. From „playing“ with carton boards in Bordeaux to waking up unplanned in your apartment. These acknowledgements would be too long if I mention everything. One advice: Watch your ghosts.

Vasu, one of a few people that I know who does not drink alcohol. I have always enjoyed our discussions and parties together and I hope you will make a nice side career as a singer.

Vincent, it was difficult to miss your differently colored All Stars and three screens in front of you. I will especially remember one time that we partied together – you chugged every beer that I gave you in matter of seconds.

Wei, thank you for inviting me to the dinner before your departure from the Netherlands.

Wouter, I appreciate your help during my PhD, especially in the beginning. It was quite a journey from the dinner that I had with you and Roman after my interview until our Nature Chemistry paper was published. I am glad that we made it.

Yiming, my office mate and my drink mate. I had nice time chatting in our office and discussing various topics. I especially enjoyed our discussions with a cup of beer. Let's have more of them in future.

Yunlong, it was fun to imitate Roman's dancing every time when we partied together. I am glad that we partied once more after you left Delft.

I would further like to thank all students that were part of the group during these years. Each of you contributed to the group atmosphere. Dovile, I am glad that you did amazing work during your master project which will, hopefully soon, result in a paper. Allan, having you as an office mate was exceptional experience.

Ana Catarina, Inês, Iván, Jorge, Kars, Laura, Marco, Maria, Nishant, Philip and Vânia, it was an amazing experience to be a member of SMARTNET crew together with you. We had so many good meetings. The best part was always after all presentations finished. I hope we will meet again at some point to remember all those nice moments.

Alexey, Javier, Rohit, Tophi, Vallin, it was amazing that we formed a friend group after PhD Start-Up. I can't even remember all the things that we did together, but I am glad that we created some memories. I will always remember our trips to Croatia and Austria.

What would PhD be without some other activities in the free time? Apart from playing video games, I devoted my free time to football. I would like to thank to all the people that invited me to play football with them. Ilias and Cristobal, I am glad that we formed a team and participated in a tournament. It is nice that we also had nice time outside of a football field.

Mama i tata, puno vam hvala za podršku koju ste mi pružali svih ovih godina. Vaši savjeti i potpora su me doveli tu gdje sam danas.

I na kraju, Monica, neizmerno ti hvala što si uz mene već više od 6,5 godina i što si mi podrška u dobrim i lošim trenucima. Drago mi je da smo konačno na istom mjestu i radujem se našoj zajedničkoj budućnosti.

